Unravelling the Choreography of the EnvZ/OmpR Transmembrane *Pas de Deux*

by

Robert J. Lawrence

Student number: 652740

School of Pharmacy and Biomedical Sciences

The thesis is submitted in partial fulfilment of the

requirements for the award of the degree of

DOCTOR OF PHILOSOPHY

of the University of Portsmouth

November, 2019

Preface

This PhD was fully funded by the Faculty of Science and Health within the University of Portsmouth. The project began in October 2016 and was completed in November 2019.

The project was supervised by Dr Roger Draheim, Dr Marianna Cerasuolo and Dr Andrew Pickford.

Experiments were conducted within the School of Pharmacy and Biomedical Sciences at the University of Portsmouth

Robert Lawrence

Abstract

Two-component regulatory systems allow bacteria to respond to and survive the environments in which they are situated. Specifically focusing on the sensor kinase element of these systems, much is left unknown regarding the overall functions of many of these protein types. This work centres on the EnvZ/OmpR system within *Escherichia coli* and more specifically how the osmosensing kinase EnvZ transduces signal across the membrane. Many studies have detailed the mechanisms of cytoplasmic and periplasmic sections of these proteins, yet the transmembrane helices have remained relatively untouched due to difficulties in probing within the membrane *in vivo*. Transmembrane helix movements have been detailed within similar kinase proteins, which are described for comparison.

The experimental approach centred around three mutant libraries of EnvZ – two single-cysteine libraries (transmembrane helix 1 or 2) and one double-cysteine library (both transmembrane domains). The cysteines replaced residues within the transmembrane helices of EnvZ and were predicted to form a sulphydryl crosslink between two dimerising proteins under oxidising conditions. This was proposed to occur only if the positions were within an appropriate proximity meaning that some area of the helix would crosslink and others would not, revealing an interaction profile. The signal output of the system was also tested for tolerance to each mutation. These experiments were performed in the presence and absence of a hyperosmotic stimulus in order to suggest differences in the interaction and signal output profiles of the active versus inactive forms of EnvZ.

The single-cysteine libraries revealed no differences in the interaction profile of the first transmembrane helix and a non-piston type movement within the second transmembrane helix. The double-cysteine library generally corroborated these results, adding a TM1/2 interaction profile. This profile included residues within the periplasmic and cytoplasmic ends of the helices but not within the membrane core. The dynamic range of the system was also calculated for the double-cysteine library and compared to “absence of stimulus” signal output

results. This revealed an exponential decay relationship across the 89-member library, with only five outliers to this trend.

While the overall movement of the EnvZ transmembrane helices cannot be conclusively stated from this work, several interesting features of this mechanism have been described. In particular, the lack of interaction between TM1 and TM2' helices may suggest an inner membrane space is created that contributes to the sensing mechanism of the system. Ultimately, the results collected do not support the piston-type displacements seen in similar kinases, leading to the proposal of a new model. Further work is required to test the proposed model as well as understanding the role of EnvZ within a wider context.

Keywords: Two-component systems, EnvZ/OmpR, Transmembrane signaling, Transmembrane four-helix bundle.

Declaration

Whilst registered as a candidate for the above degree, I have not been registered for any other research award. The results and conclusions embodied in this thesis are the work of the named candidate and have not been submitted for any other academic award.

Word count: 41,187

Contents

List of Figures

List of Abbreviations

1X-Cys	Single-cysteine mutation within EnvZ
2X-Cys	Double-cysteine mutation within EnvZ
A/Ala	Alanine residue
ABR	Antibiotic-resistant
ADP-P	Adenosine diphosphate and phosphate
Amp	Ampicillin
AMR	Antimicrobial resistance
APS	Ammonium persulphate
AS1	First helical region of the HAMP domain (Amphipathic sequence 1)
Asp/D	Aspartate residue
ATP	Adenosine triphosphate
C/Y	CFP/YFP ratio
CA	Catalytic ATPase
CC	Coiled coil
cCFP	CFP value corrected for background fluorescence
CEG	Conditionally essential genes
CFP	Cyan fluorescent protein
cYFP	YFP value corrected for background fluorescence
Cys/C	Cysteine residue
D/M	Dimer/monomer ratio
DHp	Dimerisation and histidyl phosphotransfer domain

E. coli	*Escherichia coli*
EDTA	Ethylenediaminetetraacetic acid
EG	Essential genes
EHEC	Enterohaemorrhagic *Escherichia coli*
EnvZc	Cytoplasmic domain of EnvZ
HAMP	Domain present in histidine kinases, adenylate cyclases, methyl-accepting proteins and phosphatases
His	Histidine
His/H	Histidyl residue
HK	Histidine kinase
HP	Helical propensity
IPTG	Isopropyl-β-D-thiogalactopyranoside
MDR	Multidrug resistance
Met/M	Methionyl residue
MMA	Minimal medium A
MzrA	Modulator of EnvZ/OmpR A
NEM	*N*-ethylmaleimide
OM	Outer membrane
OmpC	Outer membrane protein C
OmpF	Outer membrane protein F
OmpR-P	Phosphorylated OmpR
Osm	Osmolarity
P	Phosphate group

PBD	Protein database
PD	Periplasmic domain
Pro	Procaine
RR	Response regulator
SDM	Site-directed mutagenesis
SDS	Sodium dodecyl sulphate
SDS-PAGE	Sodium dodecyl sulphate-polyacrylamide gel electrophoresis
SHK	Sensor histidine kinase
TBS	Tris-buffered saline
TBS-T	Tris-buffered saline with tween 20
TCS	Two-component regulatory system
TEMED	*N, N, N, N*'-tetramethyl-ethylenediamine
TM	Transmembrane
TM1	Transmembrane helix 1
TM2	Transmembrane helix 2
TM5	Transmembrane helix 5
TMD	Transmembrane domain
TMHMM	Transmembrane Helix prediction with a hidden Markov Model
Trp	Tryptophan
WT	WT
YFP	Yellow fluorescent protein

List of Bacterial Strains and Plasmids

***Escherichia coli* Strain**	**Function or Feature**	**Citation**
K-12 MG1655	F- λ- *ilvG rfb50 rph1*	(1)
MDG147	MG1655 Φ(*ompF*$^{+}$-*yfp*$^{+}$) Φ(*ompC*$^{+}$-*cfp*$^{+}$)	(1)
EPB30	MDG147 *envZ::kan*	(2)
MC1061	F- *hsdR2(rK*$^{-}$ *mK*$^{+}$*) mcra0 mcrB1*	(3)
DH10B	Electrocompetent cell	(3)
Plasmid	**Function or Feature**	**Citation**
pEB5	*ΔenvZ* –empty control vector	(4)
pEnvZ	Contains *envZ*	(5)
pRD400 (pEnvZ-V5)	pEnvZ with linker (GGSSAAG) and V5 tag	(6)

Disclaimer

This thesis contains work taken from Heininger et al, 2016 and Yusuf et al, 2017 (preprint only via Biorxiv), on both of which RL is a contributing author. Sections 2.4-8, 3.1-4, 4.1-3, 6.1-2 and appendix section A have been adapted from these articles. RL provided additional Western blotting experiments essential for completion of these projects. All other work was entirely organised and completed by RL.

Acknowledgements

During my seven years at the University of Portsmouth, I have achieved a bachelor's degree in Pharmacology, spent a year volunteering (and worrying that I should have done a master's) and now I approach the end of my PhD. It has always been in my nature to try and go it alone when it comes to my work, but to get this far I have learned the importance of finding help wherever I can.

First and foremost, my brilliant fiancée Hannah Elliott (Lawrence one day soon!) has been my number one fan throughout this entire process. She gives me so much confidence in myself and is never afraid to tell me when I'm about to do something stupid – which is often thanks to a severe lack of common sense! Hannah, you're my best friend, greatest confidant and I really wouldn't have made it this far without your unwavering loyalty, honesty and love.

My parents have always given me the best opportunities to go out and achieve anything I set my mind to and for that I will be eternally grateful. I've never felt pressure to do anything that my heart wasn't drawing me towards, so that has served as an excellent guiding force to get into a career I will genuinely enjoy for many years to come. My sister Hannah is a stupendous overachiever so it has always been fun trying to catch up to her! I will remind her that, all going well, I will receive my PhD at a younger age than she did and I got my first publication before her too. Oh, and the small matter of working in a real science! In all seriousness, she has provided amazing support to me over my doctoral years and maybe one day I can teach her something too (not likely unfortunately).

My friends at UoP have been hugely helpful over the years as the Draheim group has steadily grown in size since 2015. Rahmi, Than, Fadhael, Peltine and Joy - you are all excellent scientists in your own ways and I know that in ten years' time there will be an impressive alumni of students that started their research lives with Roger. Speaking of whom, Roger has been a mentor to the fullest extent of the word ever since I met him. I came to him

looking for a little micro experience to kill time before I tried to apply for more PhDs and he gave me the opportunity to start a research career. He has certainly taught me to take any opportunity and turn it into the best possible outcome for my career. I feel I have come a long way in this area and feel confident knowing that I have the ability to compete in such a competitive community.

Thank you to all of my students over the years: Aarie, Kanchan, Nesrine, Berenice, Linh, Huda, Thanusha, Krishna, Nathan, Sarah, Laura, Hannah, Huma, Florianne, Pilar, Clara, Sam, Ambika, Malcolm, Jess, Teresa, Komal, Lauren, Cecilia, Patri, Hugo, Declan, Charlotte, Abi, Kuky and Parwana. It has been a pleasure and a challenge to train so many people in my methods, but I wouldn't change a single one of you. I wish you all the best in your careers wherever they may take you – I know that you have all helped mine!

Next, I'd like to thank the university – it's been a home from home for quite some time now and I feel truly prepared to go out and find the next challenge somewhere new. I see so many familiar faces around campus and I will really miss that when I leave. Many lecturers within my school have been excellent allies over the years – Jan, Tony and Paul thank you all for your advice and encouragement that has taken me where I want to go!

Finally, I want to thank Hannah again – you are well worth a double mention and I dedicate my thesis to you! I'm fairly sure you'll never want to read past this page; I imagine most other people are with you on that. However, all the hard work and effort I've put into this work is truly representative of my commitment to you.

Rob Lawrence 

Chapter 1: Introduction: An overview of the Two Component System

1.1: Two-Component System Structure

The most crucial goal for any bacterium is to survive and propagate its existence to the furthest degree possible within the environment it is situated. Therefore, the environment will inevitably present the primary barrier to this goal and so the bacterium must be appropriately equipped to deal with its vast array of environmental changes. The two-component regulatory system (TCS) is specifically engineered to allow bacteria to react to their environments (7–12) or pathogenically (12–14) and symbiotically (15,16) interact with eukaryotic hosts and partake in essential cellular pathways (7,17). Some TCSs are essential to bacterial viability such as WalK/WalR that regulates cell wall metabolism and virulence yet most of its physiological role remains uncharacterised. Others regulate homeostatic processes important for virulence such as the KdpD/KdpE system which regulates potassium ion levels, a critical factor in bacterial virulence (18–21). EnvZ/OmpR is a TCS that regulates outer membrane porin expression and while it is not essential to cell viability, it has control over the permeability of the outer membrane to small hydrophilic molecules (22).

A TCS is formed of sensor and effector components known more specifically as the sensor histidine kinase (SHK) and the response regulator (RR) respectively. This basic structural architecture can become more complex, with additional elements added but the SHK and RR are consistent throughout (**Figure 1-1 A-D**)(23). Depending on the specific nature of the stimulus it is designed to detect, the SHK will often be bound within the inner membrane. The RR is found in the cytoplasm and will often be exclusively linked to its SHK, receiving input only via this interaction (24,25). These features describe the TCS somewhat two-dimensionally, however the reality of their function is far more complex as they form a

sophisticated network. These networks function via the crosstalking of TCSs and these processes must be tightly regulated to ensure signals are properly transduced.

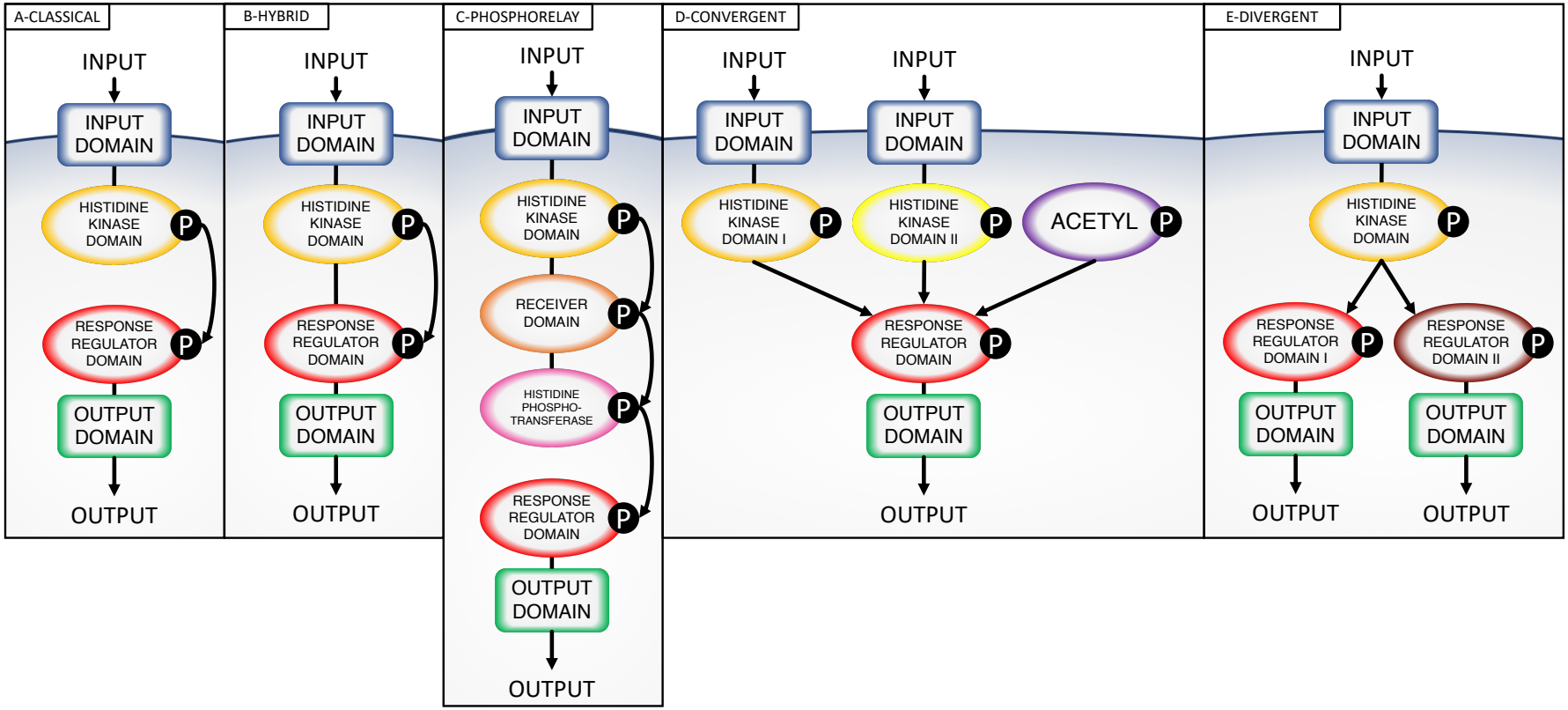

Figure 1-1: Classifications of two-component systems by their architecture. The classical structure (**A**) consists of a sensor including an input domain and a histidine kinase (HK) domain. The HK domain becomes phosphorylated following input detection, which allows for phosphorylation of the RR. Once the RR is phosphorylated, the attached output domain produces an output. The hybrid system (**B**) is similar to the classical system, yet it is formed as one continuous protein, rather than two separate polypeptides. The phosphorelay system (**C**) requires four separate phosphotransfer events, as the membrane-bound component is more complex than the classical system. The two additional phosphotransfers occur within the kinase protein as the phosphate group is passed to a receiver domain then a histidine phosphotransferase domain before it is moved to a conserved aspartate within the response regulator. Upon completion of these transfer events, an output is generated. The convergent (**D**) and divergent (**E**) systems are the opposite of one another. The former perceives stimuli via multiple sensor HKs that communicate and activate a shared response regulator. The latter perceives stimulus via a single sensor HK which communicates with multiple response regulators, subsequently producing multiple outputs. (23)

1.2: Crosstalk Versus Specificity

As previously mentioned, an SHK is almost certain to be specifically linked to its cognate RR – without such a system there would be an overabundance of crosstalk leading to a fatal breakdown in communication from external signals to internal processes. Therefore, SHKs utilise a set of phosphotransfer-related mechanisms to maintain specificity to their cognate RR including molecular recognition, phosphatase activity and competition for substrates. The foremost of these mechanism is the SHKs ability to recognise specific residues within the RR, thereby allowing it to discriminate cognate from non-cognate (26,27). Phosphatase activity, found in most SHKs, allows the TCS to regulate the signal output generated by its RR through means of phosphate removal. This also aids specificity and reduces unwanted crosstalk as phosphorylated non-cognate RRs will be acted upon by the phosphatase activity of the SHK before they have chance to generate an inappropriate output (28–31). Some response regulators are activated by the acetyl-phosphate available within the cytoplasm (**Figure 2-1D**) via its own phosphatase activity. Similar to the activation of non-cognate RRs previously discussed, SHKs will detect and correct these erroneous phosphorylation events (2,32–34). Finally, the RRs compete for phosphorylated kinases and therefore cellular concentrations of both will contribute to regular function in response to signal. It is exceedingly common for [RR] to exceed its cognate [SHK]; for example EnvZ (SHK) and OmpR (RR) are maintained at a ratio of around 1:35, which is similar to most other pathways (35,36). This relationship of concentrations allows the cognate RR to easily outcompete any non-cognate RRs, thus maintaining regular signal function. These mechanisms contribute to reduction of unwanted crosstalking, therefore most TCS communication is one-to-one (**Figure 1-2A**). However, some TCS must engage in crosstalk, either multiple SHKs to a single RR or the converse, to allow specific physiological events to occur (24,37,38). In terms of targeting a TCS, the balance of specificity with crosstalk and the impact on cell survival could be of great importance. Causing an overabundance of unregulated crosstalk will most likely cause

detrimental effects to the overall cell function, resulting in either bacteriostatic or bactericidal effects. Consequently, investigation into defining TCSs as therapeutic targets has taken place

1.3: Domain structure and related functions within the SHK

The fundamental purpose of a TCS system is to allow a bacterium to respond to specific environmental cues such as changes in pH, osmotic pressure, nutrient levels and antibiotic presence (39). These systems are also able to crosstalk at the level of transcription, thereby creating a complex signal transduction network capable of facilitating survival across a wide range of environments (40,41). The process of signal transduction is largely conserved between different systems (**Figure 1-2**) and while the ability of the dimerisation and histidyl phosphotransfer (DHp) domain and catalytic ATPase (CA) domain to form a dimer and facilitate trans-autophosphorylation (**Figure 1-3**) is well understood (42), the role of the transmembrane helices transferring signal to this cytoplasmic four-helix bundle is much less well understood in SHK proteins generally. Unsurprisingly, mutation and allosteric modulation of TCSs has been shown to result in various mechanisms of resistance across a range of different bacteria (39,43–47). Thus, modulation of signal output from these systems appears to be viable target for chemotherapeutic treatment.

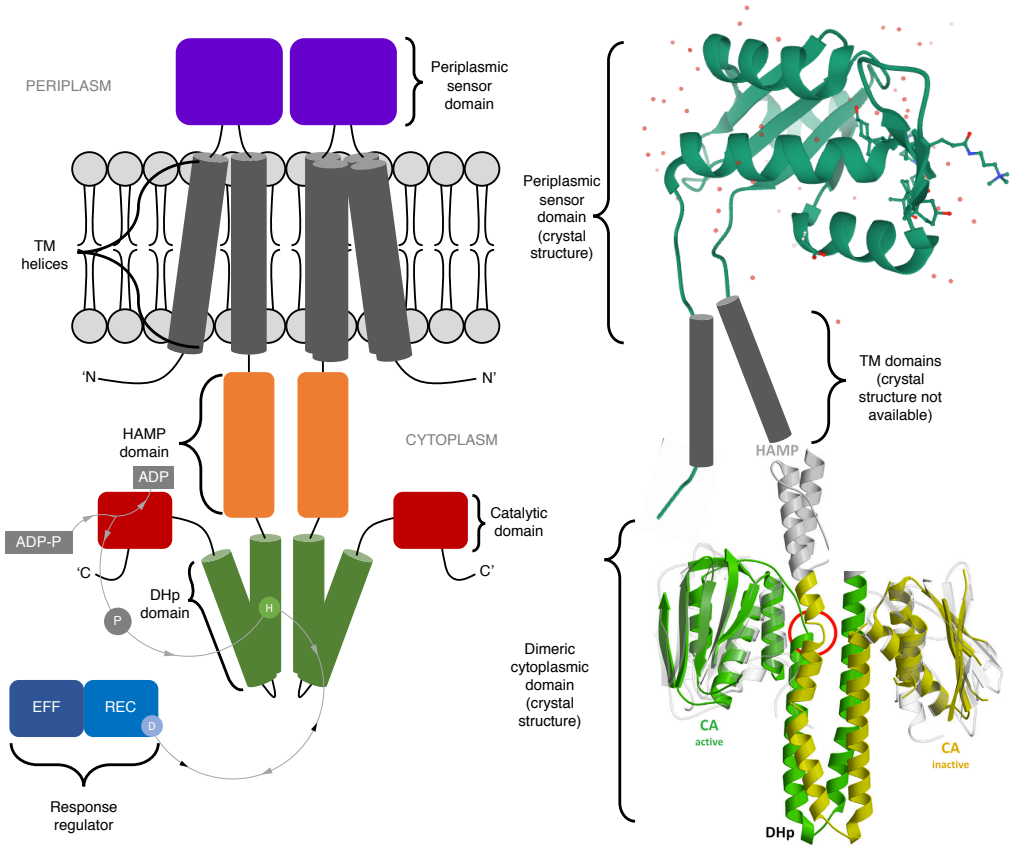

Figure 1-2: A TCS from sensory input to gene transcription output with EnvZ crystal structures for comparison. The SHK is the larger protein within this figure, formed of various domains that each contribute a specific function. A sensor domain (purple) detects stimuli that will effect conformational change. The transmembrane domains (grey) will contribute to the passage of signal across the membrane. The HAMP (present in **H**istidine kinases, **A**denylate cyclases, **M**ethyl-accepting proteins and **P**hosphatases) domain (orange) will contribute to this transduction downstream, ensuring the signal is not passed on inappropriately. The DHp domain (green) contains a conserved histidyl residue (H) that will be autophosphorylated by the CA domain (red) from the other protein in the dimer formation with an (adenosine diphosphate and phosphate) ADP-P (grey) providing the phosphoryl group (P). Once the histidyl residue is phosphorylated, it will be available for transfer to an aspartate residue (D) in the receiver domain (light blue) of the RR, a separate cytoplasm soluble protein. This allows the effector domain (dark blue) of the RR to effect gene transcription. As well as providing a phosphoryl group to the RR (grey arrows), the SHK can also remove this phosphoryl group via its phosphatase activity (black arrows), which serves as a regulatory function. Crystal structures for the EnvZ SHK have been discovered for both the periplasmic (PDB ID: 5XGA) and cytoplasmic regions (48) of this protein. The cytoplasmic regions are depicted in a dimeric form, hence the presence of two DHp domains and two CA domains These can be seen left of this figure, yet there it not yet a crystal structure of the transmembrane domains of EnvZ, therefore they are depicted as grey cylinders.

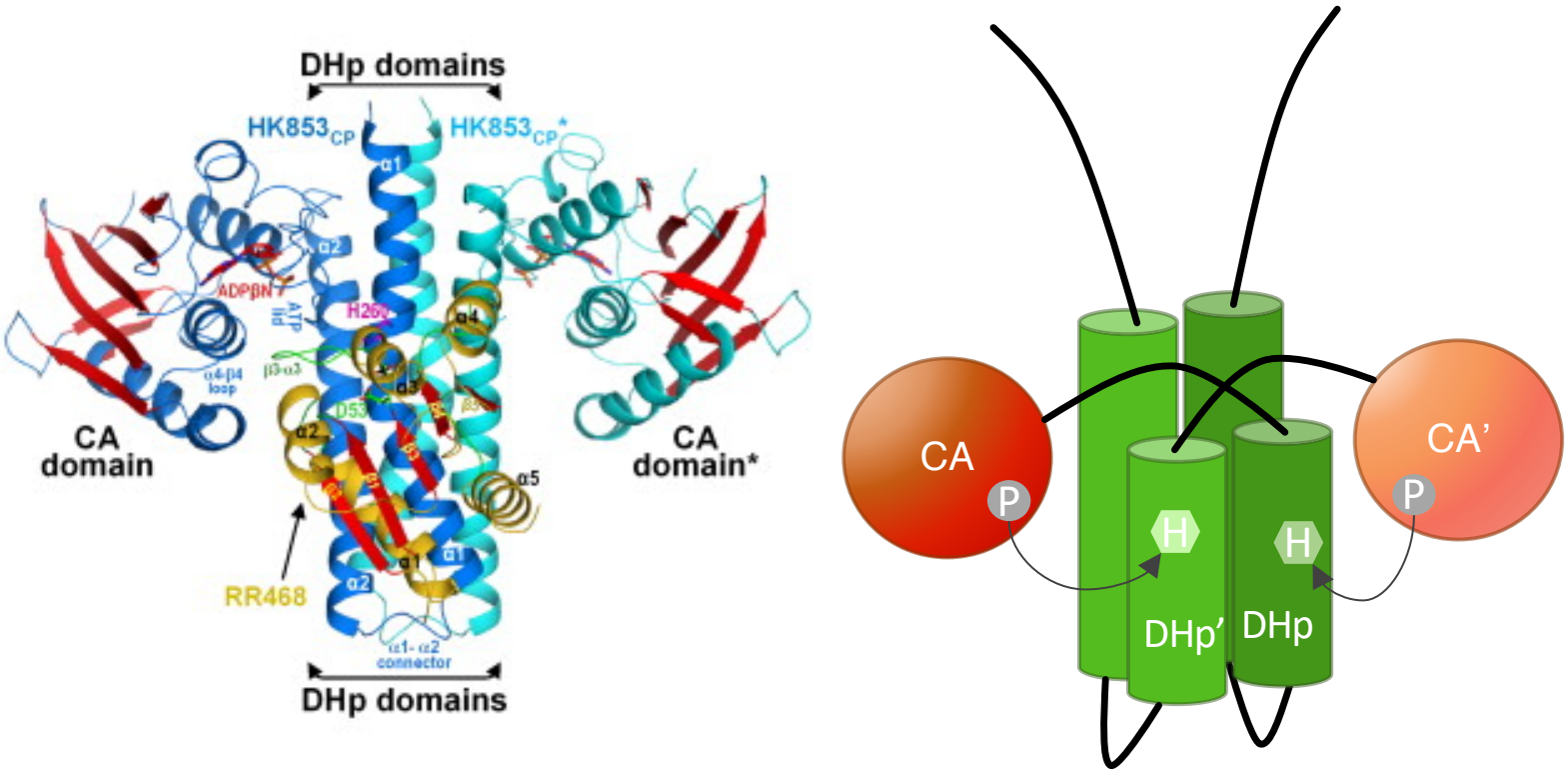

Figure 1-3: Process of autophosphorylation within an SHK homodimer. The kinase core conserved across HKs consists of the DHp and catalytic domain, in which ATP can bind. The dimeric core of the HK853 kinase is shown (left, protein database (PDB) ID: 3DGE) and a simplified version of this relationship is also shown (right). The HK853 kinase is chosen for is high resolution crystal structure and comparability to EnvZ (27).

1.4: EnvZ/OmpR – A structural and functional overview

The EnvZ/OmpR TCS is present within many Gram-negative bacteria and was initially shown to respond to changes in external osmolarity by modulation of porin expression within the outer membrane (**Figure 1-4**) (22,49) . EnvZ, an osmosensing SHK found within the inner membrane of *Escherichia coli* (*E. coli*), is among the most well-known of the *E. coli* SHKs. It is structurally complex and therefore studies that attempt to elucidate its function and structure remain ultimately inconclusive (50). Comprising of 450 amino acids, the EnvZ monomer consists of a 115-residue periplasmic domain (51,52), two transmembrane domains (TM1 and TM2) (53), a HAMP (linker) domain and a kinase domain within the cytoplasm. Biochemical studies have shown that EnvZ can autophosphorylate a conserved His-243 residue using an adenosine triphosphate (ATP) molecule (54). This phosphate is then used to phosphorylate the conserved Asp-55 residue (55) located within OmpR, the cognate RR linked with EnvZ. Through phosphatase capabilities, EnvZ may dephosphorylate OmpR-P to return it to its original state (30,56). More specifically, the process is a trans-autophosphorylation as the ATP-binding domain of one EnvZ subunit will phosphorylate the conserved His-243 residue located on the other EnvZ subunit of the dimer (42,57,58). In addition, EnvZ/OmpR has been shown to control virulence within *E. coli* making it a potential target for virulence-attenuation (59). Two of the major porins expressed within the outer membrane and governed by EnvZ of E. coli are outer membrane protein F (OmpF), a large-diameter porin, and outer membrane protein C (OmpC), a small-diameter porin. When the EnvZ/OmpR TCS causes more OmpC (low permeability) than OmpF (high permeability) to be present in the outer membrane, the permeability of the cell membrane to antibiotics and other small molecules (<650 Da) is significantly reduced (22).

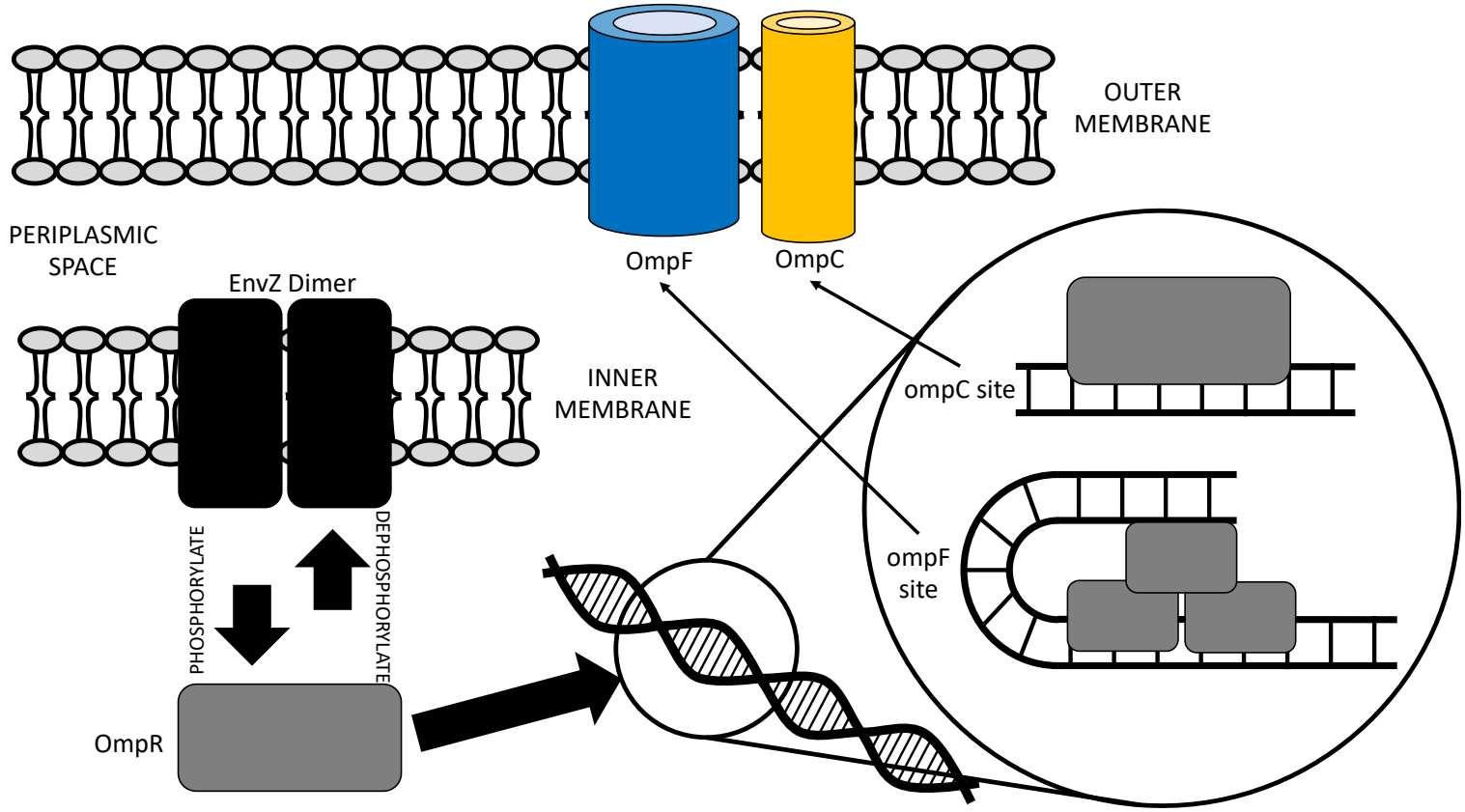

Figure 1-4 The EnvZ/OmpR TCS found within *E. coli*. EnvZ is an SHK that becomes activated by the following stimuli: Osmolarity increase, Modulator of EnvZ/OmpR A (MzrA) interaction. The EnvZ homodimer autophosphorylates, allowing for phosphorylation of its RR named OmpR. Phosphorylated OmpR (OmpR-P) will then bind to the DNA within *E. coli* at sites promoting transcription of outer membrane porins OmpF or OmpC. If the concentration of OmpR-P is high due to increased EnvZ activation, then multiple OmpR-P units will bind to the *ompF* sites as the affinity is greater. However, the units will create a multimer that bends the DNA around itself and ultimately blocks off the *ompF* site from being activated any further. This causes OmpR-P units to bind at the lower affinity *ompC* sites, therefore when [OmpR-P] levels are increased, *ompC* transcription will also be increased and *ompF* transcription will be decreased. The key difference between OmpF and OmpC is their effect on permeability, with the former promoting increased permeability across the outer membrane.

The molecular mechanisms of perception and response to environmental stimuli by EnvZ have long been studied but remain somewhat unclear and occasionally contradictory. However, over the last few years, three stimuli have been studied in greater molecular and biophysical detail than previously possible: changes in extracellular osmolarity, periplasmic interactions with MzrA and changes in intracellular pH.

The cytoplasmic domain of EnvZ (EnvZc) contains the HAMP domain and the kinase domain, the latter of which consists of several regions that are highly conserved among other histidine kinases (60,61). The EnvZc domain has consequently been used as a model example for kinase domains within all HKs and retains all the enzymatic activities of a complete EnvZ protein when expressed in an EnvZc only form (62,63). EnvZc contains two functional domains – the DHp domain contains the His residue 243 (64). This domain is not only responsible for the phosphorylation of OmpR but also dephosphorylation – the conserved His-243 is vital in these processes (65). The CA domain contains the ATP binding site as a phosphate group is transferred over. These domains have been studied structurally via NMR, revealing more specific features within both the DHp and CA domains as well as detailing their relationship to function (66,67). Two helices were revealed within domain A that form a 4-helix bundle as a dimer (66). The CA domain displays a similar folding pattern seen within other ATPase proteins. The conserved regions previously mentioned have involvement in the structural formation of the binding pocket within this domain.

The HAMP linker domain, found between the DHp domain of the kinase region and TM2, plays an essential role in signal transduction between the receptor and kinase domains. Its structure consists of two α-helices of identical length yet offset by a single helical turn. These helices form a 4-helix bundle within an EnvZ dimer yet the core residues of this bundle are packed unusually. It is expected that a knob to hole packing would be observed within a 4 coiled coil structure, yet the HAMP domain arranges in a knob to knob packing mode

(complementary *x-da* packing), which consequently would require a rotational shift of 26° to organise into the more usual packing format. This would cause downstream elements to rotate to the same degree, thereby revealing the signal transduction functionality of the HAMP domain (68,69) (**Figure 1.2**).

The periplasmic domain (PD) has been determined as a crystal structure in the presence of the CHAPS detergent but attempts to crystallise the PD without a detergent have not been successful. Multiple features within the PD have been identified from these studies, such as two helices and β-sheets and their interfaces within a dimer formation have been suggested based on similar proteins such as NarQ/X and PhoQ (**Figure 1.2**). However, unlike domains of EnvZ within the cytoplasm such as the HAMP domain and the kinase domain, the PD does not intrinsically form a homodimer structure and such interactions are shown to be relatively weak in solution (70–77). It is therefore proposed that this weakness is intentional to allow the sensing functionality within the periplasmic domain. As the affinity of the PD dimeric interface is modulated, downstream structural effects within the cytoplasmic domains will allow for or prevent its kinase functionality (78). Regarding the transmembrane domains of EnvZ, little has been discovered regarding their structure and specific role within the signal transduction process of this HK. Some mutants affecting the transmembrane domains (TMDs) have shown to supress EnvZ kinase and/or phosphatase functionality suggesting they have an important role in the overall process. However, as structural studies are much more difficult within transmembrane regions of proteins, alternative methods to those previously discussed with the periplasmic and cytoplasmic domains of EnvZ are required.

Additional studies have identified MzrA, a small inner membrane protein that interacts with the periplasmic domain of EnvZ *in vivo*. These MzrA-EnvZ interactions have been shown to result in increased EnvZ signal output (79,80). MzrA and osmosensing act independently to modulate EnvZ signal output because modulation of porin expression due to changes inextracellular osmolarity still occurred in the absence or during overexpression of MzrA

(79,80). Finally, building on the aforementioned studies, intracellular pH was shown to have a dramatic effect on the activities of EnvZ. The phosphatase activity of EnvZ has been shown to be regulated by intracellular pH, with a shift towards acidic conditions decreasing phosphatase activity (81). Furthermore, given the broad conservation of the residues involved in this phosphatase activity switch, such a regulatory mechanism likely reflects a general pH-response mechanism for the vast majority of bacterial TCSs (81). In addition, OmpR has been shown to respond in a phosphorylation-independent manner to changes in intracellular pH (82).

Based on these various classes of effectors, it appears that the both periplasmic and cytoplasmic domains are important for allosteric interaction that modulate EnvZ signal output as measured by changes in the intracellular level of phospho-OmpR. Thus, it remains important to better understand the role of the (TMD) and its transmembrane (TM) helices during stimulus processing by EnvZ in order to predict how porin balance can be targeted. In addition, recent evidence has also shown that lipid-mediated allostery is important for overall EnvZ activity. Models of transmembrane helix movement during signal transduction are of particular importance when considering the physical shifting the protein undertakes in order to achieve trans-autophosphorylation (83). There have been several contradictory claims to the model of movement exhibited by the transmembrane domains of EnvZ. These claims are often based upon the models of similar histidine kinases rather than direct evidence obtained from experiments involving the EnvZ/OmpR system. Firstly, several models of movement for transmembrane helices as well as models that involve the HAMP domain will be discussed then this information will be summarised to suggest how it may inform the discovery of a model of movement for EnvZ.

1.5: Transmembrane Communication within SHKs by the TM-cable-HAMP Module

Multiple SHKs and receptors contain a transmembrane communication module that consists of four transmembrane helices embedded in the membrane, a control cable and a HAMP domain functioning as a single unit. Each of these is discussed below. When joined together these function as an integrated signal processing unit. Other proteins exist that share similarities in their structural and functional characteristics when compared to the SHK and more specifically, EnvZ (**Figure 1.5**). It is important to understand how the various functional units of these proteins work, especially as certain domains such as the HAMP domain, are highly conserved amongst these protein types. The proteins exampled in **Figure 1.5** each have two transmembrane domains, akin to EnvZ (far left of **Figure 1.5**). Understanding the role of transmembrane helices in similar proteins may be useful to put EnvZ transmembrane communication into context.

If a sensor histidine kinase includes a periplasmic domain that perceives stimulus, such as EnvZ, it must transduce the presence of stimulus across the cytoplasmic membrane. Initial models for transmembrane communication that have been proposed for related receptors include piston-type displacements and scissor-type motions. Over the last few decades, various *in vivo*, *in vitro* and *in silico* methodologies have been employed in an attempt to elucidate specific mechanisms of signal transduction within SHKs and other related receptors via both ligand-based and environmental stimuli for example, NarQ (nitrate levels) and EnvZ (osmolarity changes) respectively.

In addition to the transmembrane domain, significant analysis has also been undertaken on the HAMP domain, which is often found adjacent to the inner leaflet of the cytoplasmic membrane (84–86). The HAMP domains form a discrete parallel four-helix-bundle that configures alternately between the on- and off kinase states. Initially, a rotational or gearbox model for HAMP signaling was proposed based upon the solution structure of an

isolated domain and subsequently these studies began to involve chimeric SHKs which supported the initial studies (84). In parallel, mutagenic studies have led to a dynamic bundle model for HAMP signaling (87). These two models have been compared and contrasted many times. Very recently, the *apo* and ligand-bound form of an X-ray structure of a four-helix-bundle, TMD and HAMP domain has been solved (88). Connecting these domains is the so-called control cable, a somewhat flexible short residue stretch between the end of transmembrane helix 2 (TM2) and the beginning of the HAMP domain (89,90). The Tsr chemoreceptor protein is found within *E. coli* and contains a similar TM/HAMP region to an SHK and therefore useful comparisons may be drawn in its signal transduction mechanisms. The Tsr control cable has been shown to mediate structural interactions between misaligned registers of TM2 and the first HAMP domain helix, known as AS1 (91,92). It is suggested that the inward displacement of TM2 causes the side-chain environment within the control cable to alter and subsequently the control cable helix breaks allowing the HAMP helices to pack more stably thus promoting a kinase-off output. This helix-clutch model supports piston type movements within transmembrane domains yet does not suggest a specific HAMP domain model of movement. Evidence for these differing models have been found across several different types of proteins, including SHKs. This information will be useful to understand how a piston type movement may display and also considers the connection the HAMP domain may have with TM movements.

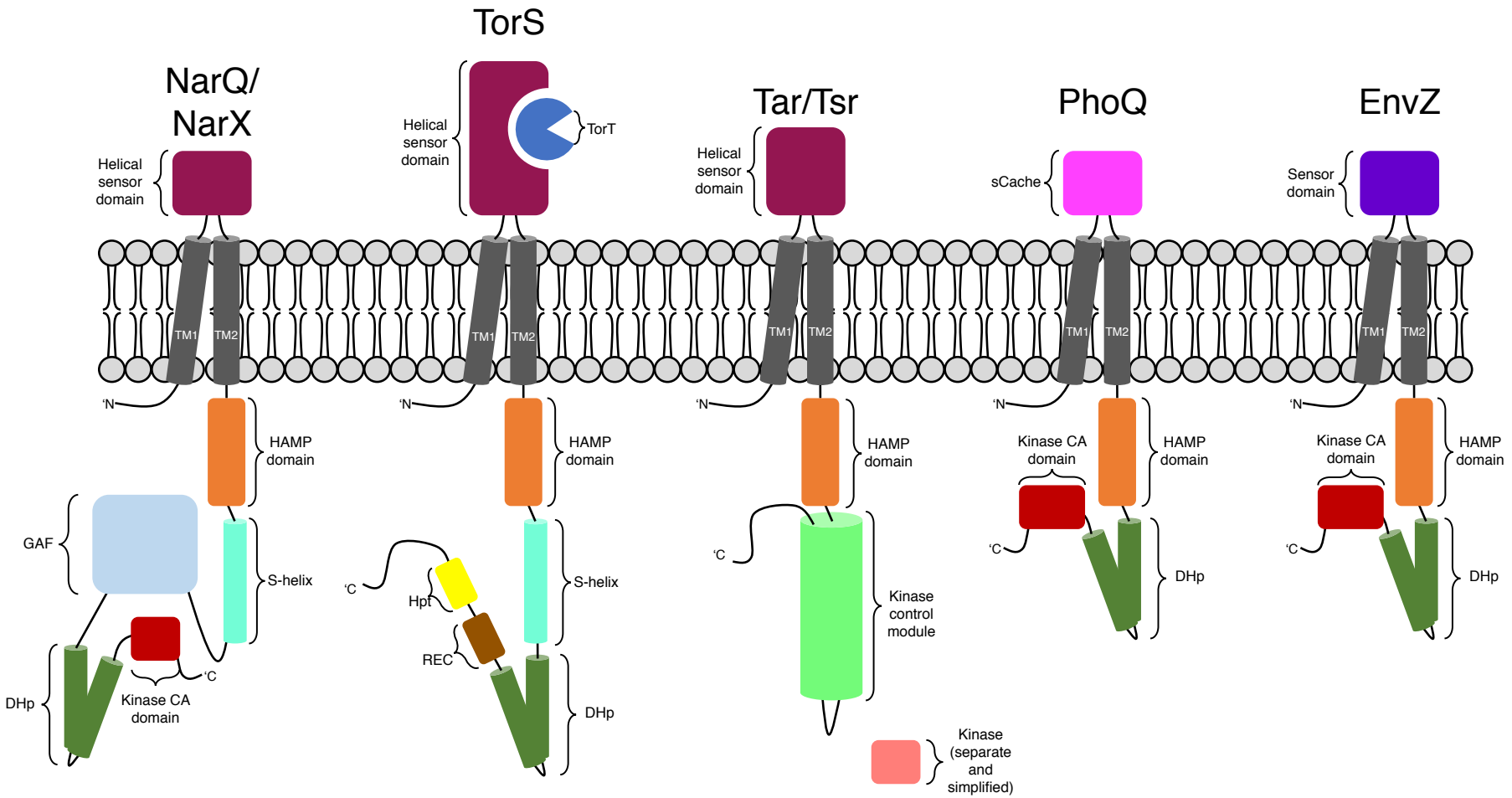

Figure 1-5: Examples of bacterial proteins with structural similarities to EnvZ. Four examples of proteins that contain structural domains similar to EnvZ plus EnvZ structure for comparison. These examples are all membrane bound sensor kinases who share the function of transmitting transmembrane signal to an interior kinase domain. Each protein contains two transmembrane domains followed by a HAMP domain then a kinase domain. Each system contains a different arrangement of domains downstream of the HAMP domain and this may explain difference in transmembrane and HAMP domain conformational changes between different sensor kinase systems. This figure has been adapted from Gushchin and Gordeliy, 2018 (167).

1.5.1: Piston-type Models of Transmembrane Communication

The piston model suggests a slight displacement of TM2 towards the cytoplasm upon activation of the SHK (**Figure 1-6**) (93), evidenced using analogous substitutions in the transmembrane region (94). This piston-like motion is induced by stimulus at the periplasmic side and is transformed into a combination of longitudinal and transversal movements of the helix resulting in the modification of the HAMP domain (95). The movement seen in the piston model is thought to primarily involve the β-helices, as α-helices are generally more resistant to compression and extension (96). Experiments in *E. coli* were carried out at the Tsr protein to specifically analyse TM2 movement in this model. This showed the input and output domains to communicate through three main areas, the TM2, HAMP, and cable control helix showing changes in serine occupancy to promote a piston-like displacement of TM2 normal to the plane of the membrane initiating a signal transmission. The signal may then be transmitted to the first helical region of the HAMP domain (AS1) allowing activity predicted by the gearbox and scissor models (89).

Tar, Tsr, Trg, TorS and NarX have all been reported to display a piston-like sliding motion during signal transduction (97–101).The Tar chemoreceptor has been shown to display piston type movement in the alpha-4 periplasmic helix within its homodimer form. As it binds aspartate to activate, the *apo* and *holo* forms of the protein were compared using cysteine cross-linked dimers in order to show the piston movement (102). Further experiments that substitute alaninyl residues within TM2 of Tar for the aromatic amino acid tryptophan (Trp) altered wild-type (WT) signaling patterns. Additionally, six positions around the mutant W209A were individually substituted for Trp, which abolished signal output for 5 of these positions. These results were found to support a piston model of movement as they are generally consistent with previous predictions (99). Despite these findings, a study concerning the HAMP domain suggests helical rotations of TM2 are responsible for signal transduction, refuting a piston-type movement (69,98). Sulphydryl reactivity has been used in similar

experiments to show piston-like displacements in the transmembrane helices of other chemoreceptors such as Trg furthering the usefulness of this technique as it allows usage of whole, intact cells within their native environment (88). SHKs such as NarX and TorS have also exhibited piston type movement, proven via analyses of their *apo* versus *holo* three-dimensional structures (97,100).

The piston model is able to combine with other models to explain the conformational changes in the transmembrane domain. Examples include the “swinging-piston” as explained by Hall et al and a “clutch” proposed by Ames et al (89,93). In the swinging-piston model, the signals are transferred by both a change in tilt and position of the helix, the scissor model may, therefore, be indicated in this. The “clutch” mechanism involves the rotation of two subunits relative to each other to displace TM2. The displacement here is due to a disengagement of a structural clutch at the TM2 aromatic belt to promote a kink in the helix. This results in a swivel motion to enhance HAMP domain packaging and shifting the protein to the off state. When this clutch is re-engaged, TM2 joins cable helices resulting in the destabilisation of the HAMP domain and therefore the activation of the protein thus incorporating the piston and gearbox models (89). The idea of combining models in a protein to show conformational change is supported by the idea that the piston model is evidenced at a periplasmic level, however, little evidence is provided for transmembrane movement (95). Tar transmembrane movement has been investigated via *in silico* simulations, revealing further evidence towards a piston-like model of movement. It shows how this movement can alter the conformation and dynamics of the HAMP domain, which is consistent with the dynamic bundle model of movement suggested within the HAMP domain itself. As such, the data collected provides further insight into the minutia of HAMP domain function at the atomic level (95). A recent study has added detail to the specific motion of TM2 during the proposed piston-like shift within Tar, as the helix is thought to bend during the piston motion (103). This slight bending is

thought to add to the rigidity and helicity of the control cable, located between TM2 and the HAMP domain, subsequently displacing this region also.

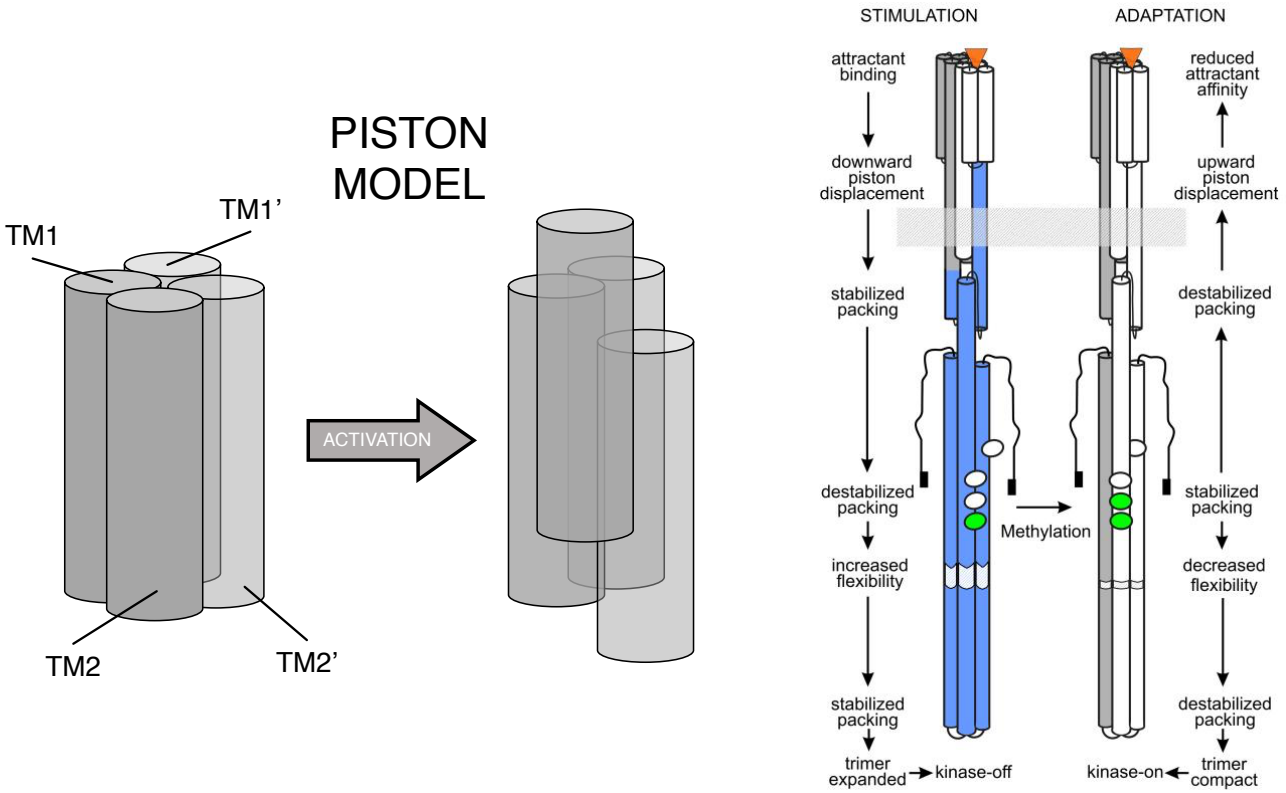

Figure 1-6: A piston model of transmembrane helix signaling. TM2 of an SHK or chemoreceptor will be vertically displaced causing initiation of signal transduction. Right is a figure taken from Hazelbaur and Lai, 2010 demonstrating how the piston movement affects the stability of domain structures downstream of the transmembrane domains within a chemoreceptor (225).

1.5.2: Scissor-type Models of Transmembrane Communication

The scissor model of transmembrane helix movement is a more recent suggestion based on the movement of TM1 in a scissor-like motion (**Figure 1-7**) (104). This model has been described in the hybrid TCS (HTCS), BT4663, which contains all the domains of a regular TCS but in a single polypeptide (105–107). Following detection of stimulus, molecular rearrangement results in the subdomains moving closer together in a scissor motion to allow trans-autophosphorylation. This scissor-like motion is seen as an increase in the tilt angle of β-TMD relative to the bilayer normal to destabilise interactions between transmembrane domains. Experiments conducted into the *Bacillus subtilus* chemoreceptor McpB concluded from crosslinking studies, with both single- and double-cysteine mutants, that piston-like motions of the transmembrane domains were unlikely. Instead, they report a rotational type movement between the on and off states between transmembrane helix 1 (TM1) and TM1' and no conformational changes across the TM2/TM2' or TM1/TM2' interfaces. Additionally, crosslinking patterns seen via double-cysteine mutants have suggested higher order signaling complexes form, such as trimers of dimers (108). A scissor model should not be absolutely ruled out as rotational movement may accompany it, therefore an expansion to their mutant library used could reveal further detail to the specific movements seen, especially if movements are more subtle than previously expected. The *Bacillus subtilis* HK DesK has shown rotational motions coupled with scissoring and tilting movements within its transmembrane helices via computational modelling simulations and X-ray structures (109,110). These motions are more complex than other HKs as DesK has 10 TMs, and the scissoring motions occur within TM1 and transmembrane helix 5 (TM5). This could suggest a scissoring motion may be more favourable in HKs with more complex TMDs.

Studies on the scissor model have also been carried out on PhoQ, a histidine kinase similar to EnvZ, which has been shown to alter structural states via diagonal scissoring of the four-helix bundle. This model was constructed based on disulphide crosslinking data using

Bayesian inference, a method of statistical inference in which Bayes' theorem is used to update the probability of a hypothesis as more evidence becomes available (111). This considers a larger range of motion including intrahelical torqueing, helix bending, or DHp domain cracking. In state 1, the periplasmic helices are in parallel configuration while in state 2, a crossing configuration is seen, consistent with scissoring. This suggests that during state 1, TM1 helices are positioned more closely displacing TM2 helices, while in state 2, the opposite is seen, allowing one pair to move toward the bundle centre accompanying the outward displacement of the other (111).

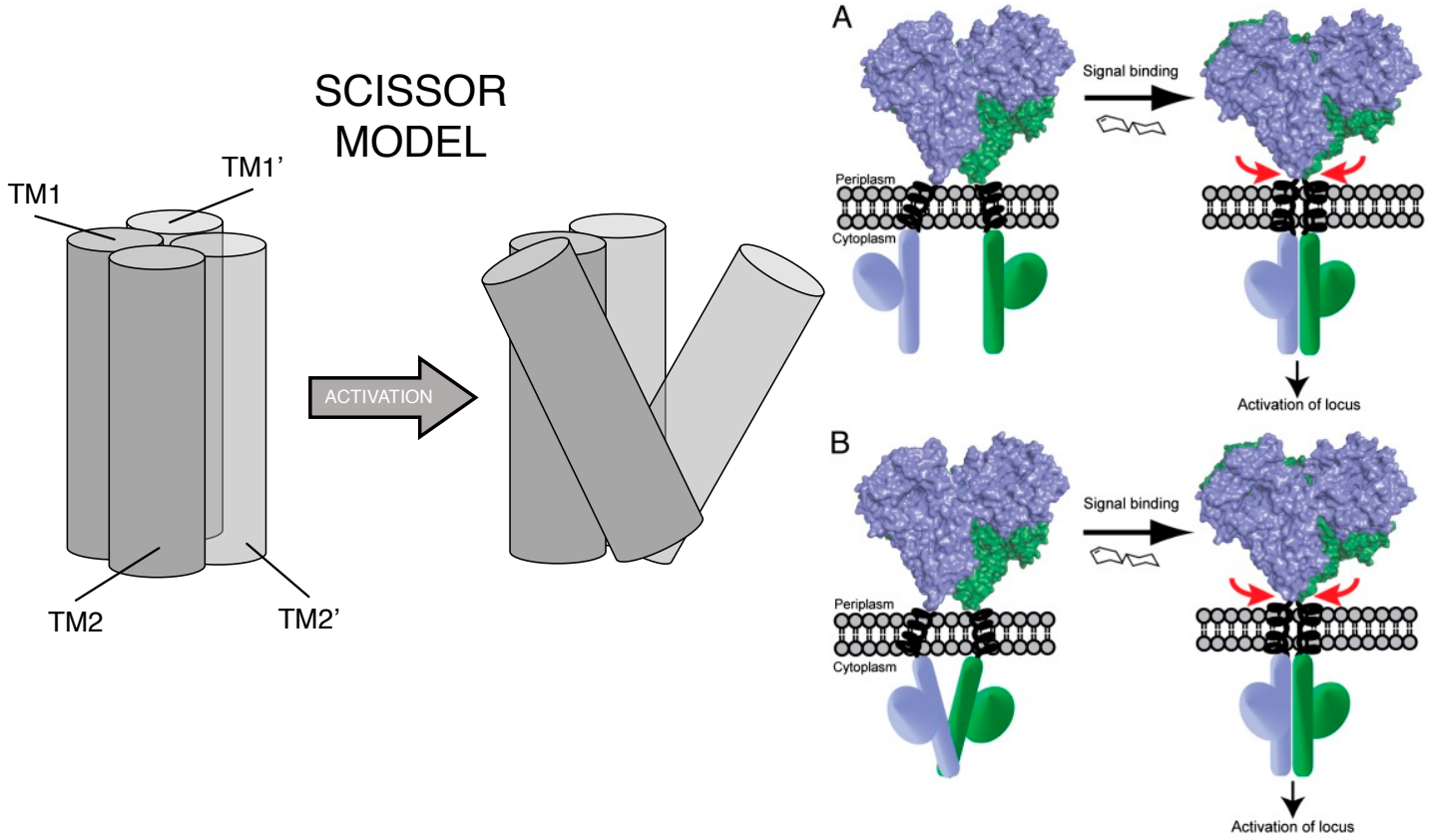

Figure 1-7: A scissor model of transmembrane helix signaling. Right is a proposed model of transmembrane movement in the hybrid two component system BT4663 following ligand binding. The C-domain termini are brought closer together by ~15Å with a movement similar to that of scissor blades. This figure has been adapted from Lowe et al, 2012 (226).

1.5.3: Gearbox Models of SHK Communication

Gearbox models in HKs (**Figure 1-8**) are seen in combination with other models, namely scissor models as previously discussed, or as an independent model of transmembrane domain signal transduction. Rotational movement of the helices upon stimulus detection can allow specific side chains to either move closer together in the central core of the TM helix bundle or move them apart. Depending on the chemical properties of these shifting side chains, the overall stability or flexibility of the helical bundle may be adapted to either promote or reduce signal transduction to cytoplasmic domains of the SHK. Crosslinking experiments have shown the TM helices of *S. aureus* HK, AgrC, to rotate anticlockwise approximately 80° following an activating stimulus and following an inhibitory stimulus, the helices rotate approximately 30° in the opposite direction (112).

1.5.4: Models of Transmembrane Communication involving the HAMP Domain

There are models of movements that concern the mechanisms of the HAMP domain alone, known as the gearbox model (**Figure 1-8**) and the dynamic bundle model (**Figure 1-9**). These models specifically describe the movements of the four-helix bundle formed by two opposite HAMP domains during dimerisation. The gearbox model also shows additional mechanisms known as knob packing in which residues slot into spaces within other residues on the interacting helix (69,87). The dynamic bundle model is more difficult to specifically define, and it is suggested as an alternative to the gearbox model.

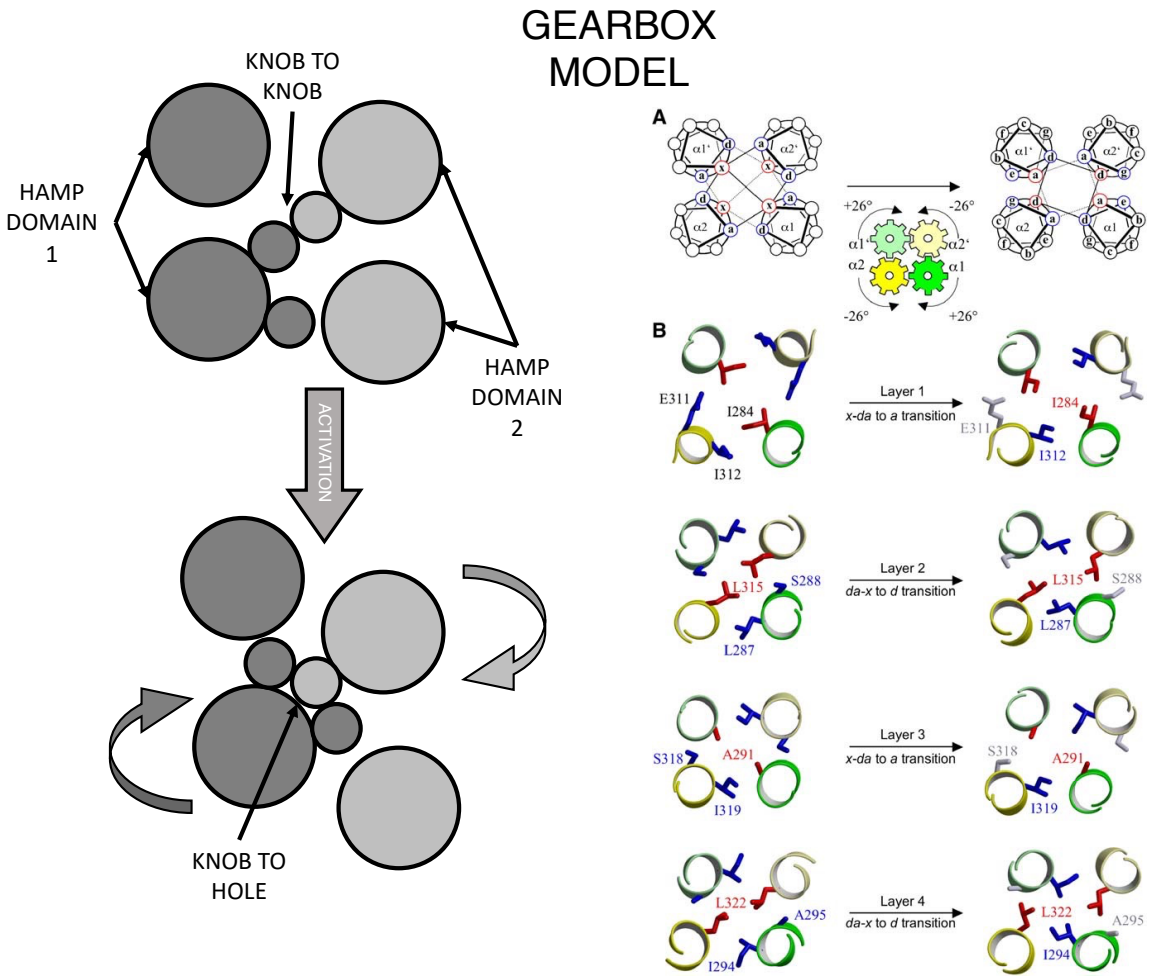

Figure 1-8: A gearbox model of HAMP domain helix signaling. Helices, depicted overhead, rotate allowing residues to align into a space (knob to hole packing) thus allowing signal transduction. Residues will also align against another residue (knob to knob packing), a conformation that will not allow signal transduction. The left side depicts the layer by layer transitions within the helices as the gear is shifted and residues move to their new positions following stimulus. This figure has been adapted from Hulko et al, 2006 (69).

1.5.4.1: The gearbox model of HAMP domain function

Generally speaking, the HAMP domain is thought to confer signals downstream based on changes in the helix rotation and bundle radius (113). The HAMP domain of EnvZ forms a parallel dimeric four-helix coiled-coil, this allows conformational changes to be seen by fusing Af1503 HAMP to the dimerization/histidine phosphorylation domain. This model then suggests that the HAMP domains reverse the direction of input helices to rotate layers in opposite directions resulting in either activation or inactivation (114). It is proposed that the incoming signal initiates a helical rotation around an axis perpendicular to the membrane (113). However, this rotation causes no change in the location of His243 suggesting this does not determine activation state. Instead activation is suggested to be via a catalytic domain HAMP recognition at the proximal end of the DHp. This is supported by the fact that when no stimulus is present, EnvZ remains in the phosphatase state with a phenylalanine bound at the cleft. Following conformational changes including axial helical rotation producing a binary switch in helical core layer and therefore a change in DHp, this cleft is then closed releasing the catalytic domain and allowing kinase activity (114).

Initially a knob-to-hole theory was put forward as the packing mechanism for the gearbox model suggesting a protruding residue on one helix would fall into a space on the neighbouring helix surrounded by side chains. In the HAMP domain experimentation however a knob-to-knob packing system is seen (69). The use of the knob-to-knob packing suggests that a more conventional packing system such as knob-to-hole may be the main HAMP signaling conformation requiring a 26˚ counter rotation (87). Further experiments found seryl and isoleucyl residues to rotate out of the core during the transition from knob-to-knob packing to knob-to-hole packing (115).

1.5.4.2: The Dynamic Bundle Model of HAMP domain function

It is increasingly recognised that signaling proteins may be dynamic in their mechanisms rather than set to a few, strict conformations (116) (**Figure 1-9**). Thus, there exists a range of HAMP domain formations based on stability; the most stable of these is the four-helix *x-da* bundle and the least stable formation would be an entirely denatured bundle (87). It is presumed that the HAMP domain has evolved to oscillate through this range of dynamic states dependent on circumstance. Both stimulus inputs and methylation of lower domains within the protein will modulate HAMP stability to either begin or end a signal response. As such, the methylation state of lower domains will directly impact on the kinase activity via effects on the dynamic state of the HAMP domain. A lower methylation state will lead to less kinase activity, perhaps due to increased HAMP dynamism compared to a higher methylation state (117–121). Mutational analyses regarding *E. coli* chemoreceptor Tsr show that the dynamic bundle agrees with conformational suppression effects more comfortably than a conventional two-state model. These movements will work in conjunction with TM2 piston type movements and the consequent adjustments to control cable dynamics, which would alter HAMP conformation and therefore stability. The *x-da* bundle and ways in which the HAMP domain changes the stability of this form is integral to the dynamic bundle model. This bundle is the most stable as it is formed of layers in which complementary side chains, within a four-helix coiled coil unit, may interact stabilising the bundle. Further work has described a biphasic dynamic bundle in Tsr, suggesting that intermediate packing of both the HAMP domains and the methylation bundle will lead to increased kinase activity. If the HAMP domain packing loosens, the methylation bundle packing will tighten followed by reduced kinase activity. If the HAMP domain packing tightens and the methylation bundle loosens then the kinase activity will also reduce. This model allows for the previously described dynamic range of packing stabilities. The two reduced kinase states each represent a different scenario; the former occurs in presence of an attractant and the latter results from severe HAMP destabilisation (122).

Figure 1-9: A dynamic bundle model of HAMP domain helix signaling. A model without a conventional 2-state design, the dynamic bundle is capable of moving into multiple states of HAMP domain helix orientation. A specific diagram is difficult to create due to the dynamic nature of this model, therefore it can be represented as an overall destabilisation. This figure has been adapted from Gushchin and Gordeliy, 2018 (167).

1.6: Model combinations

As mentioned previously, these models can combine in order to achieve successful signal transduction. For example, the piston model may use a combination of elements from other models to transmit signal across the membrane (111). Different combinations could therefore be used in different classes of receptor depending on the structure and function of the protein involved, this has been seen previously in the swinging piston model (96,111,123). The PhoQ study previously mentioned indicates that the conformational changes seen between state 1 and state 2 are too complex to be explained by the piston or gearbox model alone, as well as showing large radial displacement or toward tilt to displace the helices indicating the scissor model to have a predominant role over either of these models (87).

The HAMP region is seen to convert the known piston like movements into a conformational change, which can be seen in the kinase control region. Research carried out on chemokine receptors showed no support of the alternate bundle structure required for the gearbox model instead suggesting it functions based on the stability of the HAMP bundle (87). This is supported by the clutch model as the helical rotations seen in TM2 were not seen to elicit the signaling shifts predicted by the gearbox model suggesting the piston displacements are converted to another signaling conformation at the membrane rather than being transmitted through the HAMP domain. The rigid structure of the TM2-AS1 interaction also contradicts the scissor model as this structure would be unable to produce a signal reversal at the cytoplasmic domain of TM2 (89). The HAMP rotation in the gearbox model may coexist with the piston model in a variety of proteins by the piston-like displacement triggering the HAMP rotation to generate transmission (115). Alternatively, due to the piston-like motion of TM2 following stimulation a change in tension may be seen between AS1 and TM2 functioning as a control cable to alter the tension in HAMP without helical rotations (87,89). The piston model also allows the coexistence of the scissor model, a study involving CheA kinase utilising disulphide scanning and X-ray crystallography showed the piston displacement in TM2 while

providing evidence that the subunit interface remains static suggesting the scissor model involvement (111). This is further supported by the separation of neighbouring residues in the α1 and α2 helices, although this could also be seen in the gearbox model (124).

1.7: Models of EnvZ Transmembrane Signaling

Although these models have been investigated in an assortment of proteins, few experiments have been carried out to determine EnvZ transmembrane signaling mechanisms. However research has been undertaken in other histidine kinases such as PhoQ which is suggested to undergo activation via the scissor model with dynamic movement of both TM1 and TM2 (111). Other research into histidine kinases suggest the presence of a HAMP rotation as seen in the gearbox model controlling activation by the accessibility of the catalytic domain and the HAMP/DHp proximal end (114). Alternatively, it is suggested that the transmission at EnvZ may be due to the increased helical stabilisation upon increased osmolarity near the conserved histidyl residue (83) which is supported by the evidence that intrahelical binding follows an increase in intracellular osmolarity (68,69). This is also evidenced as the helix displays unfolding in a stretched state and increased folding in a relaxed state which then increases autophosphorylation (125).

Further research has been undertaken to map the EnvZ TM1 dimerisation surface used in dimerization and signal output, this showed the main TM1-TM1' interface to consist of residues 19, 23, 26, 30, and 34 (104). Cystyl residues were substituted into each position within TM1 resulting in altered function suggesting that the TM1 interface remains unchanged during signaling. This utilised a single cysteine (1X-Cys) mutant library with mutations in positions 11-41, this showed an increase in signaling but no change in the TM1-TM1' interface. The data suggested that the TM1 domains crossed at an angle which resulted in the TM helices becoming more distal from the membrane core suggesting a scissor-like conformation

(104). A follow up study was then completed, this is as yet unpublished, to investigate the conformational changes elicited at the TM2-TM2' interface using the same methods.

1.8: A closer look at disulphide crosslinking studies

Disulphide crosslinking has been utilised for many years to map relative distances between residues within dimers. Its key advantage over methods with similar ends but different means, is the ability to perform it *in vivo* thereby providing us with more convincing snapshots of true biochemical and biophysical processes within a cell. For the disulphide crosslink to form, they must fall within a certain distance and this will only occur under oxidising conditions. Therefore, these adducts will not occur naturally as the cytosol and nuclear environments are reducing allowing event to be controlled by adding an oxidising agent (126,127).

A cysteine replaces strategically chosen residues throughout TM1 and TM2 within EnvZ and any pre-existing cysteines are removed. Provided WT function of the protein is retained with its WT cysteine substituted, experiments involving the substitution of other residues within EnvZ for a cysteine may proceed as any alteration in signal output can then be attributed to this further mutation not the loss of the sole pre-existing cystyl residue at position 277. This residue is removed for cysteine mutants to remove any opportunity of a dimer forming via this position. The aim of a cysteine substitution is to identify parts of the protein that come into close proximity, parts that are far apart and anything in between. This is because the degree to which the mutant crosslinks will indicate an approximate distance between the mutated residues (128). For example, if two mutant cystyl residues, each from a separate monomer in the dimer structure, come as close together as possible, within a few angstroms, they will almost certainly form a disulphide crosslink within an oxidative environment (**Figure 1-10**). The cells containing crosslinked proteins will then be prepared for sodium dodecyl sulphate-polyacrylamide gel electrophoresis (SDS-PAGE) and Western blotting, as described in **Section 2.5**. The closer the residue, the more likely a crosslinking will

occur and therefore a larger percentage of the cell population will contain crosslinked dimers. These dimers will migrate through a polyacrylamide gel more slowly than a non-crosslinked monomer and the intensity of both bands (monomer and dimer) observed after Western blotting will indicate the degree to which the protein was able to crosslink. Therefore, a dimer/monomer (D/M) ratio is calculated to represent the proportion of dimer formation with a disulphide linkage to monomers that have not achieved that linkage. If a higher number of proteins form a dimer, the upper band will appear darker than the lower band and the ratio will be greater than 1. If the bands are of a similar intensity, the ratio will be close to 1 and if the lower band is more intense than the upper band, the ratio will be less than 1. If an upper band is not detectable but a lower band is present, the ratio is recorded as monomer only and quantified as 0. This quantification is useful across different samples of the same mutation as the data effectively normalises itself because it is a ratio. As the protein expression can only be controlled to a certain degree, cases may occur in which two different cell samples of the same mutation may have a ten-fold difference in protein expression. The two separate samples of the same mutant strain may have a significant difference in overall intensity but as long as the ratio is the same for each, for example if two equally intense bands were produced as well as two equally weak bands, then the ratio would be roughly 1 for both. (**Figure 1-11**). Crosslinking efficiency is dependent on a number of biophysical factors including the relative orientations of the cystyl residue side chains, their availability to oxidants, and the dynamics of the actual sulphydryl group that will be involved in the disulphide crosslink (111,129–131).

The next step to gaining insight into specific protein movements is to analyse the differing D/M ratio outcomes under varying conditions. In the case of the following experiments involving the EnvZ/OmpR TCS, the cells are grown under two different osmolarity conditions termed **low osmolarity** (0% sucrose in minimal media A (MMA) – EnvZ signal **off**) and **high osmolarity** (15% sucrose in MMA – EnvZ signal **on**). The MMA itself contains no sucrose therefore the osmolarity of the media may be stated as low if no sucrose is added. It is

hypothesised that the transmembrane domains (TM1 and TM2) shift positions from the off state to the on state. Any changes in disulphide crosslinking results between these two growth conditions will indicate that these shifts have occurred. The patterns created by these changes can be used to map the protein interface in the dimeric structure.

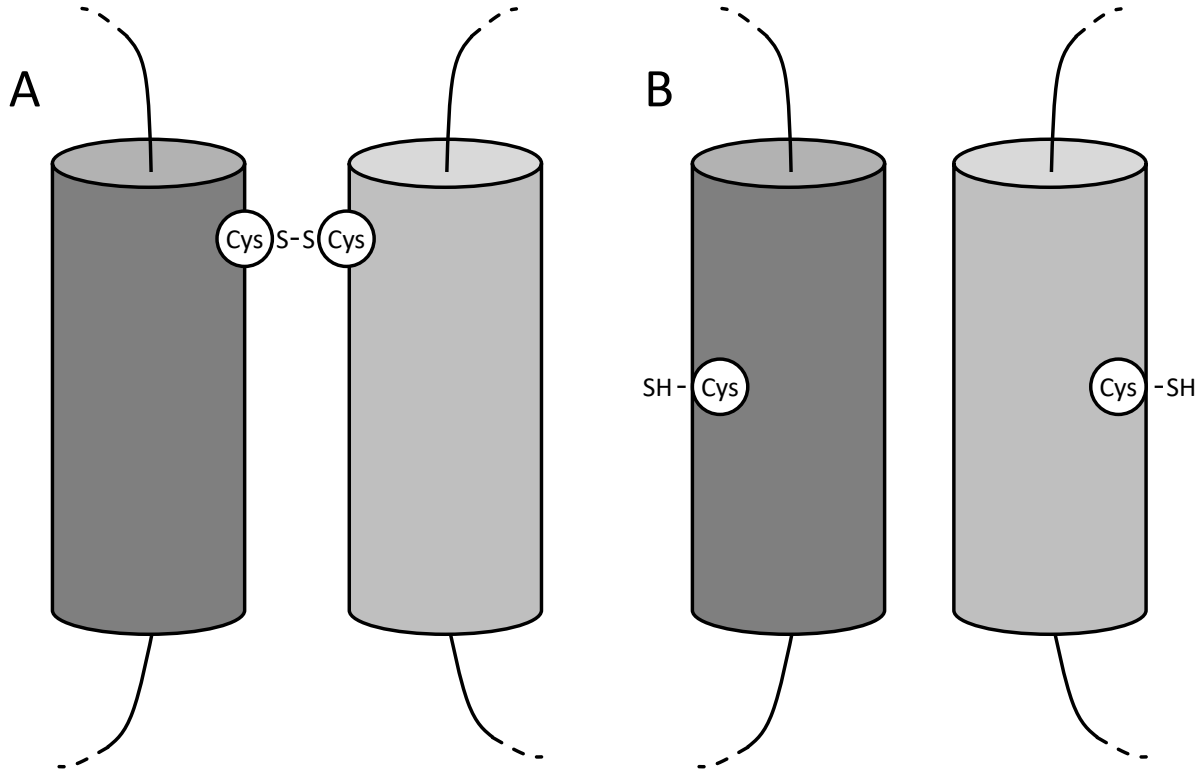

Figure 1-10: Cysteine residues form disulphide linkages based on proximity. (A) Cysteine residues substituted into positions within the TM helices that are close during the dimer formation will form a disulphide linkage. (B) Cysteine residues substituted into positions within the TM helices that are not close during the dimer formation will not form a disulphide linkage. Cylinders represent a TM helix each from a separate EnvZ protein within a homodimer.

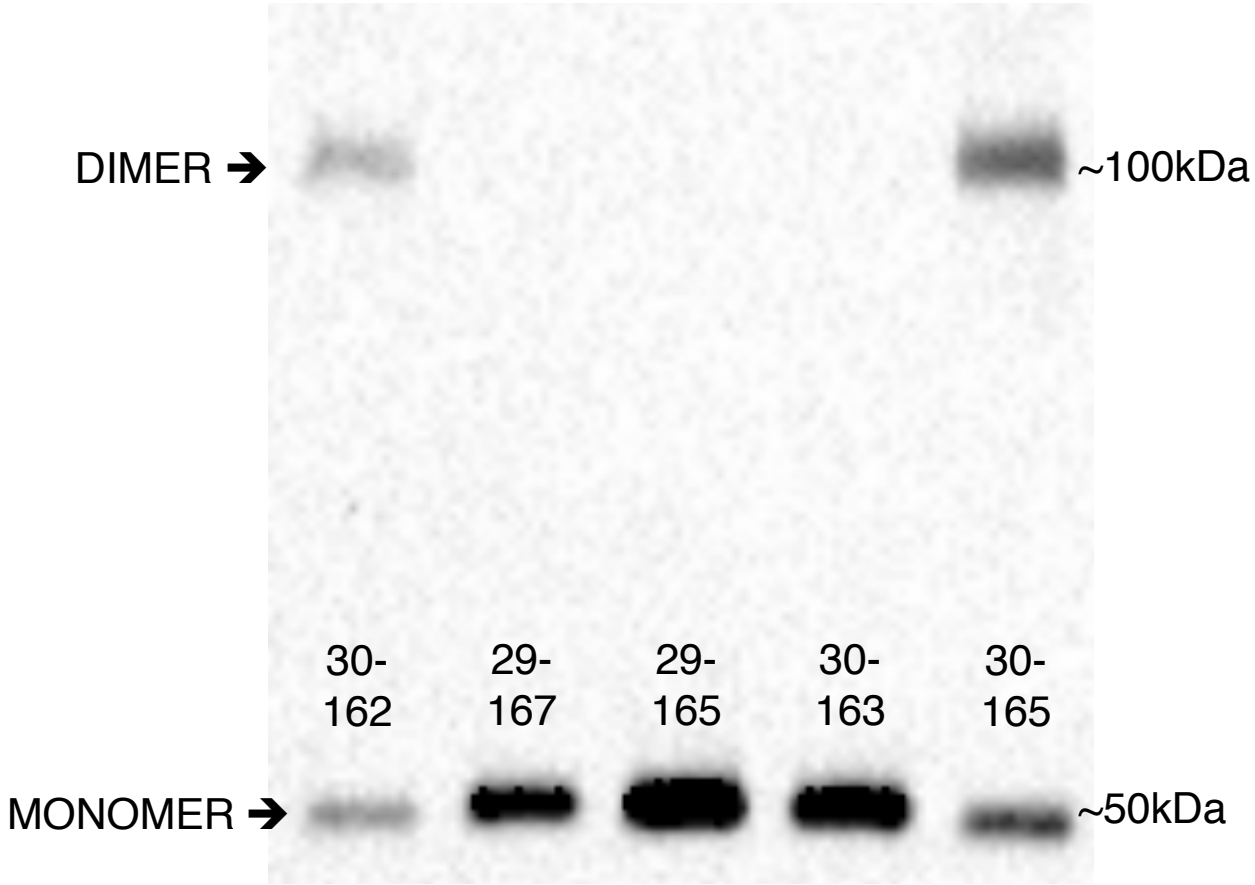

Figure 1-11: A demonstration of different band intensities for immunoblotting with cysteine mutants. Five different double-cysteine-containing mutants are shown to demonstrate the potential outcomes. The 30-162 mutant in the far-left lane displays dimer (upper) and monomer (lower) bands of similarly weak intensity. As the intensities are similar, the dimer/monomer (D/M) ratio will be close to one following quantification. The 30-165 mutant in the far-right lane displays dimer and monomer bands of increased overall intensity. However, the dimer band is slightly less intense than the monomer band and the D/M ratio will therefore be below one following quantification. The three mutants (29-167, 29-165 and 30-63) in the middle lanes display intense monomer bands only. This is a clear indication that the mutated positions do not come into close proximity with each other during dimer formation under these conditions.

1.9: Signal output measurements via fluorescence

Through gene fusions of cyan fluorescent protein (CFP) and yellow fluorescent protein (YFP) to the protein outputs of EnvZ function, OmpC and OmpF, signal output can be quantified as described in **Section 2.4**. These gene fusions were included within the strains used as described in **Section 2.1**. As EnvZ is activated by various stimuli (**Figure 1-12A**), the balance of *ompC* to *ompF* expression shifts and the quantified CFP and YFP values that are recorded will demonstrate these shifts (**Figure 1-12B**). A CFP/YFP (C/Y) ratio may be calculated from these values, which assists the comparison of repeats within mutant groups. For example, one repeat of mutant 15-177 may produce a CFP value of 500 and a YFP value of 100 giving a ratio of 5. A second repeat of the same mutant may produce a CFP value of 1000 and a YFP value of 200, which would give the same ratio of 5 and therefore the same relationship may be inferred despite the significant increase in signal output overall for the second repeat. This is important as while the expression of the EnvZ protein can be controlled to some extent via the concentration of the transcription triggering element, certain mutants will ultimately prove to be idiosyncratic in their expression magnitude. However, as long as the CFP/YFP ratio and by extension their OmpC to OmpF relationship remains the same, the repeats can be trusted.

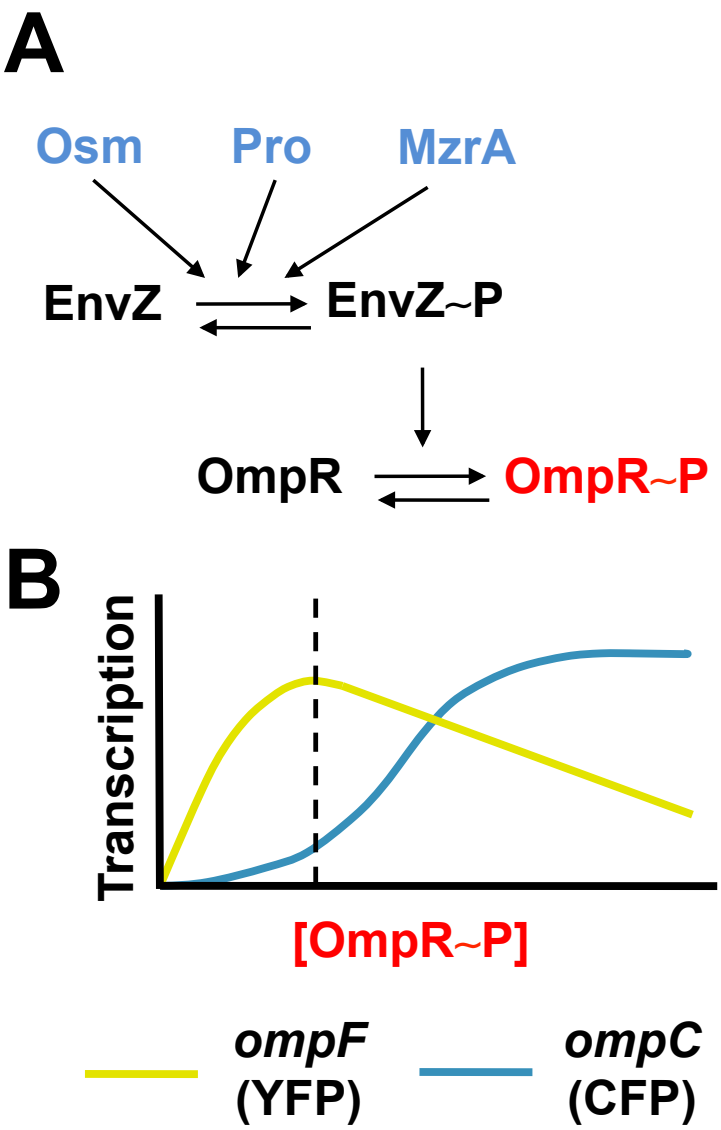

Figure 1-12: The EnvZ/OmpR signal output relationship. (A) EnvZ is bifunctional and possesses both kinase and phosphatase activity. The ratio of these activities is modulated by presence of extracellular osmolarity (51,227), procaine (228) or MzrA(79)(80). OmpR serves as the cognate response regulator (RR) of EnvZ and thus the intracellular level of phosphorylated OmpR (OmpR-P) is governed by EnvZ activity. (B) OmpR-P levels control transcription of *ompF* and *ompC*, which can be monitored by employing MDG147 (4) or EPB30 (2) cells that contain a transcriptional fusion of *yfp* to *ompF* (yellow) and of *cfp* to *ompC* Figure (blue). This allows the intracellular levels of OmpR-P (red) to be estimated by monitoring the CFP/YFP ratio. The dashed line represents the baseline level of OmpR-P from EPB30/pRD400 cells expressing WT EnvZ grown under the low-osmolarity regime (0% sucrose).

1.10: Double cysteine capabilities

By creating a mutant library of EnvZ in which two positions in both TM1 and TM2 are substituted for cysteines, the depth of results collected from both crosslinking and signal output experiments can be significantly increased. The methods, described in **Chapter 3**, will be optimised and modified to accommodate for slight changes in properties and desired outcomes of a double cysteine mutant crosslinking study. The cystyl (Cys) residues are carefully paired so that each mutant contains a Cys-substitution within each transmembrane domain, and these substitutions will be approximately aligned to each other (**Figure 1-13**). Two cysteines in a single monomer (one in each TM helix) will provide opportunity for three different crosslinking events to occur during dimerisation, as opposed to the one crosslinking event that may occur with a single cysteine mutant. These crosslinking events may connect TM1-TM1' (green), TM2-TM2' (blue) or TM1-TM2' (red) (**Figure 1-14**). A 2X-Cys mutant is not only capable of each of these crosslinks, it is also capable of crosslinking at more than one of these positions at once. The previously described SDS-PAGE and Western blotting experiment, described in **Section 2.5**, has been adapted for this library and its results remain central to the project. Each crosslinked dimer of a different formation will migrate through the acrylamide gel to a distinctly different distance. Therefore, we can identify the band by this distance especially in comparison to other known bands that are run directly adjacent to it. The bands will be quantified, and a ratio will be calculated but, with a multiple band sample several ratios will need to be calculated to identify specific dimer band quantities. As multiple interactions can occur for a single mutant, ways in which residues position themselves in a three-dimensional space can be deduced. This is a significant advantage over a 1X-Cys mutant, which is only capable of a more two-dimensional look at the dimer interface.

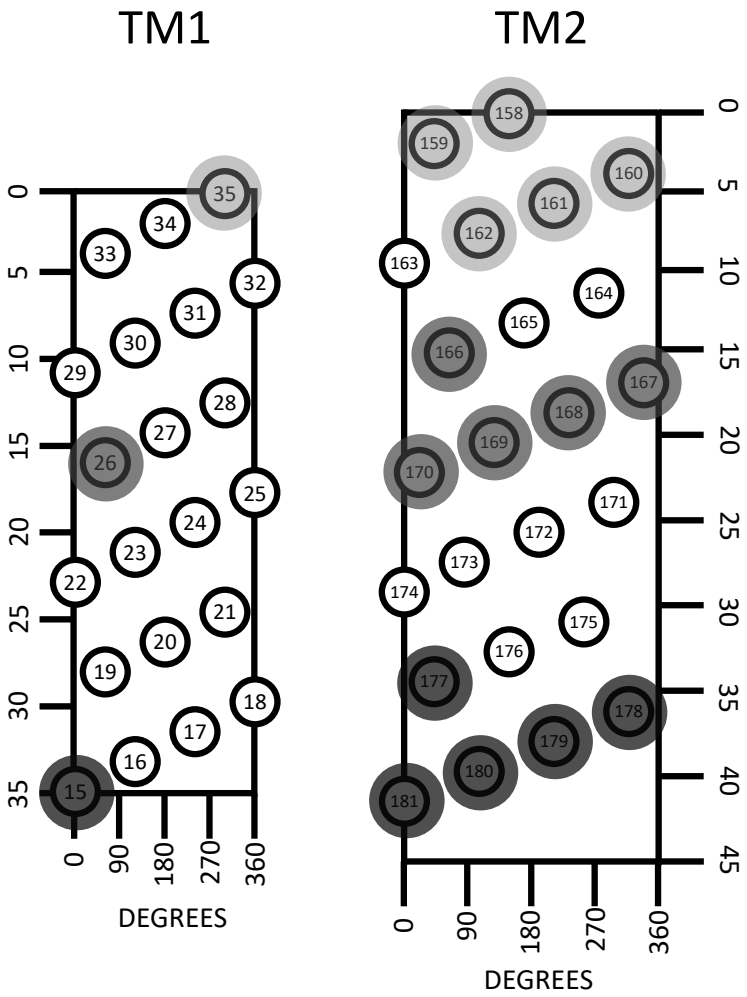

Figure 1-13: Demonstration of 2X-Cys mutant pairing logic. Pairing was designated based on the proximity of the TM1 (left) position to its TM2 (right) pairings. A TM1 residue position located in the periplasmic extremity of the TM1 helix (35) will be paired with the five residues located in the periplasmic extremity of the TM2 helix (158-162). The bracket of five TM2 residues will be shifted up one place as the TM1 residue shifts down one place, for example 34 is paired with 159-163.

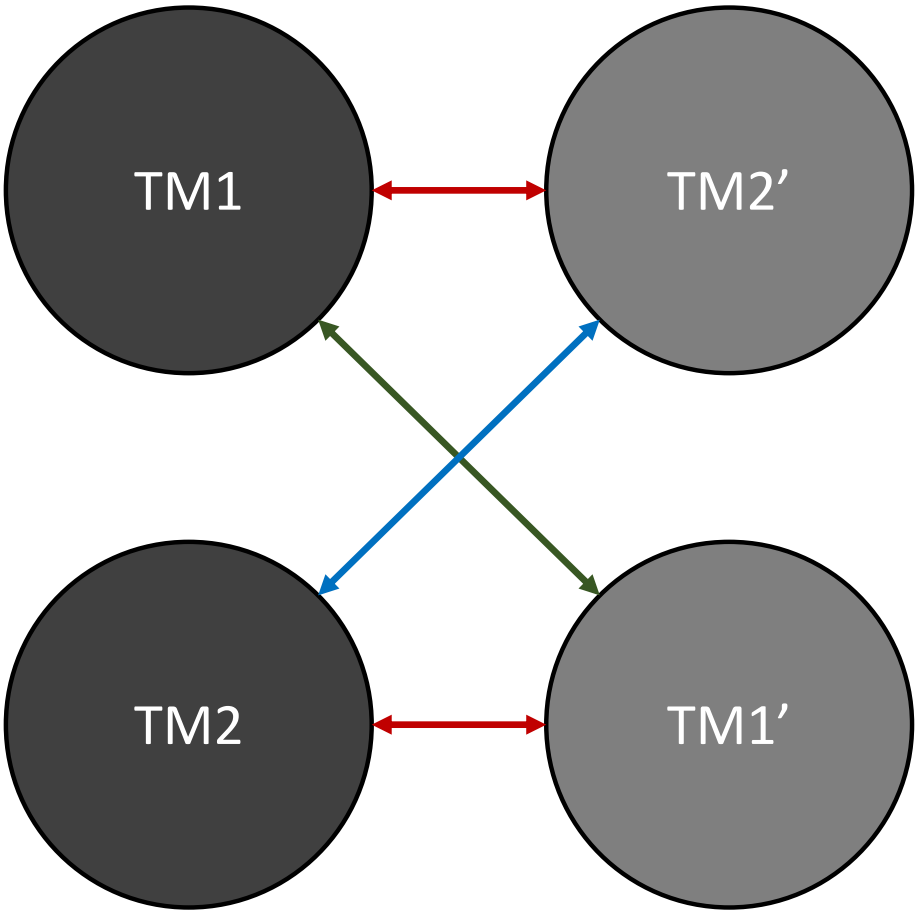

Figure 1-14: Head-on view of potential TM interactions. The TM four-helix bundle can interact in three distinct ways including TM1-TM1’ (green arrow), TM2-TM2’ (blue arrow) and TM1-TM2’ (red arrows) interactions.

1.11: Summary

Despite the multiple models of transmembrane signaling it is still unclear how the signal is transmitted across the membrane via EnvZ, yet the evidence provided suggests a combination of models that could be involved. Future work must identify the key interactions of the transmembrane domains during activation of EnvZ and identify structural differences between the active and inactive structure. If this mechanism was known, artificial activation of the protein may be possible to modulate porin expression and by extension permeability in antibiotic resistant bacteria. Although research has been undertaken to understand both the TM1 and TM2 interfaces individually it is important to achieve complete understanding of the transmembrane interactions including the conformational changes seen between TM1-TM2' interfaces during as this may be critical in understanding the full mechanism of transduction during trans-autophosphorylation (42). Further to this, the knowledge surrounding the transmembrane helices of EnvZ is generally lacking an up-to-date definition regarding not only its function but also its structure (131). Difficulties in elucidating the latter of these properties are apparent – NMR and *in silico* studies are notoriously difficult to complete with protein domains contained within the membrane. However, the nature of the proposed experiments should, in theory, reveal both structural and functional information on these helices. This research could be completed in a similar way to that carried out to investigate TM1-TM1' interactions by using a double cysteine mutant which instead contains one mutation in each transmembrane domain (104). Models attached to similar protein systems, such as the previously described piston and scissor models, should display clear patterns within a disulphide mapping study. These predicted patterns and whether they are seen or not will form the basis of the overall hypothesis presented within this thesis.

1.12: Hypotheses

The transmembrane helices within EnvZ do not exhibit a piston-type movement during signal transduction as described in **Figure 1-6**. Specifically, the presence and intensity of dimer bands would be different between the two signaling states (**Figure 1-15**). If a simple piston was observed, this should occur along the entire interacting surface within the TM domain. If there are some areas that alter dimer band intensity, either increasing or decreasing the dimer:monomer ratio, alternate possibilities should be suggested.

Formation of TM dimers would be lesser or non-existent in one state when compared to the other. This should occur throughout the entire interaction surface if one of the helices is suggested to partially move out of the membrane in a piston type motion. If there are some areas that alter the relative preponderance between substituted Cys residues between states and some that do not, an alternate model should be suggested.

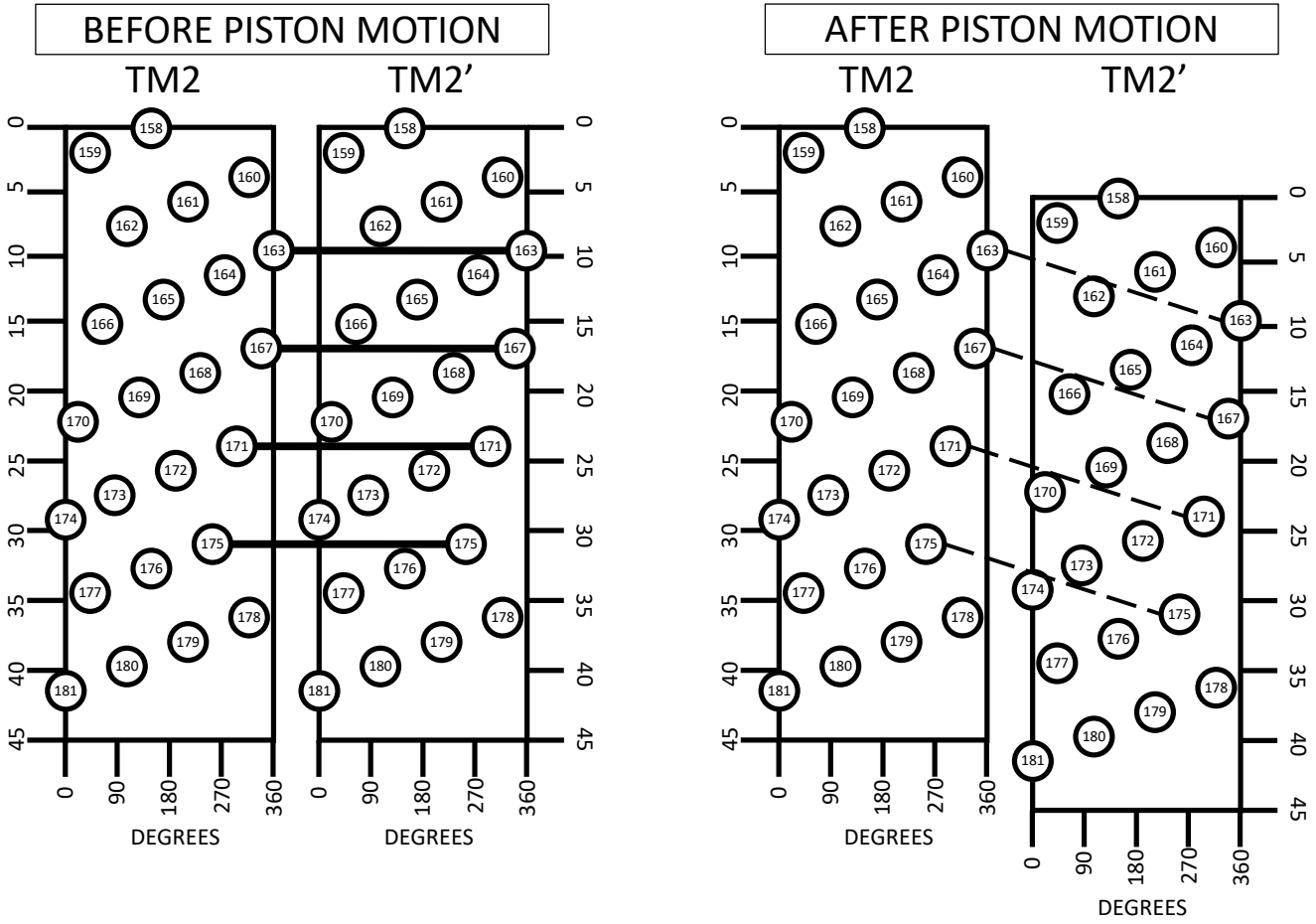

Figure 1-15: Demonstration of a hypothetical piston shift effect on crosslinking. The hypothetical piston shift shown here shows four TM2-TM2' interactions between positions 163, 167, 171 and 175 in TM2 of EnvZ. If a piston shift was present, shown left, the interactions between these residues would become weaker, depicted as a bold uninterrupted line (strong interaction) versus a thin, dashed line (weak interaction). These changes would be shown via a reduction or absence of TM2-TM2' dimer formation.

1.13: Aims

1. To identify areas within the transmembrane helices of EnvZ that have increased, decreased or unchanged signal output depending on the positioning of cysteine substitutions based on their OmpC/OmpF signal output profile via a dual-colour fluorescence assay.
2. To propose a model of movement for the transmembrane helices within an EnvZ-EnvZ' homodimer during stimulus-perception based on a disulphide-mapping study.

1.14: Objectives

Single-cysteine Analyses of the EnvZ Transmembrane Helices

1. Construct a functional library of single-cysteine-containing EnvZ receptors through TM1 and TM2 via site-directed mutagenesis
2. Map TM1-TM1' and TM2-TM2' interaction surfaces with and without the presence of stimulus to identify a pattern of movement.
3. Identify positions within TM1 and TM2 that differ to WT EnvZ signal output, dependent on their Cys substitutions.

Double-cysteine Analyses of the EnvZ Transmembrane Helices

1. Construct a functional library of double-cysteine-containing EnvZ receptors (one Cys in TM2 and one Cys in TM2) via site-directed mutagenesis
2. Map TM1-TM2' interaction surfaces with and without the presence of stimulus to identify a pattern of movement.
3. Identify positions within TM1 and TM2 that are not tolerant of Cys substitutions when compared to WT EnvZ signal output.

Chapter 2: Materials and Methods

2.1 Bacterial strains

E. coli strains DH10B (New England Biolabs) or MC1061 (gifted) (3) were used for DNA manipulations, while strain K-12 MG1655 (publicly accessible) (133) served as a non-fluorescent strain that was used to control for light scattering and cellular autofluorescence. Both YFP and CFP values were calculated for this non-fluorescent strain under both low osmolarity (MMA + 0% Sucrose) and high osmolarity (MMA + 15% Sucrose) media. These values represented fluorescence that could be attributed to sources that were not representative of the production of CFP or YFP. Therefore, these values were subtracted from the true CFP and YFP values collected for each mutant. *E. coli* strains MDG147 [MG1655 Φ(*ompF*$^{+}$-*yfp*$^{+}$) Φ(*ompC*$^{+}$-*cfp*$^{+}$)] (1) and EPB30 (MDG147 *envZ::kan*) (2) were employed for analysis of EnvZ signal output. The MDG147 strain is fluorescent but also retains envZ within its chromosomal DNA. EPB30 is a fluorescent strain without envZ within its chromosome thus the EnvZ coded within its plasmid is the sole version of this protein that will be expressed. As the C-terminus of bacterial receptors can be sensitive to the presence of an epitope tag, it was previously ensured that the addition of a V5-epitope tag did not alter the signaling properties of EnvZ (6,134). Plasmid pEB5 was employed as an empty control vector (4). Plasmid pRD400 (6) retains the isopropyl β-D-thiogalactopyranoside (IPTG)-based induction of EnvZ from plasmid pEnvZ (5) while adding a seven-residue linker (GGSSAAG) (135) and a C-terminal V5 epitope tag (GKPIPNPLLGLDST) (136). IPTG is a molecular mimic of allolactose that triggers transcription of the *lac* operon, subsequently allowing transcription of the plasmid envZ gene which is under control of a *lac* operator. A library of 1X-Cys containing mutants was previously created by Anika Heininger (104,137) – these mutants were created via site directed mutagenesis and used for all 1X-Cys experiments as well as the creation of the 2X-Cys-containing EnvZ library. A library of 2X-Cys-containing EnvZ receptors were created by standard molecular cloning methodologies from the individual 1X-Cys containing TM1 (104)

and TM2 (137) libraries. Mutant strains were grown overnight in 5mL Lysogeny broth (LB) media with Ampicillin (Amp) (10g Sodium Chloride, 10g Tryptone, 5g Yeast extract, dH_2O to 1L, 100μL Amp^{100}) at 37°C and 200rpm. Plasmid DNA was extracted using a Qiagen miniprep kit. A double restriction enzyme (Sal-I and Bgl-II) cut of two plasmids at 37°C was performed, one containing a TM1 mutation and the other containing a TM2 mutation. The cut DNA fragments were separated via agarose gel electrophoresis using a 0.8% agarose gel for 45 minutes (70V for first 15 minutes, 120V for remaining 30 minutes). The appropriate sections of DNA, 3μl TM1 band and 9μl TM2 band, were ligated with T4 DNA ligase and its appropriate buffer to form a novel plasmid with an assumed double-cysteine mutation of EnvZ. This plasmid is transformed into a DH10B strain, grown on LB Amp agar plates (15g agar, 10g Sodium Chloride, 10g Tryptone, 5g Yeast extract, dH_2O to 1L, 100μL Amp^{100})overnight at 37°C then a single colony was transferred into LB Amp media and grown overnight at 37°C, 200rpm. The plasmid DNA was extracted using the Qiagen miniprep kit and sent to Eurofins for sequencing. The sequence data received is checked against WT EnvZ sequence using the Serial Cloner software. If a correct sequence is detected, plasmid DNA taken from the same source of that which was sequenced is transformed into the EPB30 strain for experimental use. Plasmid DNA was mixed with competent EPB30 cells on ice for one hour followed by a 45 second heat shock (42°C) and then 2 minutes on ice. The cells are then transferred to 500μL LB Amp media and incubated for 1 hour at 37°C, 200rpm. The cells are centrifuged for 5 minutes at 3000rpm and approximately 90% of the supernatant is removed. The remaining 10% of supernatant was used to resuspend the pellet and transferred to an LB Agar plate upon which they were spread using a sterile spreader. Plates were incubated overnight at 37°C then a single colony was transferred to 500μL LB Amp media and stored in a cryovial at -80°C. In order to maximise potential TM1-TM2' crosslinking, Cys residue pairs were selected by identifying TM1 residues participating in helix formation (15 through 35) and

pairing each with five potential TM2 partners ranging from 158 through 181, based on putative proximity position within the membrane (**Figure 1-13**).

2.2. Creation of a cysteine-less EnvZ

WT EnvZ from *E. coli* contains a single Cys residue at position 277 (**Figure 2-1**). Pre-existing Cys residues would make it significantly more difficult to interpret the results of *in vivo* disulphide-mapping experimentation, therefore, a cysteine-less (Cys-less) version of EnvZ was created. The native Cys-277 codon was converted to a methionine (Met) (C277M) because a previous sequence analysis determined that a Met residue was the second most common, after Cys, at position 277 within EnvZ proteins from other organisms (138). A serine (Ser) residue was also chosen (C277S) because it was shown to not affect the biochemical activities of the purified cytoplasmic domain from *E. coli* ($EnvZ_c$) (139). Finally, as a small non-polar residue, an Alanyl (Ala) residue (C277A) was also selected for analysis. All substitutions were made using standard site-directed mutagenesis techniques (Stratagene protocol). The PCR mixture (Template DNA 1μL, 10X Buffer 5μL, Forward primer(0.1 μg/μL) 1μL, Reverse primer(0.1 μg/μL) 1μL, dNTPs (10mM) 1μL, Pfu turbo 1μL, dH_20 40μL) was run through the following programme 1)95°C for 1 minute, 2) 95°C for 50 seconds, 60°C for 50 seconds, 68°C for 1 minute/kb of plasmid length (step is repeated 17 times or a total of 18 cycles, 3) 68°C for 7 minutes, 4) 4°C hold. Following the PCR protocol, 1μL DpnI is added to the reaction mixture and incubated at 37°C for 1-2 hours to digest parental DNA. 5μL of the reaction mixture was run adjacent to undigested parental DNA to ensure a difference in band pattern.They were expressed from pRD400 (6), which results in the addition of a seven-residue linker (GGSSAAG) and a C-terminal V5 epitope (GKPIPNPLLGLDST) that have previously been used within bacterial receptors, including Tar and EnvZ, resulting in minimal effect to steady-state signal output (6,90,98,99,134,135,140,141).

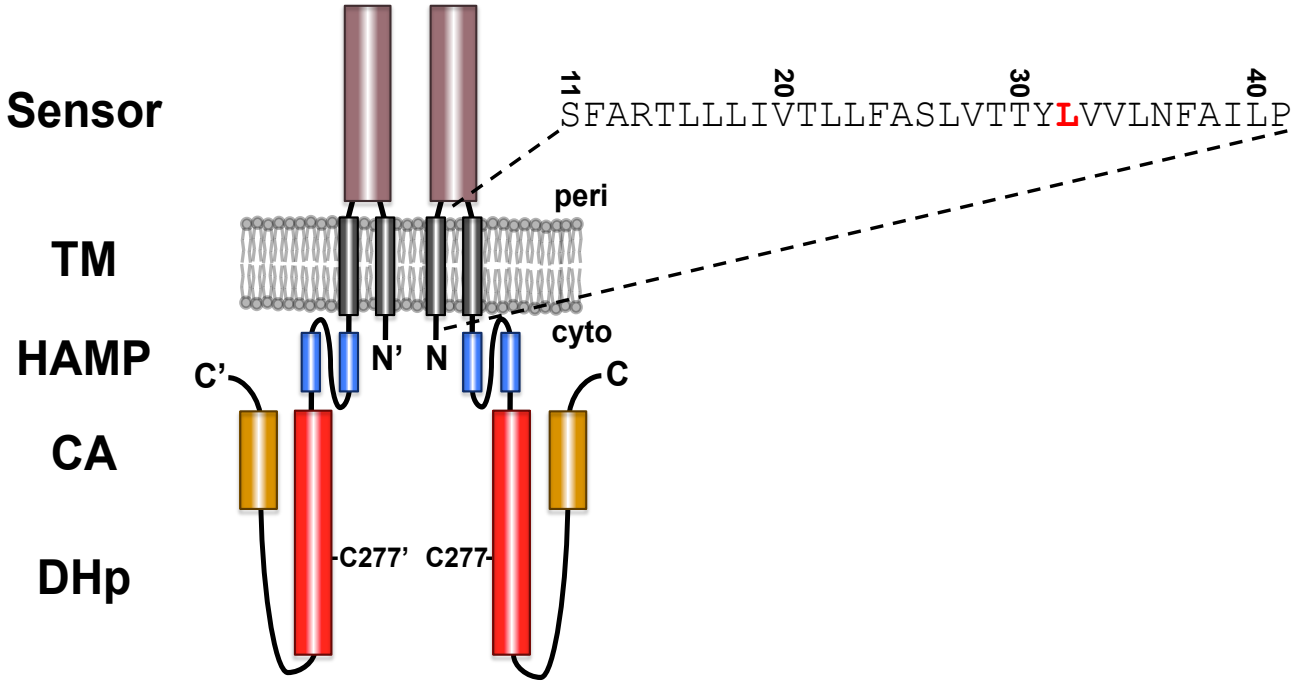

Figure 2-1: EnvZ structure highlighting TM1. EnvZ functions as a homodimer with a cytoplasmic N-terminus, the TM1(grey, proximal to the N-terminus), a large PD (brown), TM2 (grey, proximal to the C-terminus), a membrane-adjacent HAMP domain (blue) and the DHp, (red) and CA activity (orange). The residues subjected to Cys substitution are highlighted. Leu-32, indicated in red, could not be substituted for a Cys residue. In addition, the location of the original Cys residue at position 277 is provided.

2.3: Selection of residues comprising TM1 and TM2 in EnvZ

The primary sequence of EnvZ (NP_417863.1) from *Escherichia coli* K-12 MG1655 was subjected to a full protein scan with DGpred using a minimal window of nine residues and a maximal window of 40 residues (142). This software searched for putative TM helices by employing a sliding window of variable lengths and calculating the ΔG_{app} for transmembrane insertion throughout the length of the sequence and suggested that residues between Phe-12 and Val-34 comprise TM1. Alternatively, a software package that identifies TM helices with a Markov model (TMHMM v2.0) (143) was employed and suggested that the residues between Thr-15 and Phe-37 compose TM1. In both cases, a motif commonly found within TM helices that consisted of positively charged residues and adjacent aromatic resides bracketing a core of aliphatic residues was found within the putative TM segments (144). It was also established that there are no WT Cys residues within or close to the TM regions. The sole WT Cys residue within EnvZ is found at position 277 and removed for cysteine mutants as previously described. The same software packages also suggested that Leu-160 to Ile-181 and Leu-160 to Ile-179 comprise TM2 respectively. Based on these observations, and to maximise the probability of including all residues within either TM1 or TM2, all residues between positions 11 to 41 and 156 to 184 respectively were targeted for the creation of a library of single-Cys-containing EnvZ receptors.

2.4: Analysis of EnvZ/OmpR signal output *in vivo*

Bacterial cultures were grown as described previously (6) with minor modification. MDG147 or EPB30 cells were transformed with pRD400 expressing one of the single-Cys-containing EnvZ receptors or pEB5 (empty). Fresh colonies were used to inoculate 2-ml overnight cultures of Minimal Media A (MMA) (145) supplemented with 0.2% glucose. 5X MMA was first made (5g Ammonium sulphate, 22.5g Potassium phosphate monobasic, 52.5g Potassium phosphate dibasic, 2.5g Sodium citrate tribasic, dH_2O to 1L) which was then used to make 1X

MMA (200mL 5X MMA, 1mL 1M Magnesium sulphate, 10mL 20% glucose, 0.5mL Amp^{100}, 50μL IPTG, 500mL 30% Sucrose (if high osmolarity media is required, replace with dH_2O if low osmolarity media is required), dH_2O to 1L, vacuum filtered). Cells were grown overnight at 37°C and diluted at least 1:1000 into 7 ml of fresh medium. Upon reaching an $OD_{600nm} \approx 0.3$, chloramphenicol was added to a final concentration of 170 μg/ml to stop cell growth and protein production. Fluorescent analysis was immediately conducted with 2 ml of culture and a Varian Cary Eclipse (Palo Alto, CA). CFP fluorescence, indicating ompC transcription, was measured using an excitation wavelength of 434 nm and an emission wavelength of 477 nm, while YFP fluorescence, indicating ompF transcription, was measured using an excitation wavelength of 505 nm and an emission wavelength of 527 nm. These values were corrected for cell density and for light scattering/cellular autofluorescence by subtracting the CFP and YFP fluorescence intensities determined for MG1655/pEB5 cells.

2.5: Analysis of EnvZ sulphydryl reactivity *in vivo*

Cells were grown as described above with minor changes. Upon reaching an optical density $(OD)_{600nm} \sim 0.3$, cells were subjected to 250 μM molecular iodine in ethanol for 10 min while incubating at 37 °C in order to create an oxidising environment needed for the crosslinking event to occur between Cys residues. The parameters for iodine concentration and exposure time were determined via a series of experiments changing these variables in order to produce the most reliable bands for Western blotting. The reaction was terminated with 8 mM *N*-ethylmaleimide (NEM) and 10 mM ethylenediaminetetraacetic acid (EDTA). Cells were harvested by centrifugation and resuspended in standard 6X non-reducing SDS-PAGE buffer (0.4mL 0.5M Tris HCl, 1.25mL 10% SDS, 10mL Sodium phosphate buffer, 250μL 0.5M EDTA, 1.25g sucrose, 2.5μg bromophenol blue, 0.25mL 0.5M NEM, water to 10mL). Cell pellets were analysed on 10% (1X-Cys mutants) and 7% (2X-Cys mutants) SDS/acrylamide gels (Separating gel (makes 2 gels): 6mL (10%)/7.5mL (7%) dH_2O, 5mL (10%)/3.5mL (7%) 30%

acrylamide, 3.75mL 1.5M Tris HCl, 150μL 10% SDS, 25μL TEMED, 37.5μL 20% Ammonium persulphate. Stacking gel (makes 4 gels): 3.05mL dH_2O, 0.65mL 30% acrylamide, 1.25mL 0.5M Tris HCl, 50μL 20% SDS, 25μL TEMED, 12.5μL 20% APS). Gels were run in 1X SDS PAGE running buffer (10X SDS PAGE running buffer: 30.3g Tris base, 144g glycine, 10g SDS. 1X SDS PAGE running buffer: 100mL 10X SDS PAGE running buffer, dH_2O to 1L) for 15 minutes at 70V and 60 minutes at 120V. Filter paper and nitrocellulose membranes were soaked in 1X SDS PAGE semidry transfer buffer (10X SDS PAGE semidry transfer buffer: 58.2g Tris base, 29.3 glycine, 3.75g SDS, dH_2O to 1L. 1X SDS PAGE semidry transfer buffer: 100mL 10X SDS PAGE semidry transfer buffer, 200mL Methanol, dH_2O to 1L). The gel was removed from the SDS PAGE tank and soaked in 1X SDS PAGE semidry transfer buffer on a shaking platform at 30rpm for 30 minutes. A sandwich consisting of two filters, one nitrocellulose membrane, one gel (with stacking gel removed) and two filters (in this order bottom to top) was placed in a semidry transfer chamber and run for 30 minutes at 15V. The filters and gel were discarded and the membrane is inserted into a 50mL falcon tube containing 10mL blocking solution (10X Tris Buffered Saline (TBS): 12.1g Tris base, 87.6g Sodium chloride, dH_2O to 1L. 1X TBS: 100mL 10X TBS, dH_2O to 1L. Blocking solution (for 4 membranes): 40mL 1X TBS, 0.8g milk powder) and rolled for 1 hour at 4°C. The blocking solution was removed, and the membrane was washed with 10mL 1X TBS-tween 20 (TBS-T) (100mL 10X TBS, 500μL tween 20, dH_2O to 1L) for 5 minutes, rolling at 4°C. This step was repeated. The TBS-T was removed and replaced with 10mL of primary antibody solution (40mL TBS-T, 0.8g milk powder, 4μL Anti-V5 primary antibody (1 in 10,000 dilution, Invitrogen)) and incubated overnight, rolling at 4°C. The membrane was then washed twice for 5 minutes in TBST and 10mL of secondary antibody solution (40mL TBS-T, 0.8g milk powder, 0.5μL peroxidase-conjugated anti-mouse IgG (1 in 80,000 dilution, Sigma) was added to the membrane and incubated for 5 hours, rolling at 4°C. The membrane was washed twice in TBS-T (5 minutes each, rolling at 4°C) and once in TBS (5 minutes, rolling at 4°C). The

membrane was dried and an enhanced chemiluminescence (ECL) solution (ECL1: 2.5mL 250mM Luminol (in DMSO), 1.1mL 90mM p-coumaric acid (in DMSO), 221.4mL Tris HCl, pH, dH_2O to 250mL. ECL2: 160μL 30% H_2O_2, 25mL 1M Tris HCl, pH 8.5, 224.8mL dH_2O. ECL solution for imaging: 1mL ECL 1, 1mL ECL 2.) was added and then incubated for 3 minutes at room temperature in darkness. The excess ECL is removed and the mebrane is placed in the imaging dock and 100 images are taken over an exposure time of 10 minutes (146). Digitised images were acquired with a ChemiDoc MP workstation (Bio-RAD), analysed with ImageJ v1.49 (147) and quantified with QtiPlot v0.9.8.10.

Chapter 3: TM1 results

3.1: Overview of sulphydryl-reactivity analysis

A primary interest is to determine how the TMD of EnvZ allosterically processes and couples different sensory inputs into a single unified output. To determine which residues of EnvZ compose TM1, the primary sequence was subjected to a full protein scan with DGpred (143), which suggested that residues Phe-12 to Val-34 comprise TM1. TMHMM v2.0 (144) was also employed, which suggested that the residues between Thr-15 and Phe-37 compose TM1. These results are similar to previously proposed TM1 composition (55, 56), therefore, sulphydryl-reactivity experimentation was employed between residue positions 11 and 41 in order to ensure that the entirety of TM1 was encompassed.

Sulphydryl-reactivity possesses several distinct advantages. Firstly, it is well-characterised and has been employed on many soluble and membrane-spanning proteins and higher-order complexes (149). Based on these previous results, it has been possible to compare our results with those from other membrane-spanning receptors. Secondly, these reactions can be performed *in vivo*, which allows EnvZ to remain within its native environment while retaining the ability to adjust extracellular osmolarity. In addition, this leaves all accessory proteins, such as MzrA, present and modulatable within the host cell membrane. Finally, the use of an *in vivo* methodology allowed us to monitor signal output with a dual-colour fluorescence-based system (**Figure 2-2B**) have previously been employed to determine which surfaces of TM1 are intolerant of Cys substitutions (1,4,6). In summary, the *in vivo* nature of this assay facilitated mapping of the TM1-TM1' interface under different osmotic conditions, which is an important first step toward understanding how EnvZ processes different allosteric signal inputs into a single uniform modulation of bacterial porin balance.

3.2: Optimising a cysteine-less EnvZ

To measure steady-state signal output from EnvZ/OmpR osmosensing circuits possessing the Cys-less variants, two-colour fluorescent reporter strains were used. MDG147 is a derivative of *E. coli* strain K-12 MG1655 that possesses transcriptional fusions of *cfp* to *ompC* and of *yfp* to *ompF* within its chromosome. This allows the ratio of CFP to YFP fluorescence (CFP/YFP) to provide a rapid and sensitive measure of the ratio of *ompC* to *ompF* transcription, which estimates the intracellular level of phosphorylated OmpR (**Figure 2-2B**) (1,4,6). MDG147 cells harbouring the empty vector pEB5 (1) were grown in glucose MMA under either the low- (0% sucrose) or high- (15% sucrose) osmolarity regime and both CFP and YFP fluorescence were measured. As previously observed, an increase in CFP fluorescence (291 to 922 fluorescence values, low to high osmolarity) along with a concomitant decrease in YFP fluorescence (780 to 318 fluorescence values, low to high osmolarity, resulting in an increased CFP/YFP ratio (0.38 to 3.20, low to high osmolarity, ~8.5 fold increase), was observed when MDG147/pEB5 cells were grown under the high-osmolarity regime (**Figures 3-1A** and **3-1B**) (4,6).

To assess whether plasmid-based complementation could produce similar steady-state signal output, EPB30 (MDG147 *envZ::kan*) cells (2) were complemented with the Cys-less EnvZ variants expressed from plasmid pRD400 (6). EPB30/pRD400 cells expressing the C277M variant resulted in CFP and YFP fluorescence similar to those harbouring the control vector (EPB30/pEB5) under both osmotic regimes, therefore, it was not considered for further analysis (**Figure 3-2**). The C277A variant facilitated steady-state output similar to plasmid-based WT EnvZ under both regimes, while C277S resulted in slightly lower steady-state signal output (**Figure 3-3**). Based on these results, it was elected to continue with the C277A under conditions that produced results similar to MDG147/pEB5 cells (**Figures 3-1A**, **3-2B** and **3-3**).

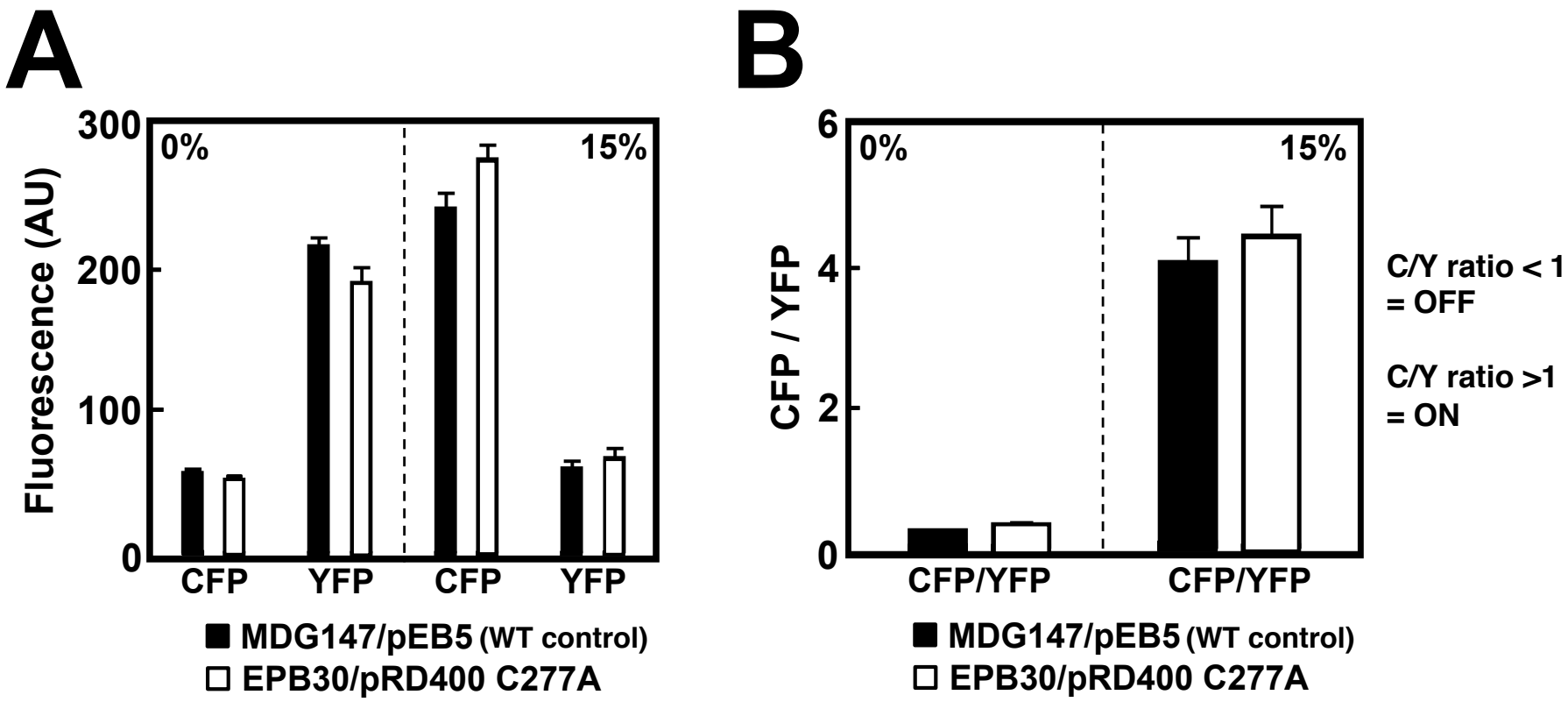

Figure 3-1: Signal output of the Cys-less variant of EnvZ. (A) CFP and YFP fluorescence from MDG147/pEB5 (filled) and EPB30/pRD400 C277A (Cys-less; empty) cells grown under the low- (0% sucrose) and high-osmolarity (15% sucrose) regimes. (B) The CFP/YFP ratio from MDG147/pEB5 (filled) and EPB30/pRD400 C277A (Cys-less; empty) cells grown under the low- and high-osmolarity regimes estimates EnvZ signal output. Error bars represent standard deviation of the mean with a sample size of $n \geq 3$.

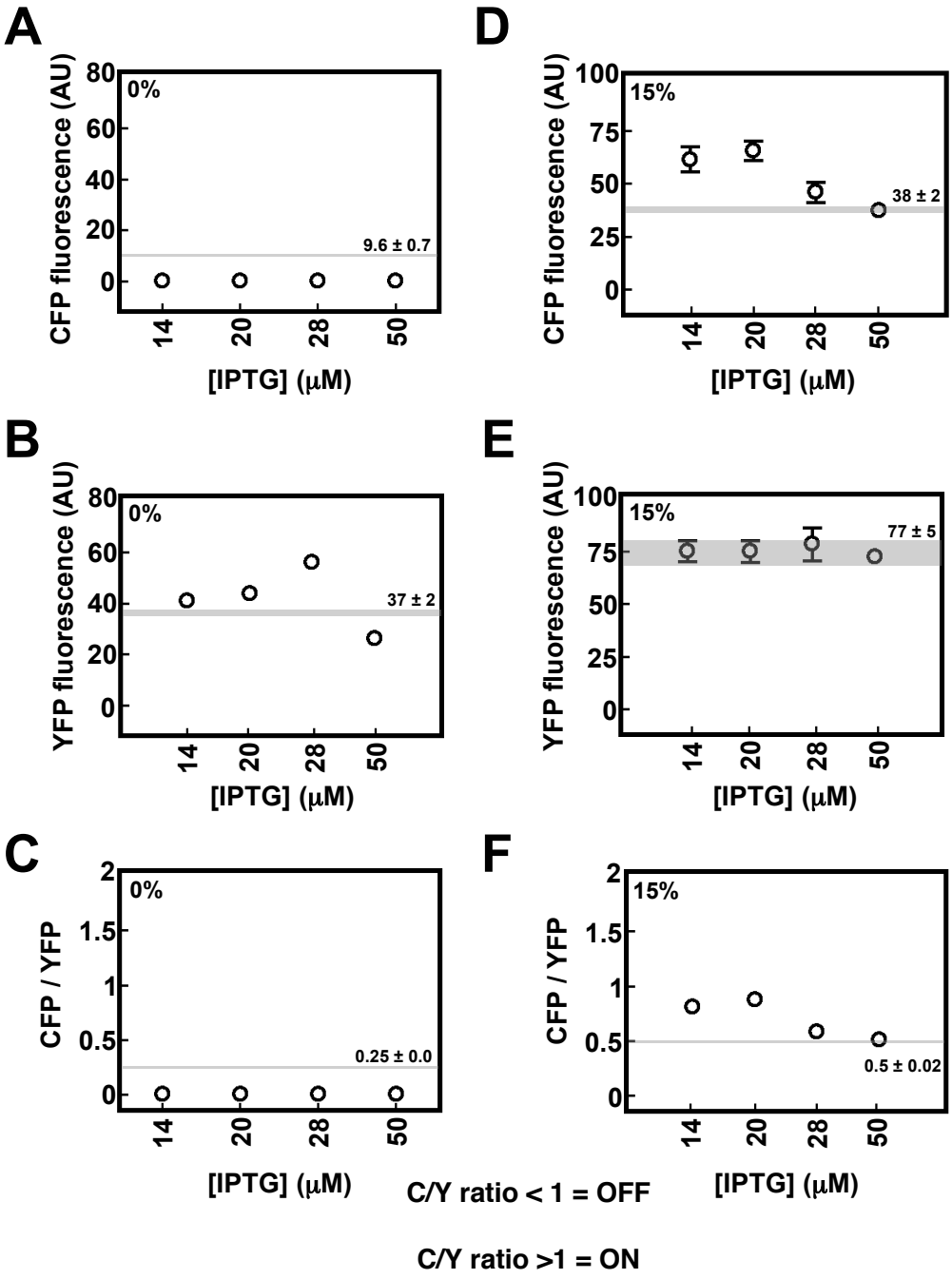

Figure 3-2: Comparison of signal output from EPB30/pEB5 (Δ*envZ*) cells and those expressing the C277M variant of EnvZ. CFP fluorescence (A), YFP fluorescence (B) and CFP/YFP ratio (C) from EPB30/pRD400 cells grown under the low-osmolarity regime (0% sucrose) expressing the C277M variant of EnvZ at different concentrations of IPTG. CFP fluorescence (D), YFP fluorescence (E) and CFP/YFP ratio (F) from EPB30/pRD400 cells grown under the high-osmolarity regime (15% sucrose) expressing the C277M variant of EnvZ at different concentrations of IPTG. In all panels, the shaded area represents the mean with a range of one standard deviation of the mean from EPB30/pEB5 (50μM iodine). Values represented by the shaded area are also provided to aid in comparison. Error bars represent standard deviation of the mean with a sample size of n ≥ 3.

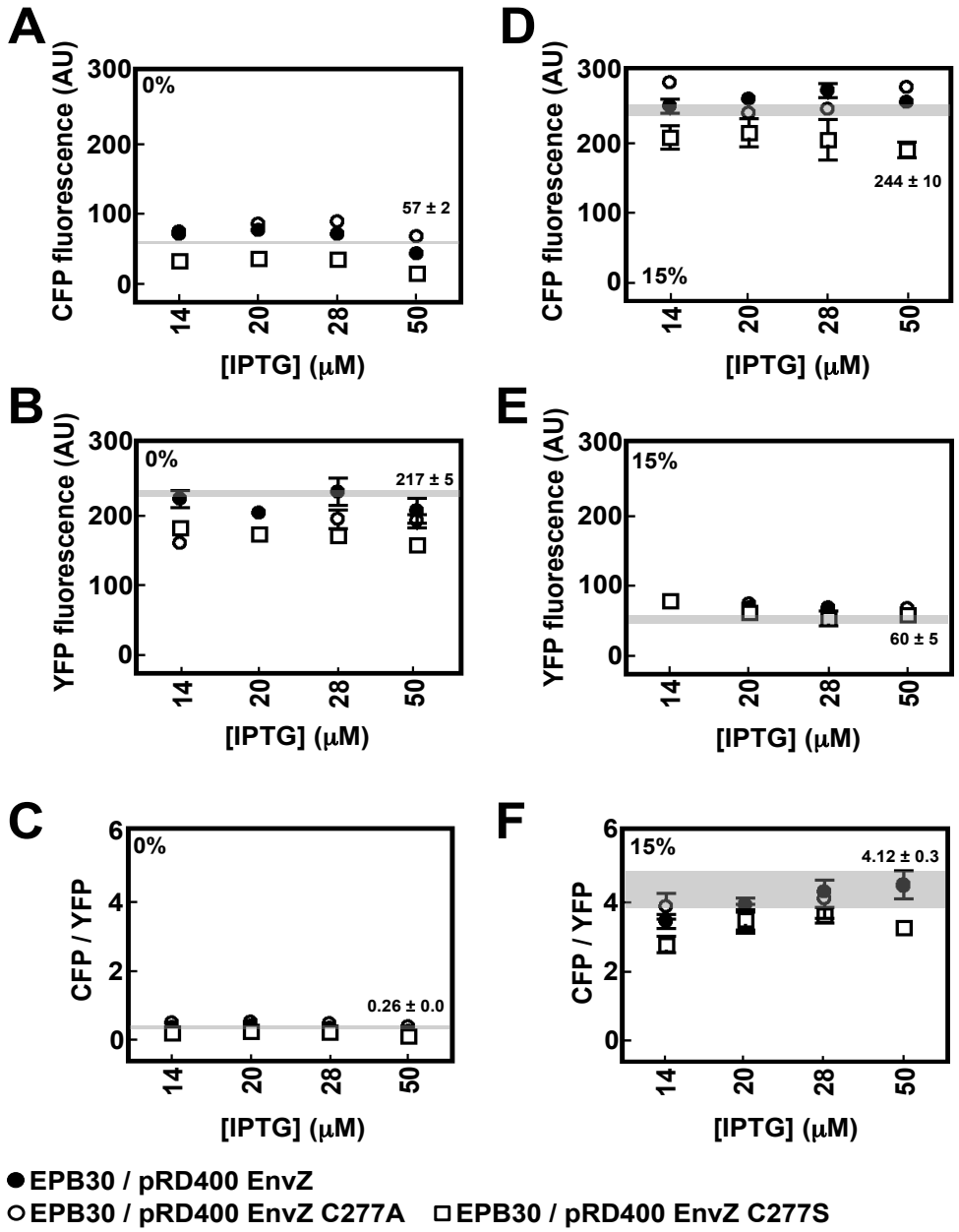

Figure 3-3: Comparison of signal output from the WT (filled circles), the C277A (empty circles) and the C277S variants (empty squares) of EnvZ. CFP fluorescence (A), YFP fluorescence (B) and CFP/YFP ratio (C) from EPB30/pRD400 cells grown under the low-osmolarity regime (0% sucrose) expressing the WT, C277A or C277S variant of EnvZ at different concentrations of IPTG. CFP fluorescence (D), YFP fluorescence (E) and CFP/YFP ratio (F) from EPB30/pRD400 cells grown under the high-osmolarity regime (15% sucrose) expressing the WT, C277A or C277S variant of EnvZ at different concentrations of IPTG. In all panels, the shaded area represents the mean with a range of one standard deviation of the mean from MDG147/pEB5 cells (50μM iodine). The values represented by the shaded area are also provided to aid in comparison. Error bars represent standard deviation of the mean with a sample size of $n \geq 3$.

3.3: Mapping TM1 surfaces responsible for maintenance of EnvZ signal output

As described above, positions 11 through 41 were selected to ensure that all residues potentially comprising TM1 were converted to a Cys residue. A library of single-Cys-containing EnvZ proteins was created by employing standard site-directed mutagenesis (see **Section 2.2**) using pRD400 containing the C277A variant as a template (**Figure 3-1**). Although several attempts were made, a Cys residue could not be placed at position 32. It was observed that the entire library, with a few exceptions, was expressed within EPB30/pRD400 cells grown under the low- or high-osmolarity regime (**Figure 3-4C**). Under both the low and high osmolarity regimes the L23C variant was found at significantly lower steady-state levels. In addition, the monomeric form of the P41C variant was only quantifiable when EPB30/pRD400 cells were grown under the high-osmolarity regime (**Figure 3-4C**).

For EPB30/pRD400 cells each expressing a single-Cys-containing TM1, CFP fluorescence and YFP fluorescence were measured to calculate the CFP/YFP ratio, which serves as an estimate of steady-state EnvZ signal output. EPB30/pRD400 cells expressing the C277A variant were used as the baseline for comparison (**Figures 3-1A**, **3-1B** and **3-3**). Under the low-osmolarity regime, a shift in signaling output toward the “on” state results in increased CFP fluorescence (**Figure 3-5A**), decreased YFP fluorescence (**Figure 3-5B**) and an overall increase in the CFP/YFP ratio (**Figures 3-6A** and **3-6B**), while a shift toward the “off” state appears as decreased CFP (**Figure 3-5A**), increased YFP (**Figure 3-5B**) and a decrease in CFP/YFP ratio (**Figures 3-6A** and **3-6B**).

Several trends were observed during analysis of the entire single-Cys-containing library. When EPB30/pRD400 cells were grown under the low-osmolarity regime, EnvZ was less tolerant of Cys substitutions at the N- and C-terminal regions of the library. In most cases, this results in a shift toward the “on” state of EnvZ, demonstrated by an increase in CFP fluorescence and a decrease in YFP fluorescence. These boundary regions appear to flank a

core of alternating increases and decreases in EnvZ signal output, suggesting that multiple tightly packed EnvZ helices exist within the hydrophobic core of the inner membrane. It should also be noted that when EPB30/pRD400 cells where grown under the low-osmolarity regime, a Cys at residue position 22 prevented cellular growth, however, this was not observed when cells were grown under the high- osmolarity regime (**Figures 3-4C**, **3-5** and **3-6**). Interestingly, these results occurred adjacent to the position that possessed the most-biased steady-state signal output (Cys-23). When EPB30/pRD400 cells were grown under the high-osmolarity regime, a similar pattern of changes was observed in the CFP fluorescence (**Figure 3-5C**), YFP fluorescence (**Figure 3-5D**) and in CFP/YFP ratio (**Figure 3-6C**), however, these changes were smaller in magnitude, perhaps due to the fact that the EnvZ/OmpR circuit was already activated and thus disturbances due to altered surface interactions would be of a smaller magnitude.

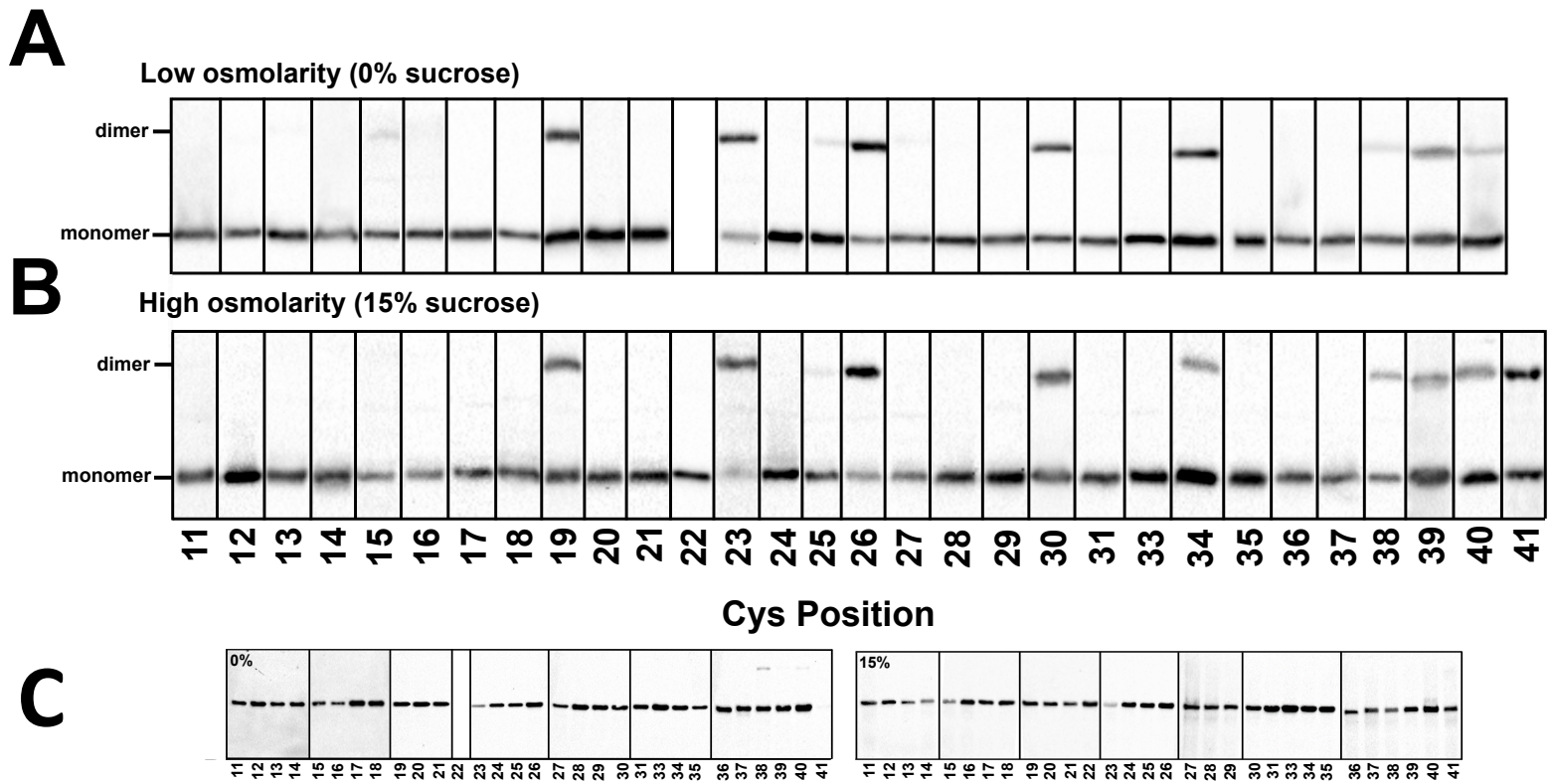

Figure 3-4 Immunoblotting analysis of the sulfhydryl-reactivity experimentation. (A) EPB30/pRD400 cells grown under the low-osmolarity (A) or high-osmolarity (B) regimes were subjected to conditions described in Figure 7-8. It was observed that particular single-Cys- containing variants resulted in the presence of dimeric EnvZ moieties. A minimum of four immunoblots were used to determine the data points presented in Figure 9-1. (C) Steady-state expression of the single-Cys-containing variants of EnvZ. EPB30/pRD400 cells grown under the low- (0% sucrose) or high-osmolarity (15% sucrose) regime expressing one of the single-Cys-containing EnvZ variants. Cells expressing the L22C variant did not grow under the low-osmolarity regime. Lower steady-state levels of the L23C variant were also observed. In addition, the P41C variant was nearly absent when expressed in cells grown under the low-osmolarity regime. When EPB30/pRD400 cells were grown under the high-osmolarity regime, lower than normal steady-state levels of L23C were observed.

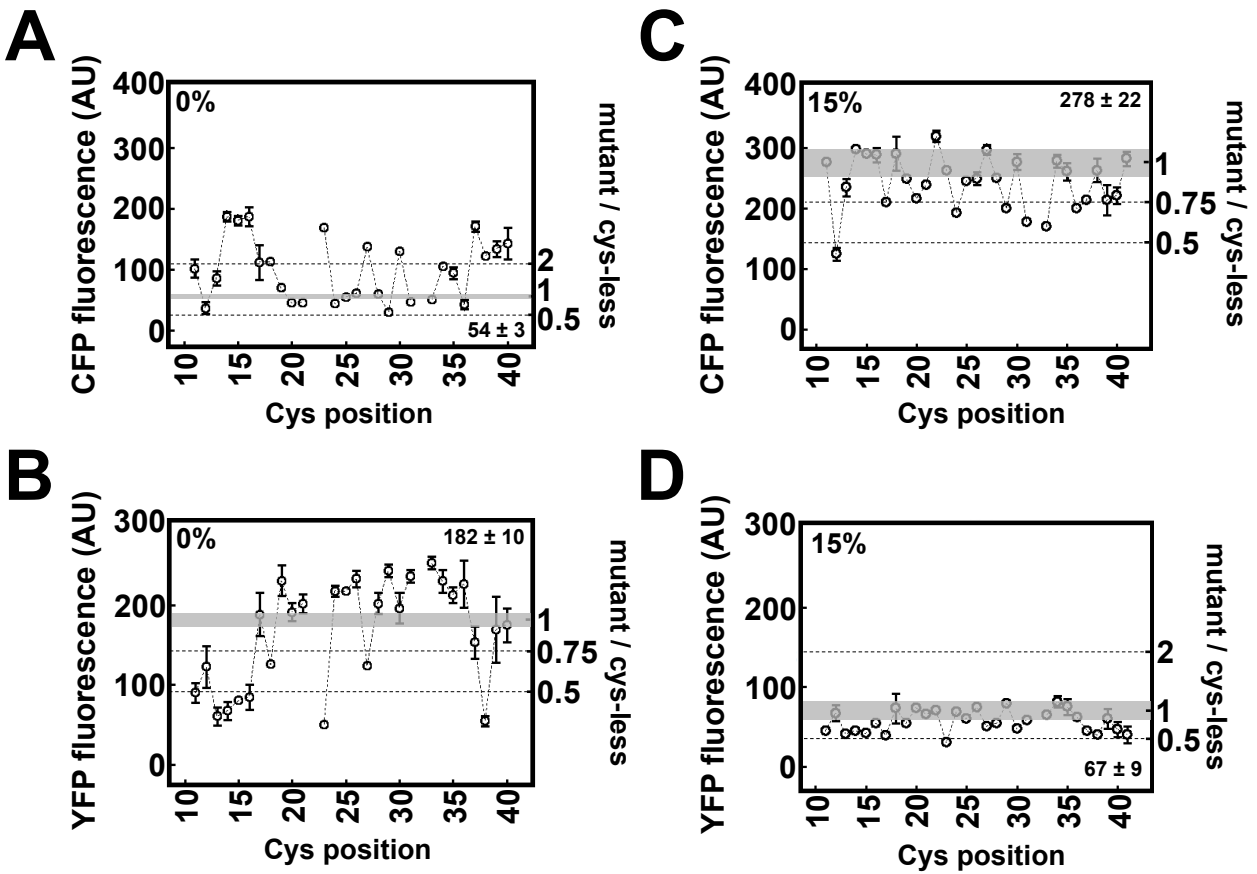

Figure 3-5: Signal output from the library of single-Cys-containing EnvZ variants represented as individual CFP and YFP values. CFP fluorescence (A) and YFP fluorescence (B) from EPB30/pRD400 cells expressing one of the single-Cys- containing EnvZ variants grown under the low-osmolarity (0% sucrose) regime. These ratios are also compared to EPB30/pRD400 cells expressing the C277A variant (Cys-less) with induction at 250 μM IPTG. CFP fluorescence (C) and YFP fluorescence (D) from EPB30/pRD400 cells expressing one of the single-Cys-containing EnvZ variants grown under the high-osmolarity (15% sucrose) regime. These ratios are also compared to EPB30/pRD400 cells expressing the C277A variant (Cys-less) with induction at 50 μM IPTG. It is important to note that the P41C variant could only be expressed within cells grown under the high-osmolarity regime. In all panels, the shaded area represents the mean with a range of one standard deviation of the mean from EPB30/pRD400 cells expressing the C277A variant (Cys-less) with induction at 50 μM IPTG. The values represented by the shaded area are also provided to aid in comparison. Error bars represent standard deviation of the mean with a sample size of n ≥

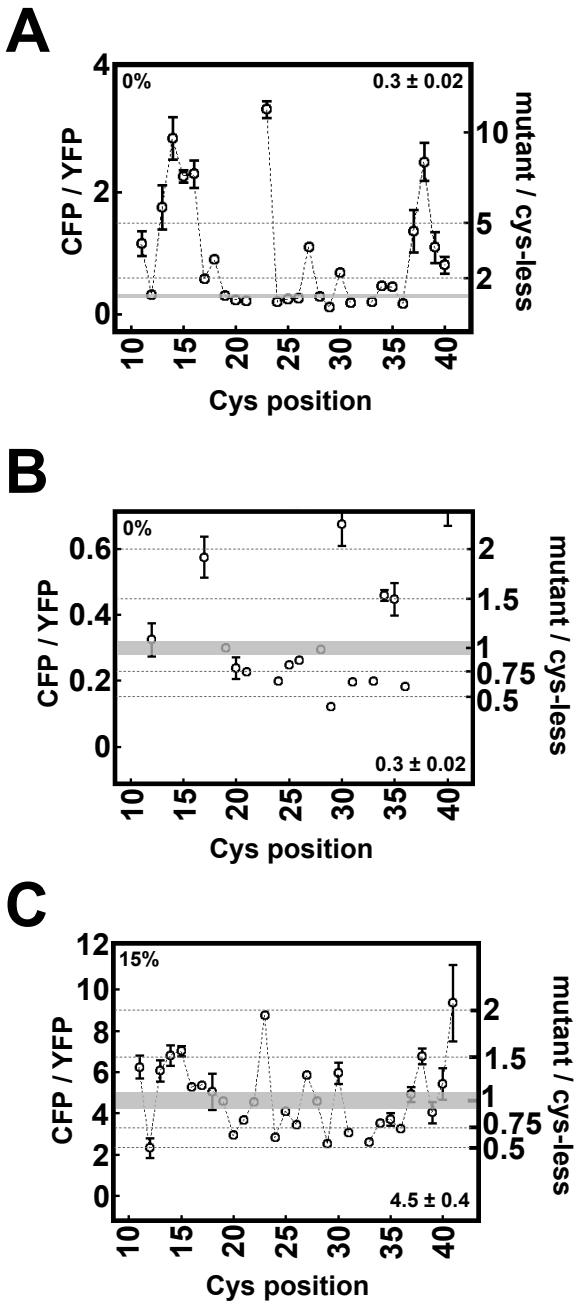

Figure 3-6: Signal output from the library of single-Cys-containing EnvZ variants represented as CFP/YFP ratios. (A) CFP/YFP ratios from EPB30/pRD400 cells expressing one of the single-Cys-containing EnvZ variants grown under the low-osmolarity (0% sucrose) regime. These ratios are also compared to EPB30/pRD400 cells expressing the Cys-less (C277A) variant and are used to demarcate the Cys-containing variants in **Figure 3-10**. (B) Magnified version of panel A in order to emphasise the region up to a 2-fold increase in CFP/YFP over cells expressing the Cys-less variant. (C) CFP/YFP ratios from EPB30/pRD400 cells expressing one of the single-Cys-containing EnvZ variants grown under the high-osmolarity (15% sucrose) regime. These ratios are also compared to EPB30/pRD400 cells expressing the Cys-less (C277A) variant and are used to demarcate the Cys-containing variants in **Figure 3-10**. It is important to note that cells expressing the P41C variant were analysed only when grown under the high-osmolarity regime. The shaded areas represent the mean and a range of one standard deviation of mean. These values are provided to aid in comparison. Error bars represent standard deviation of the mean with a sample size of $n \geq 3$.

3.4: Identifying surfaces involved in TM1-TM1' dimerisation

Based on the effect of the individual Cys substitutions on EnvZ signal output, it appears that a potential helix is present within the hydrophobic core of the membrane. Therefore, it was of interest to determine whether the helical surface participating in TM1-TM1' interaction surface could be identified. To accomplish this, the library of single-Cys-containing variants was expressed in EPB30/pRD400 cells and upon reaching an OD_{600nm} of approximately 0.3, cells were subjected to 250 μM molecular iodine for 10 minutes and subsequently analysed by non-reducing SDS-PAGE. These conditions have been previously shown to promote disulphide formation in various membrane-spanning receptors *in vivo* by creating an oxidising environment (149). As this environment is not experience by *E. coli* under normal conditions, a spontaneous crosslinking event would be unlikely to occur during dimerisation. Upon comparison of the WT and the C277A variant, under either osmotic regime, the presence of a higher molecular weight band confirmed the necessity of Cys-277 removal (**Figure 3-7**).

Based on these results, EPB30/pRD400 cells expressing the single-Cys-containing EnvZ variants were grown under the low- (0% sucrose) and high-osmolarity (15% sucrose) regimes and subjected to molecular iodine, non-reducing SDS-PAGE and immunoblotting against the C-terminal V5 epitope (**Figure 3-4**). Data were tabulated for every position with the exception of residue position 32, which could not be made as described above. Three regions were observed, each with a different extent of disulphide bond formation. The N-terminal region (region I in **Figure 3-8**), comprising residues 11 to 18, exhibited almost no cross-linking, except for a minimal amount at positions 11 and 15. The second region (II), consisting of positions 19 to 37, demonstrated alternating low and high levels of disulphide formation consistent with the hydrophobic core of TM1. The final region (III) consists of the C-terminal periplasmic positions in our library, residues 38 through 41, where the apparent helical pattern is interrupted and an overall greater extent of sulphydryl-reactivity is observed.

Altering the reaction conditions as shown in **Figures 3-9** and **3-10** further supported the differentiation of the TM1 into Regions I through III.

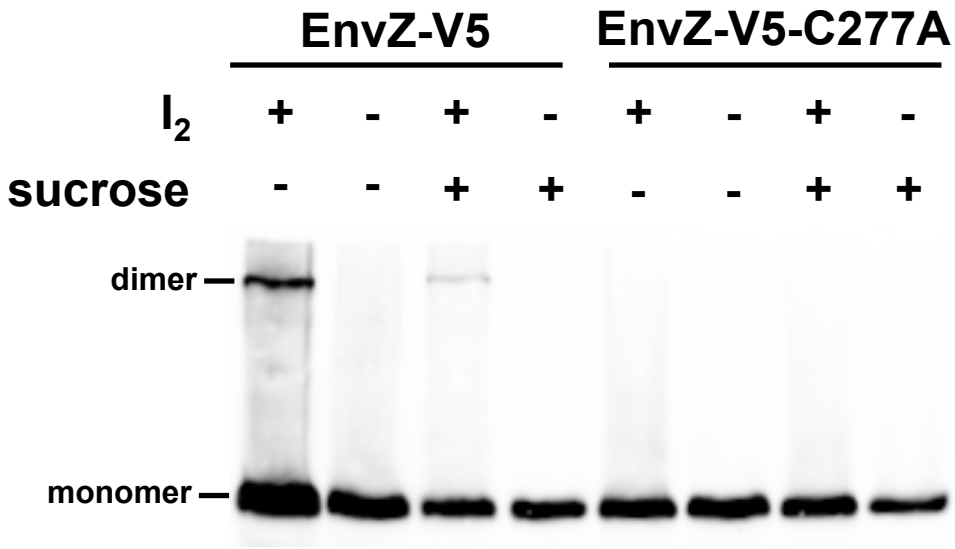

Figure 3-7 Sulphydryl-reactivity of the WT and Cys-less (C227A) variants of EnvZ. Comparison of EPB30/pRD400 cells expressing the WT and C277A variants of EnvZ upon subjecting them to molecular iodine. Cells were grown under the low- (without sucrose) or high- osmolarity (with 15% sucrose) regimes until an OD_{600nm} of approximately 0.2-0.3. Cultures were then subjected to 250μM molecular iodine. When EPB30/pRD400 cells were expressing the wild- type version of EnvZ, both under the low- and high-osmolarity regimes, a dimeric species was observed. Conversely, when the C277A variant was expressed, no dimeric species were observed. These results confirm the necessity of removing the native Cys residue at position 277.

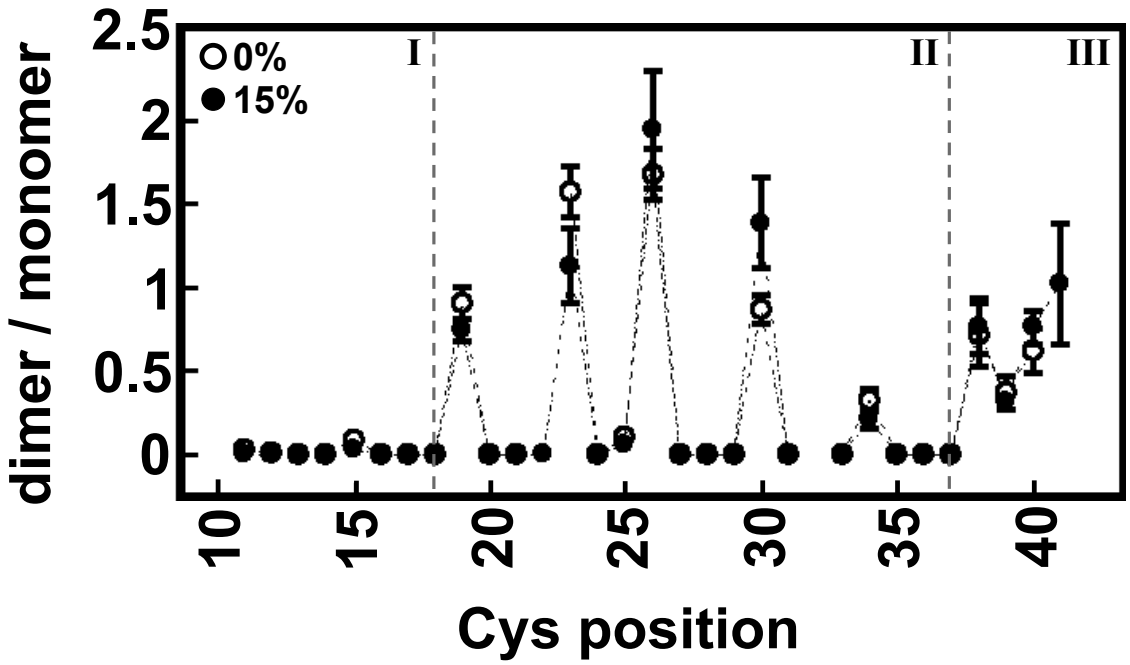

Figure 3-8: Extent of sulphydryl-reactivity for each single-Cys-containing variant. EPB30/pRD400 cells growing under the low- (empty circles, 0% sucrose) or high-osmolarity (filled circles, 15% sucrose) regimes were analysed to determine the ratio of dimeric:monomeric EnvZ at each position as shown in **Figure 3-4**. As described within the text, three distinct regions (I, II and III) were observed. Error bars represent standard deviation of the mean with a sample size of $n \geq 3$.

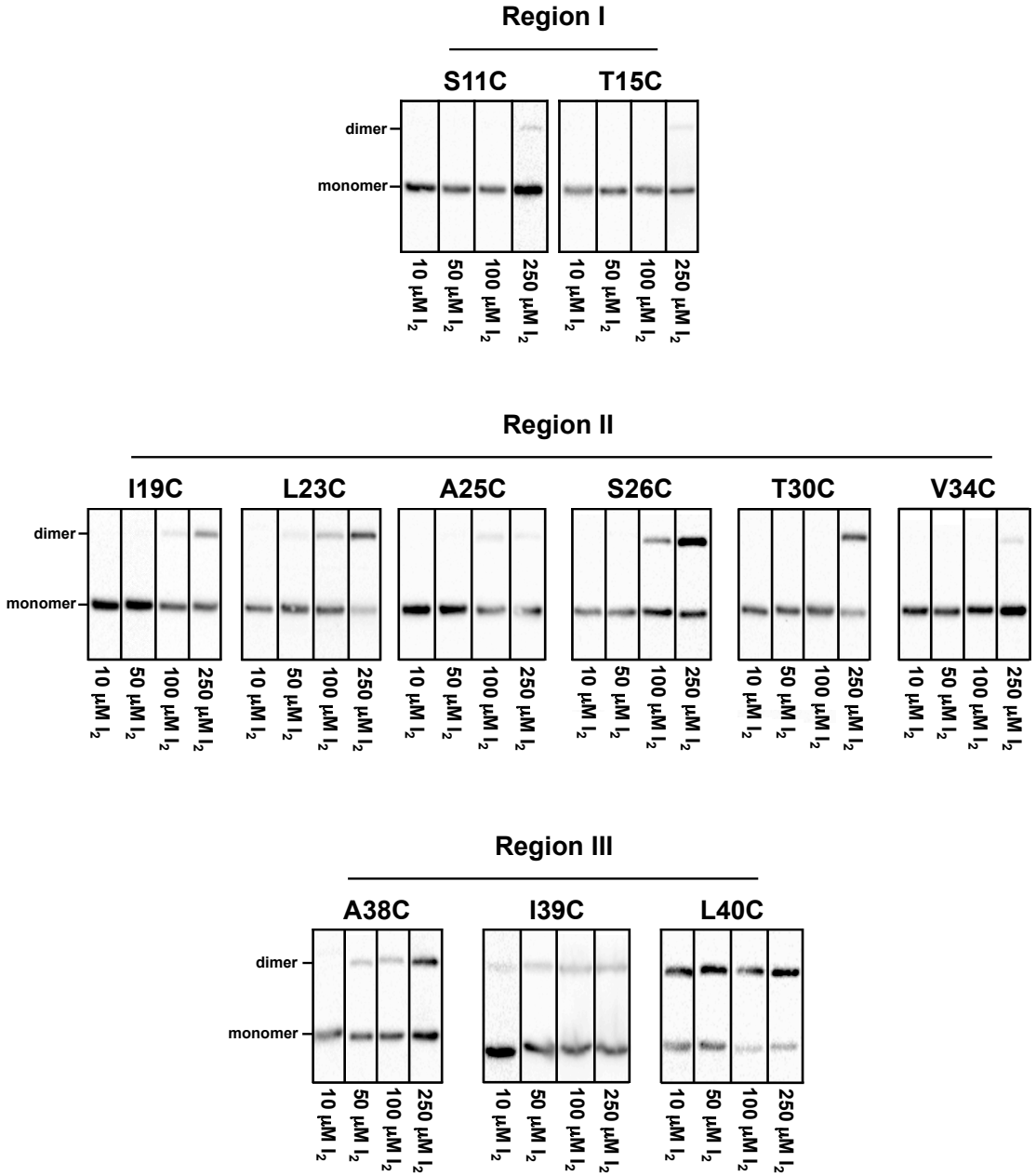

Figure 3-9: Concentration-dependent sulphydryl-reactivity analysis of the single-Cys-containing EnvZ variants. EPB30/pRD400 cells expressing one of the single-Cys-containing variants that were shown to form a disulphide under the low-osmolarity growth regime (0% sucrose) in Figure 9-1 were assessed in a modified sulphydryl-reactivity protocol. Under these conditions, the total reaction time was held constant at 10 minutes and the concentration of iodine was altered over a 25-fold range (10 μM, 25 μM, 50 μM and 250 μM final). As described in the text, these results reinforce our delineation of TM1 into Regions I-III.

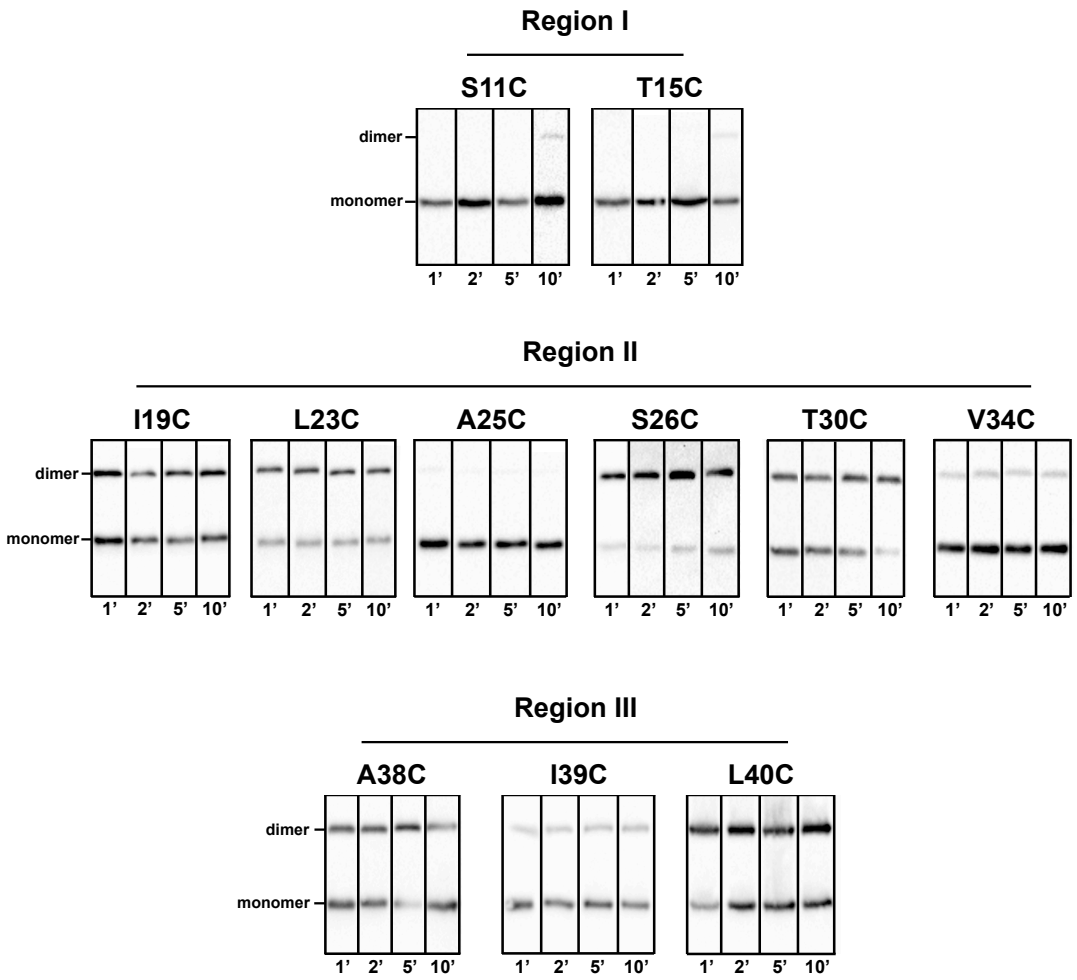

Figure 3-10: Time-dependent sulphydryl-reactivity analysis of the single-Cys-containing EnvZ variants. EPB30/pRD400 cells expressing one of the single-Cys-containing variants that were shown to form a disulphide under the low-osmolarity growth regime (0% sucrose) in **Figure 3-4** were assessed in a modified sulphydryl-reactivity protocol. Under these conditions, the concentration of iodine was held constant at 250 μM final and the reaction time was altered over a 10-fold range (1, 2, 5 and 10 minutes). As described in the text, these results reinforce our delineation of TM1 into Regions I-III.

Chapter 4: TM2 results

4.1: Creating a single-cysteine containing library within TM2 of EnvZ

The cys-less EnvZ (C277A) was used for the TM2 library as described in Section 2.6. Residues which comprise TM2 were determined by subjecting the full EnvZ sequence to DGpred (142) and TMHMM v2.0 (143), which suggested that Leu-160 to Ile-181 and Leu-160 to Ile-179 comprise TM2 respectively. Based on these analyses, site-directed mutagenesis was employed using the Cys-less variant as a template to create a library of single-Cys-containing EnvZ proteins that spanned from positions 156 to 184 (**Figure 4-1**). It was observed that nearly the entire library was expressed within EPB30/pRD400 cells grown under the low- or high-osmolarity regime. Variants possessing a Cys at position 156 showed low levels of expression when grown under the low-osmolarity (0% sucrose) regime. However, when grown under the high-osmolarity regime, no variants showed reduced expression level (**Figure 4-4C**). These results indicate that the library was suitable for further *in vivo* experimentation.

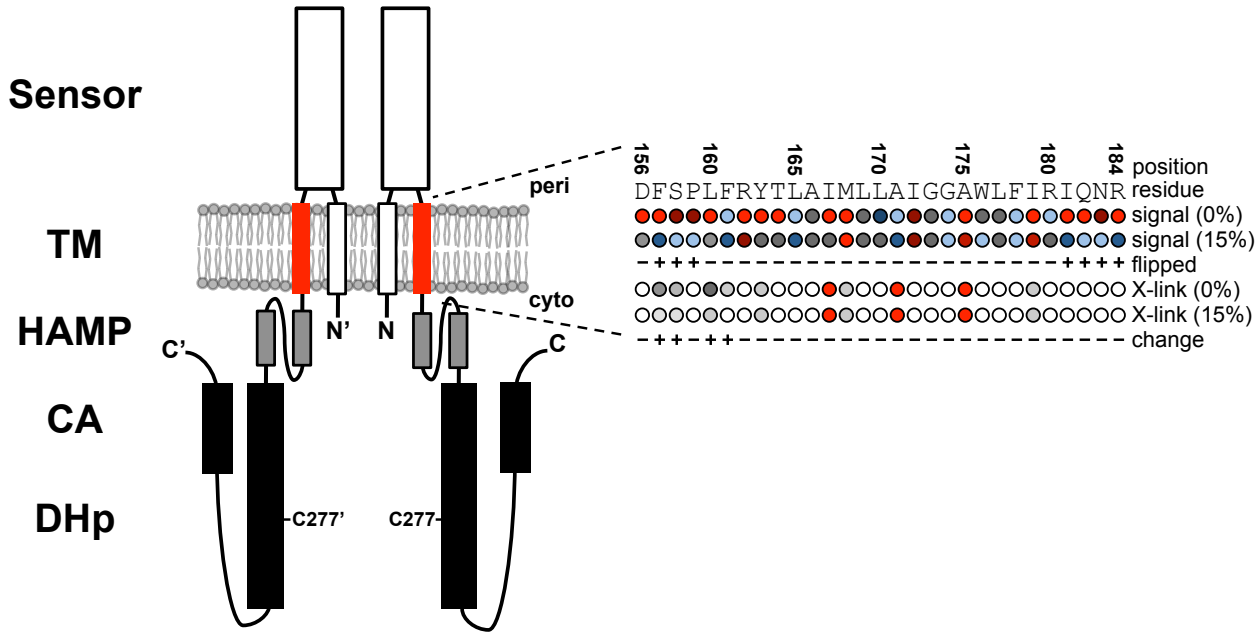

Figure 4-1: EnvZ functions as a homodimer with a cytoplasmic N-terminus, the first transmembrane helix (TM1, white), a large periplasmic domain (sensor, white), the second transmembrane helix (TM2, red), a membrane-adjacent HAMP domain (grey) and the DHp (black) and CA (black). The position of the original Cys-277 residue that was mutated to Ala to produce the Cys-less EnvZ is provided. The residues subjected to Cys substitution and their position in the primary sequence is provided. Signal output from each single-Cys-containing variant is compared to the Cys-less (C277A) variant: less than 50% of Cys-less (light blue), between 50% and 75% of Cys-less (dark blue), between 75% and 125% of Cys-less (grey), between 125% and 200% (dark red) and greater than 200% (light red). Residue positions exhibited flipped signal output are indicated with a plus. The extent of sulphydryl-reactivity is also presented in five categories based on dimer-to-monomer ratio: no dimer present (white), less than 0.05 (light grey), between 0.05 and 0.2 (medium grey), between 0.2 and 0.5 (dark grey) and greater than 0.5 (red). Positions that exhibit a significant change in cross-linking between the low- and high-osmolarity regimes are indicated with a plus.

4.2: Mapping TM2 surfaces important for maintenance of EnvZ signal output

Each of the single-Cys-containing variants in EPB30/pRD400 cells was expressed, which allowed measurements of CFP fluorescence, YFP fluorescence, and to calculate the CFP/YFP ratio that estimates steady-state EnvZ signal output (**Figure 3-1B**). Cells expressing the Cys-less C277A variant were used as a baseline comparison (**Figure 3-2**). When EPB30/pRD400 cells are grown under the low-osmolarity regime, a shift in signaling output toward the “on” or kinase-dominant state results in increased CFP fluorescence, reduced YFP fluorescence and an increase in the overall CFP/YFP ratio, while a shift toward the “off” or phosphatase-dominant state appears as decreased CFP, increased YFP and a decrease in CFP/YFP ratio (**Figures 4-2**). These changes in CFP/YFP are as described in Section 3.2 While the CFP/YFP ratio values are focussed upon for analysis and discussion, the CFP and YFP values have also been displayed to demonstrate the make-up of the discussed ratios (**Figure 4.3**). This is important to note as a ratio may be misleading or hide very low/high results. For example, the CFP and YFP values could be extremely low for a mutant, but also very similar leading to a ratio of approximately one. As they are particularly low, this would indicate that signal output has been virtually abolished, but the ratio would not reveal this information.

Several trends were observed during analysis of the library of Cys-containing EnvZ receptors. When EPB30/pRD400 cells were grown under the low-osmolarity regime, EnvZ was less tolerant of Cys substitutions at the N- and C-terminal regions of the library. At the N-terminus, signal output from receptors containing a Cys at positions 156, 162 and 163 were elevated, exhibiting greater than a 5-fold increase in CFP/YFP, while receptors possessing a Cys in the C-terminus at positions 179, 181, 182 and 184 were elevated, possessing over a 2-fold increase in CFP/YFP. These boundary regions flank a core of alternating increases and decreases in EnvZ signal output, as observed between residue positions 165 and 180,

suggesting that multiple tightly packed EnvZ helices exist within the hydrophobic core of the inner membrane (**Figure 4-4A and 4-4B**). When grown under the high-osmolarity regime, a pattern appeared where Cys substitutions resulted in significant decreases in signal output (**Figure 4-5C**). Of the 29 mutants analysed, 13 supported less than 75% of the normal WT signal output.

Most striking is the inverse effect on EnvZ signal output of the Cys substitutions that flank the hydrophobic core of TM2. For these residues, when grown under the low-osmolarity regime, the presence of a Cys resulted in an increase in signal output of more than 25%, i.e. shifted toward the on or kinase-dominant state (red dots in **Figure 4-2A**) and a reduction in signal output of more than 25%, i.e. shifted toward the off or phosphate-dominant state, when grown under the high-osmolarity regime (blue dots in **Figure 4-2C**). A “flipped mutant” is described as having opposite results as expected in both osmolarity regimes. These flipped positions reside at the N- and C-terminal ends of the examined region and outside of the proposed hydrophobic TMD core (**Figure 4-2**). Within the hydrophobic core, Cys substitutions show similar changes when cells are grown under the low- and high-osmolality regimes. These results suggest that the flanking regions are not simply rigid structural conduits for signal transduction but may have higher-order roles in signal transduction, such as MzrA interaction or functioning as a control cable at the N- and C-terminal regions respectively (79,80,87,90,140,141).

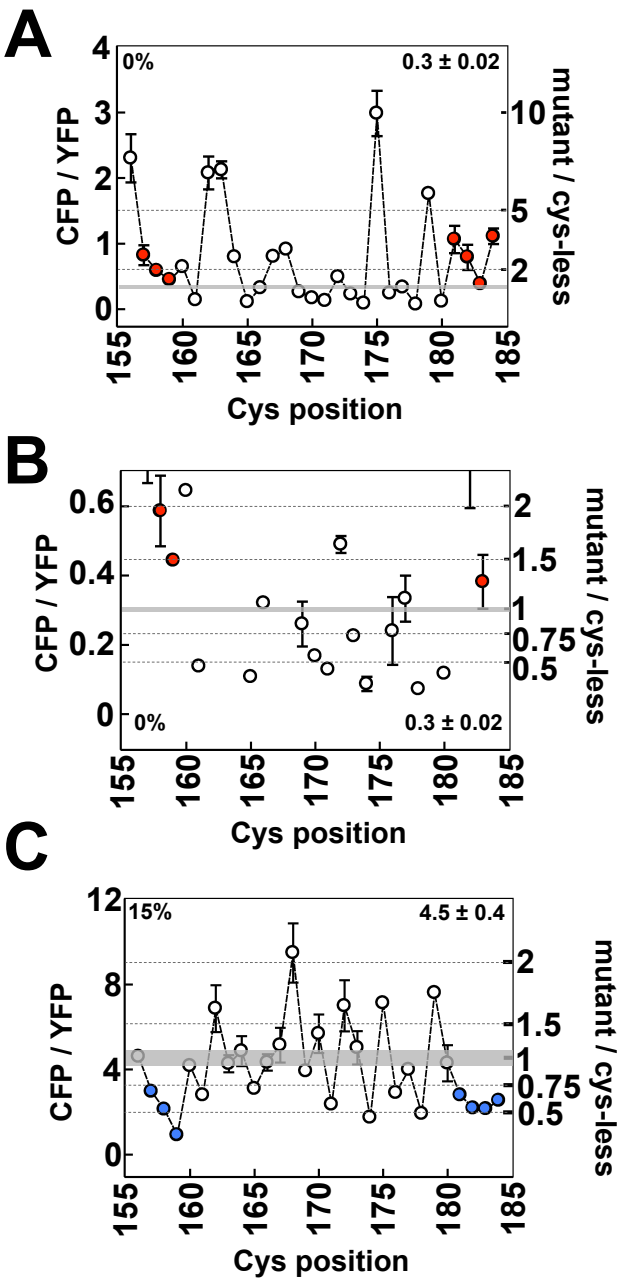

Figure 4-2: Signal output from the library of single-Cys EnvZ variants. (A) CFP/YFP from EPB30/pRD400 cells expressing one of single-Cys variants grown under the low-osmolarity (0% sucrose) regime. On the right axis, these CFP/YFP ratios are compared to the Cys-less (C277A) variant. (B) Magnified version of panel A in order to emphasise the region up to a 2-fold increase in CFP/YFP. (C) CFP/YFP from EPB30/pRD400 cells expressing one of the single-Cys variants grown under the high-osmolarity (15% sucrose) regime. On the right axis, these CFP/YFP ratios are compared to the Cys-less (C277A) variant. The flipped mutants are highlighted with a red dot in panel A (increased signal output) and a blue dot in panel C (decreased signal output). The shaded areas represent the mean signal output from the Cys-less variant of EnvZ with a range of one standard error of mean. These values are provided to aid in comparison. Error bars represent standard deviation of the mean with a sample size of $n \geq 3$.

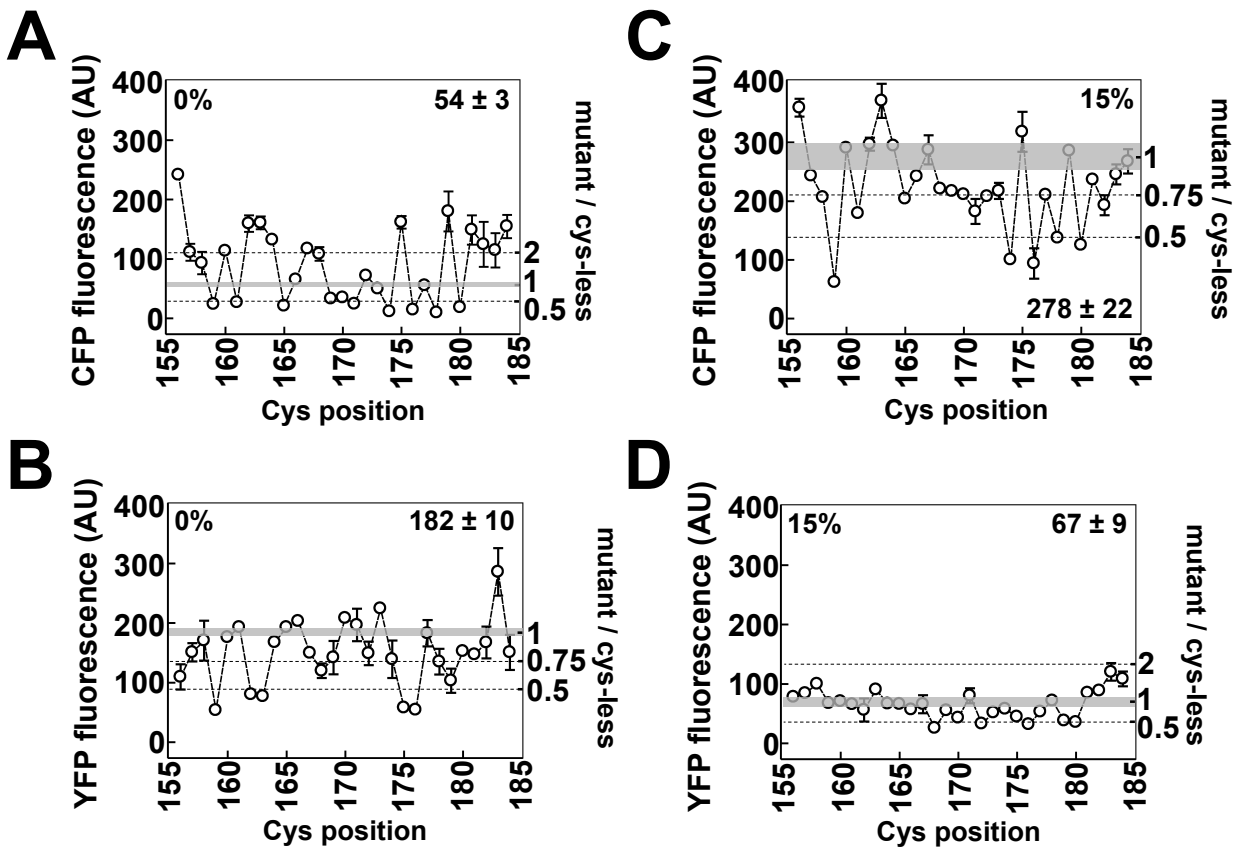

Figure 4-3: Signal output from the single-Cys-containing EnvZ variants. CFP (A) and YFP (B) fluorescence from EPB30/pRD400 cells expressing one of the receptors from the library grown under the low-osmolarity (0% sucrose) regime. CFP (C) and YFP (D) fluorescence from EPB30/pRD400 cells expressing one of the single-Cys-mutants from the library grown under the high-osmolarity (15% sucrose) regime. On the right axes, the ratio of signal output compared to EPB30/pRD400 cells expressing the Cys-less mutant is also presented to aid in comparison. In all panels, the shaded area represents the mean with a range of one standard deviation of the mean from EPB30/pRD400 cells expressing the Cys-less variant of EnvZ (Figure S3). Error bars represent standard error of the mean with an $n \geq 3$.

4.3: Identifying surfaces involved in TM2-TM2' interactions

Sulphydryl-reactivity experimentation is well-characterised and has been employed on many soluble and membrane-spanning proteins and higher-order complexes (149). The *in vivo* nature of this assay facilitated mapping of the TM2-TM2' interface under different osmotic conditions, which is an important first step toward understanding how EnvZ processes allosteric inputs from periplasmic MzrA binding and cytoplasmic osmosensing into a single uniform modulation of bacterial porin balance (**Figure 3-1**). In a similar manner to mapping TM1-TM1' interactions (104), Cys-containing EnvZ variants were expressed in EPB30/pRD400 cells and upon entering the early exponential phase ($OD_{600nm} \approx 0.25$) they were subjected to 250 μM molecular iodine for 10 minutes analysed by non-reducing SDS-PAGE and immunoblotting (**Figure 4-4A&B**).

Three distinct regions within TM2 were observed. The N-terminal region (region I in **Figure 4-2**), comprised of residues 156 to 163, exhibited significant cross-linking under the low-osmolarity regime (0% sucrose) and almost no crosslinking under the high-osmolarity (15% sucrose) regime. The second region (II) consisting of positions 164 to 179, demonstrated altering low and high levels of disulphide-formation consistent with the crosslinking of TM2 and TM2' within the hydrophobic core of the TMD. The final region (III), from residues 180 to 184, shows no crosslinking (**Figure 4-5**). It should be noted that this significant difference at the periplasmic end of the TMD between cells grown under the low- and high-osmolarity regime was not observed during similar analyses of TM1 (104).

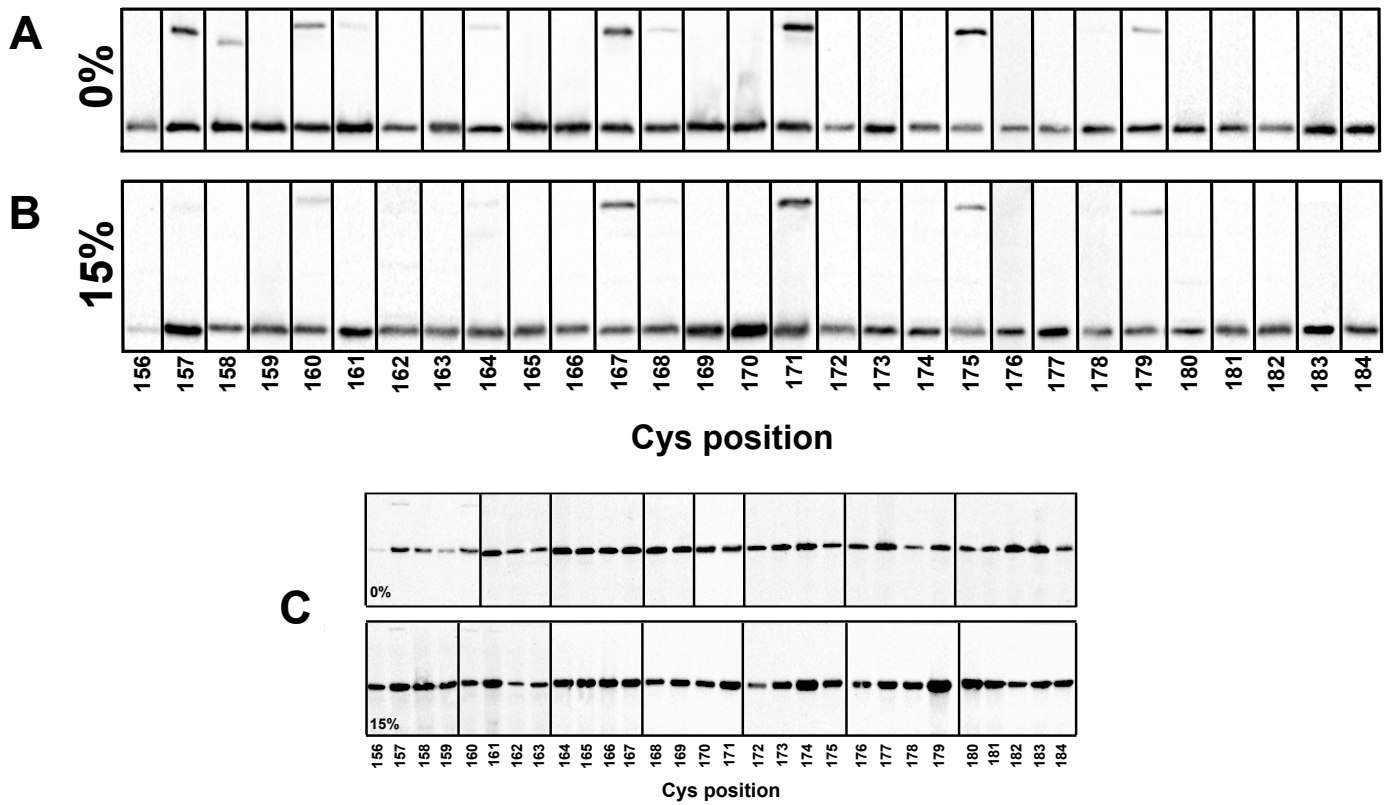

Figure 4-4: Immunoblotting analysis of the sulphydryl-reactivity experimentation. EPB30/pRD400 cells expressing one of the single-Cys-containing EnvZ receptors were grown under (A) the low- (0%) or (B) the high- (15%) regimes until an OD_{600nm} of approximately 0.25 was reached. Cultures were then subjected to 250 µM molecular iodine for 10 minutes, which resulted in the presence of dimeric EnvZ moieties that migrated at a slower rate than the monomeric species with certain Cys- containing EnvZ receptors. A minimum of three immunoblots were used for each of the data points present in Figure 8-8. (C) Steady-state expression of EnvZ variants containing a single Cys residue within TM2. EPB30/pRD400 cells expressing one of the single-Cys-containing variants were grown under the low- (0% sucrose) or high-osmolarity (15% sucrose) regimes. Under the low-osmolarity regime, reduced steady-state levels of the D156C variant were observed. In addition, disulphide formation was observed for the F157C and L160C variants in the absence of any additional oxidising agent. When EPB30/pRD400 cells were grown under the high-osmolarity regime, the F157C, L160C and F161C variants exhibited disulphide formation in the absence of any oxidising agent.

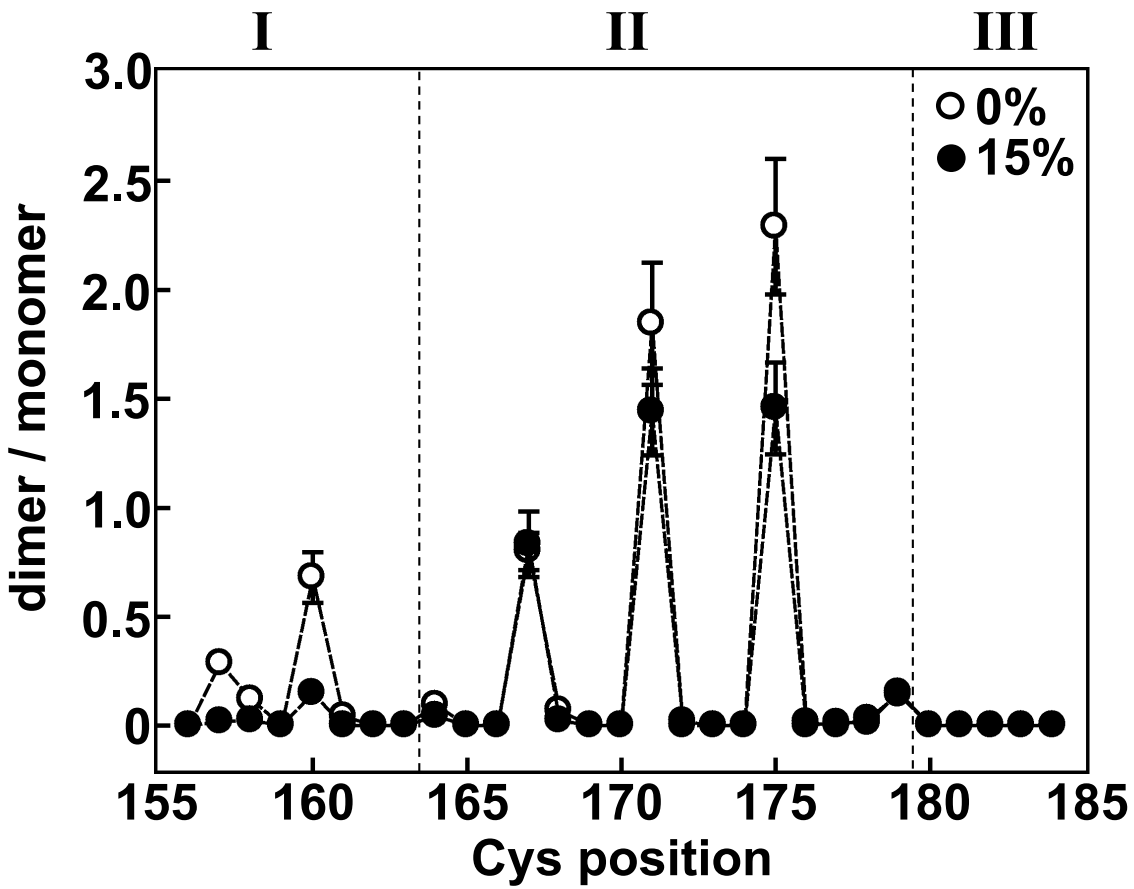

Figure 4-5: Extent of sulphydryl-reactivity for each single-Cys-containing EnvZ variant. EPB30/pRD400 cells were grown under the low- (empty circles, 0% sucrose) or high-osmolarity (filled circles, 15% sucrose) regimes and subjected to 250 μM molecular iodine for 10 minutes when their OD_{600nm} reached approximately 0.25. As shown in Figure S5, this allowed us to determine the dimer/monomer ratio represented on the Y-axis. Three distinct regions, denoted I, II and III were observed and are described in the text. Error bars represent the standard error of the mean with a sample size of $n \geq 3$.

Chapter 5: 2X Cys results

5.1: Creation of a double-cysteine EnvZ library

To create a library of EPB30/pRD400 cells containing 2X-Cys EnvZ mutations, the previous library of EnvZ proteins that contained a Cys residue in either TM1 (104) or TM2 (137) was used as a starting point. For the TM1 library, residue positions 15 to 35 were selected for analysis. These residues were selected because they were proposed to form the core of the TM1 helix. Using data from previous TM mapping experiments with the serine chemoreceptor (Tsr) (91), a range of five consecutive residues in TM2 that would likely interact with the Cys residue in TM1 were assigned. The molecular cloning was completed on 100 2X-Cys pairings and 11/100 specific Cys pairs prevented cell growth when expressed via IPTG (**Figure 5-1 and 5-2**). Cys-22, located in the membrane core region of the TM helices, had previously prevented cell growth when expressed via IPTG as a 1X-Cys mutation yet neither Cys-16, located in the cytoplasmic end of the TM helices, or Cys-21, also located in the membrane core of the TM helices, prevented cell growth when expressed via IPTG as a 1X-Cys mutant. Additionally, both Cys-16 and Cys-22 prevented cell growth across all five proposed pairings yet Cys-21 was successfully paired with and grown in four of its five pairings. The location of these unsuccessful mutations will be critical to their growth prevention as the mutation may affect the overall structure of the protein with fatal consequences. This could prove useful in locating sensitive and potentially fragile sections of the protein to interfere with and potentially elicit an antibiotic effect. All other pairs were expressed and detectable via immunoblotting.

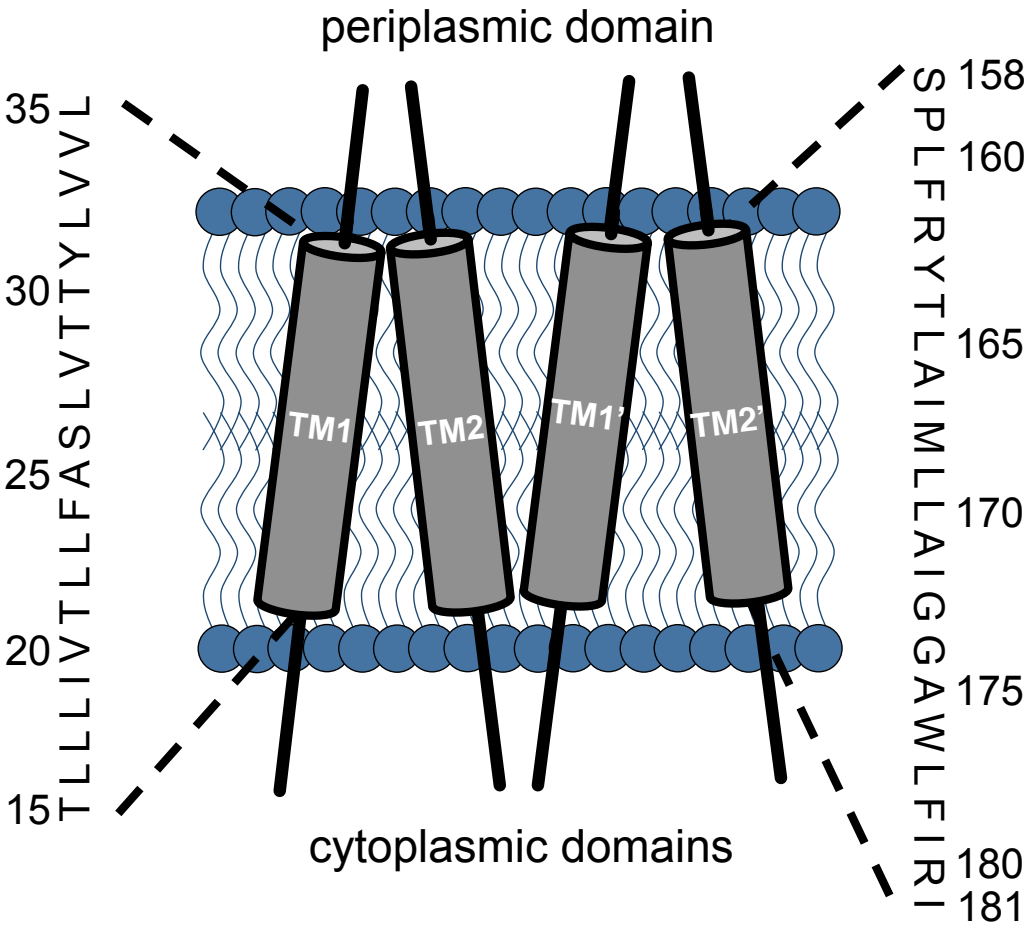

Figure 5-1: Visual depiction of TM regions targeted by cysteine mutation. A homodimer representation of EnvZ showing the transmembrane helices involved (TM1, TM2, TM1', TM2'). The residues from which the library pairings were selected from are detailed. Residues L16 and L22 did not successfully form a 2X-Cys mutation with any of their chosen pairings. Residue L32 was not successfully created as a 1X-Cys mutant with therefore was not attempted for 2X-Cys mutations. The range of residues was selected on the basis of their inclusion within the helix structure that is located within the membrane.

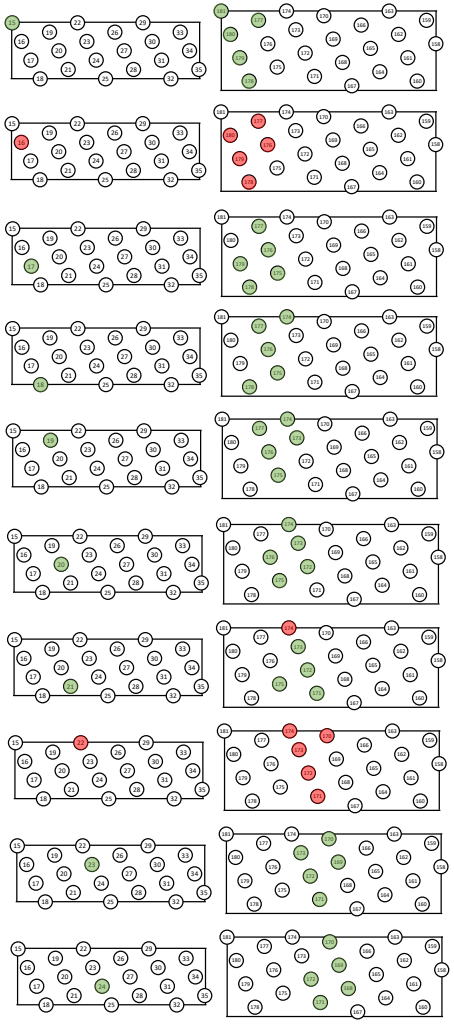

Mutant (Single Code version)	Mutant (number version)	Mutant (Single Code version)	Mutant (number version)
T15C / L177C	15-177	A25C / I167C	25-167
T15C / F178C	15-178	A25C / M168C	25-168
T15C / I179C	15-179	A25C / L169C	25-169
T15C / R180C	15-180	A25C / L170C	25-170
T15C / I181C	15-181	A25C / A171C	25-171
L16C / W176C*	16-176*	S26C / A166C	26-166
L16C / L177C*	16-177*	S26C / I167C	26-167
L16C / F178C*	16-178*	S26C / M168C	26-168
L16C / I179C*	16-179*	S26C / L169C	26-169
L16C / R180C*	16-180*	S26C / L170C	26-170
L17C / A175C	17-175	L27C / L165C	27-165
L17C / W176C	17-176	L27C / A166C	27-166
L17C / L177C	17-177	L27C / I167C	27-167
L17C / F178C	17-178	L27C / M168C	27-168
L17C / I179C	17-179	L27C / L169C	27-169
L18C / G174C	18-174	V28C / T164C	28-164
L18C / A175C	18-175	V28C / L165C	28-165
L18C / W176C	18-176	V28C / A166C	28-166
L18C / L177C	18-177	V28C / I167C	28-167
L18C / F178C	18-178	V28C / M168C	28-168
I19C / G173C	19-173	T29C / Y163C	29-163
I19C / G174C	19-174	T29C / T164C	29-164
I19C / A175C	19-175	T29C / L165C	29-165
I19C / W176C	19-176	T29C / A166C	29-166
I19C / L177C	19-177	T29C / I167C	29-167
V20C / I172C	20-172	T30C / R162C	30-162
V20C / G173C	20-173	T30C / Y163C	30-163
V20C / G174C	20-174	T30C / T164C	30-164
V20C / A175C	20-175	T30C / L165C	30-165
V20C / W176C	20-176	T30C / A166C	30-166
T21C / A171C	21-171	Y31C / F161C	31-161
T21C / I172C	21-172	Y31C / R162C	31-162
T21C / G173C	21-173	Y31C / Y163C	31-163
T21C / G174C*	21-174*	Y31C / T164C	31-164
T21C / A175C	21-175	Y31C / L165C	31-165
L22C / L170C*	22-170*	V33C / L160C	33-160
L22C / A171C*	22-171*	V33C / F161C	33-161
L22C / I172C*	22-172*	V33C / R162C	33-162
L22C / G173C*	22-173*	V33C / Y163C	33-163
L22C / G174C*	22-174*	V33C / T164C	33-164
L23C / L169C	23-169	V34C / P159C	34-159
L23C / L170C	23-170	V34C / L160C	34-160
L23C / A171C	23-171	V34C / F161C	34-161
L23C / I172C	23-172	V34C / R162C	34-162
L23C / G173C	23-173	V34C / Y163C	34-163
F24C / M168C	24-168	L35C / S158C	35-158
F24C / L169C	24-169	L35C / P159C	35-159
F24C / L170C	24-170	L35C / L160C	35-160
F24C / A171C	24-171	L35C / F161C	35-161
F24C / I172C	24-172	L35C / R162C	35-162

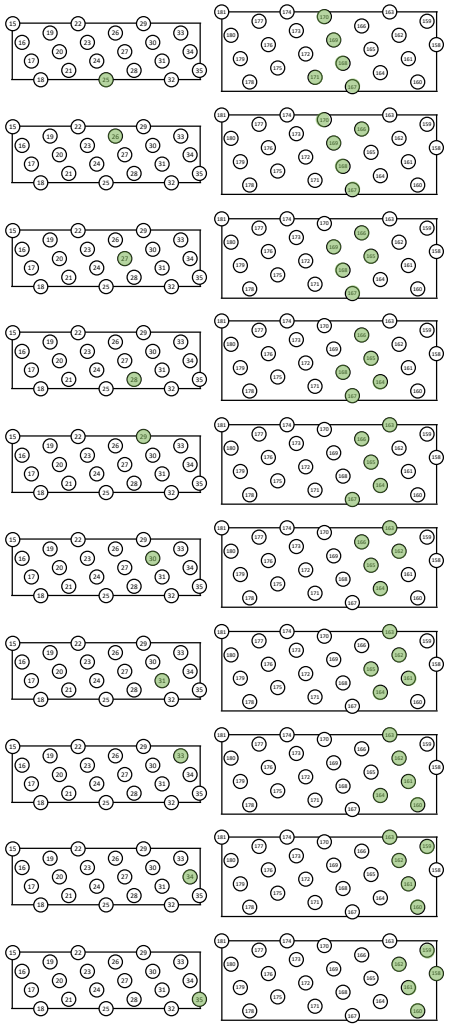

Figure 5-2: Mutant pairings accompanied by helical net depictions. Double-cysteine mutant pairings are displayed with a TM1 (15-35) and TM2 (158-181) helical net diagram to visually demonstrate the relative locations of pairing groups. Green circles indicate mutant pairings that successfully grew within an experimental strain of *E. coli* (EPB30) and red circles indicate mutant pairings that did not successfully grow within EPB30.

5.2: Sulphydryl-reactivity analysis *in vivo*

Sulphydryl-reactivity analysis has been previously employed on a wide range of membrane-spanning and soluble protein as well as higher order systems (150–152). The methodology also allows *in vivo* analysis of protein function, thus allowing EnvZ to retain its natural environment in the presence of all accessory proteins that may have modulatory functions upon EnvZ activity. An additional benefit to *in vivo* experimentation is that it allows us to record changes in signal output via a dual-colour fluorescence reporter system that have been simultaneously employed to identify position-pairings that are not tolerant to their mutations. Overall, using this *in vivo* assay we were able to map interactions within the transmembrane helix bundle under distinct osmotic conditions. This allows us to create a more complex picture of the mechanisms within the transmembrane sections of EnvZ during signal transduction.

The results from these experiments have revealed a distinct difference to reactivity experimentation involving a 1X-Cys residue (**Figure 5-3**). Several 2X-Cys mutants exhibited more than one dimer band and multiple separate interactions were possible. As each of the three possible interactions would be connected via a significantly different point along the protein structure, it is proposed that this affects their dynamics through polyacrylamide gel**.** Mutants displaying TM1-TM1' interactions migrated furthest, mutants displaying TM2-TM2' interactions migrated least far and mutants displaying TM1-TM2' interactions migrated a distance between the other two. Further to this, it was necessary to identify dimer bands and attribute them to one of the aforementioned interactions. This was achieved by running 2X-Cys mutants adjacent to their 1X-Cys constituents and lining up matching bands (**Figure 5-4**). The band identities are summarised in **Table 5-5**. With the above method of band identification, multiple 2X-Cys mutants were identified that did not produce bands as they may have been predicted. As an example of this, mutant both 19 and 175 showed strong dimer bands from 1X-Cys data yet the 2X-Cys combination of these mutants (19-175) produced only one band which aligned to the TM1-TM1' band. This shows that the 175 interaction has been lost,

suggesting the 19-19' interaction is stronger and perhaps more important to EnvZ transmembrane function.

Quantified bands were used to calculate a D/M ratio, which indicates the propensity for the crosslinking interaction (**Figure 5-6**). Where no dimer was detectable, it was deemed that there was to be no interaction and the D/M ratio has been reported as zero. In cases of 2 or more detectable bands, an overall dimer versus monomer ratio was calculated as well as individual dimers versus the sum of remaining bands, including other dimers. The latter calculation allowed measurement of specific interaction strengths where multiple bands were present. These calculations have been used to grade the interaction intensities across all helical wheel and net diagrams (**Figures 5-7, 5-8 and 5-9**). With signal, the 1-2' interactions become weaker at the periplasm proximal third of the helices as well as the area of interaction shifting towards the periplasmic space. This may suggest the helices are opening to allow access to a space between the helices. Of the 24 2X-Cys mutants that showed altered bands upon stimulus, 12 showed an addition of a band or bands and 12 showed a loss of a band or bands (**Table 5-5**). Within the cytoplasmic end, three mutants showed addition and two mutants showed loss. Within the membrane core, four mutants showed addition and four showed loss. Within the periplasmic end, five showed addition and six showed loss. The changes are seen mostly within the periplasmic end, suggesting stimulus has a significant effect upon the conformation of this area. The changes seen within the membrane core do not involve 1-2' interactions as they are not present throughout the entirety of this helix section. There is some change seen in the cytoplasmic end of the helices, but it shows the least movement of the three sections.

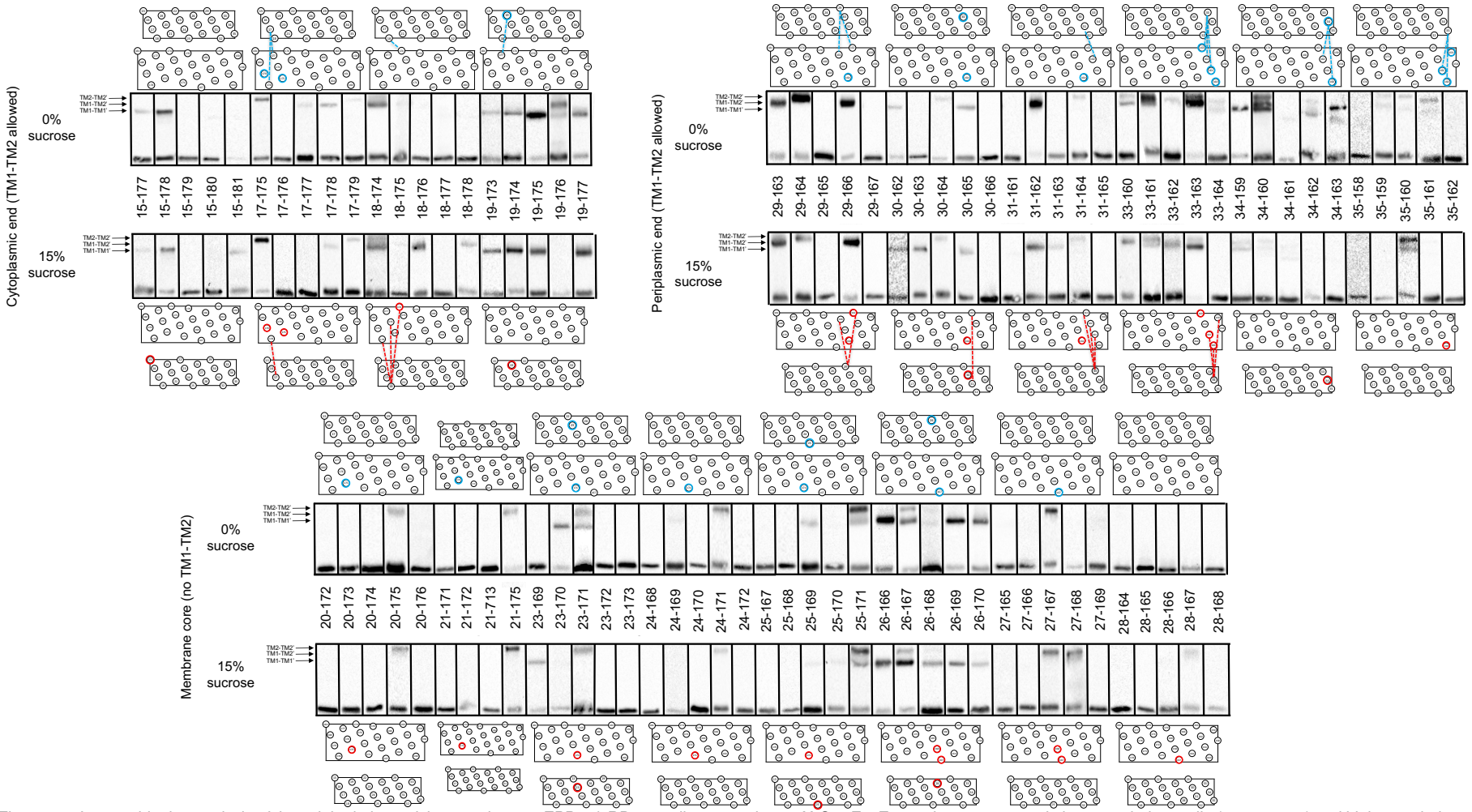

Figure 5-3: Immunoblotting analysis of the sulphydryl-reactivity experiments. EPB30/pRD400 cells expressing a 2X-Cys EnvZ mutation were grown in low osmolarity media (0% sucrose) and high osmolarity media (15%) until an OD_{600nm} of 0.3 ± 0.1 was reached. 250μM of Iodine was added to the culture for 10 minutes which resulted in the presence of dimeric EnvZ formations double the molecular weight of a monomeric EnvZ formation. Therefore, the dimeric formations migrated through the gel more slowly than the monomeric formations. Separate dimer formations were possible, which each migrated a distinctly different distance – the slowest of these interactions was the 2-2' interaction and the fastest dimer formation was the 1-1' interaction. The 1-2' interaction migrated between these two distances. Beside each set of five mutants (e.g. 15-177 to 15-181) is a pair of helical nets for both TM1 and TM2. The circles (blue = 0% sucrose, red = 15% sucrose) represent either TM1-TM1' or TM2-TM2' interactions. Dashed lines represent TM1-TM2' interactions between the connected residues. These interactions have been combined and into helical wheel and helical net figures (**Figure 5-7, 5-8 and 5-9**). The mutant library has been divided into three sections based on the 1-2' interactions observed and their position relative to protein orientation within the membrane: Cytoplasmic end (15-177 to 19-177), Membrane core (20-172 to 28-168) and Periplasmic end (29-163 to 35-162). (n=2, monomer only. n=3-8, dimer present)

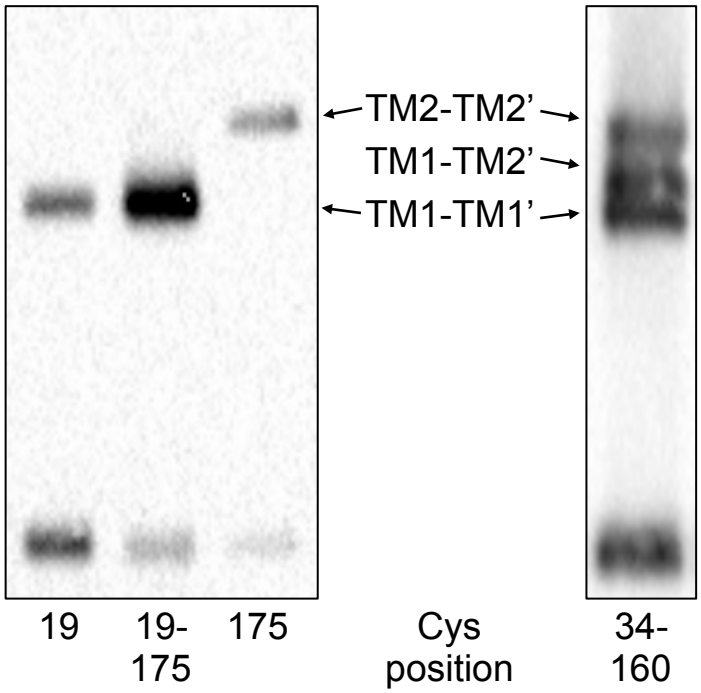

Figure 5-4: 2X-Cys mutants produce multiple dimeric formations. (Left) The 19-175 mutant was run adjacent to its 1X-Cys mutation constituents to ascertain band identity. In this instance, the band formed is shown to be a 1-1' interaction and the 2-2' interaction has been lost. (Right) The 34-160 mutant is the only example within the library in which all three dimer formations have occurred, thus proving three distinct interactions can occur.

Mutant	1X-CYS 1-1' 0%	1X-CYS 1-1' 15%	1X-CYS 2-2' 0%	1X-CYS 2-2' 15%	0% SUCROSE 2X-CYS #	0% SUCROSE 2X-CYS 1-1'	0% SUCROSE 2X-CYS 1-2'	0% SUCROSE 2X-CYS 2-2'	15% SUCROSE 2X-CYS #	15% SUCROSE 2X-CYS 1-1'	15% SUCROSE 2X-CYS 1-2'	15% SUCROSE 2X-CYS 2-2'	Δ 1-1' 0%	Δ 1-1' 15%	Δ 2-2' 0%	Δ 2-2' 15%	0% → 15%
15-177	L	L	-	-	1	✓	×	×	1	✓	×	×					
15-178	L	L	-	-	1	✓	×	×	1	✓	×	×					
15-179	L	L	L	L	0	×	×	×	0	×	×	×	(-)	(-)	(-)	(-)	
15-180	L	L	-	-	0	×	×	×	0	×	×	×	(-)	(-)			
15-181	L	L	-	-	0	×	×	×	1	✓	×	×	(-)				
17-175	-	-	**H**	H	1	×	×	✓	1	×	×	✓					
17-176	-	-	-	-	0	×	×	×	0	×	×	×					
17-177	-	-	-	-	1	×	✓	×	0	×	×	×					
17-178	-	-	-	-	1	×	✓	×	1	×	✓	×					
17-179	-	-	L	L	1	×	×	✓	1	×	×	✓					
18-174	-	-	-	-	2	×	✓	✓	2	×	✓	✓			(+)	(+)	
18-175	-	-	**H**	H	0	×	×	×	0	×	×	×			(-)	(-)	
18-176	-	-	-	-	0	×	×	×	1	×	✓	×					
18-177	-	-	-	-	0	×	×	×	0	×	×	×					
18-178	-	-	-	-	0	×	×	×	1	×	✓	×					
19-173	M	M	-	-	1	✓	×	×	1	✓	×	×					
19-174	M	M	-	-	1	✓	×	×	1	✓	×	×					
19-175	M	M	**H**	H	1	✓	×	×	1	✓	×	×			(-)	(-)	
19-176	M	M	-	-	2	✓	✓	×	0	×	×	×		(-)			
19-177	M	M	-	-	1	✓	×	×	1	✓	×	×					
20-172	-	-	**H**	H	0	×	×	×	0	×	×	×			(-)	(-)	

20-173	-	-	-	-	0	×	×	×	0	×	×	×					
20-174	-	-	-	-	0	×	×	×	0	×	×	×					
20-175	-	-	**H**	H	1	×	×	✓	1	×	×	✓					
20-176	-	-	-	-	0	×	×	×	0	×	×	×					
21-171	-	-	-	-	0	×	×	×	0	×	×	×					
21-172	-	-	**H**	H	0	×	×	×	0	×	×	×			(-)	(-)	
21-173	-	-	-	-	0	×	×	×	0	×	×	×					
21-175	-	-	**H**	H	1	×	×	✓	1	×	×	✓					
23-169	H	H	-	-	0	×	×	×	1	✓	×	×	(-)				
23-170	H	H	-	-	1	✓	×	×	0	×	×	×		(-)			
23-171	H	H	**H**	H	2	✓	×	✓	1	×	×	✓		(-)			
23-172	H	H	-	-	0	×	×	×	0	×	×	×	(-)	(-)			
23-173	H	H	-	-	0	×	×	×	0	×	×	×	(-)	(-)			
24-168	-	-	L	L	0	×	×	×	0	×	×	×			(-)	(-)	
24-169	-	-	-	-	0	×	×	×	0	×	×	×					
24-170	-	-	-	-	0	×	×	×	0	×	×	×					
24-171	-	-	**H**	H	1	×	×	✓	1	×	×	✓					
24-172	-	-	-	-	0	×	×	×	0	×	×	×					
25-167	L	L	M	M	0	×	×	×	0	×	×	×	(-)	(-)	(-)	(-)	
25-168	L	L	L	L	0	×	×	×	0	×	×	×	(-)	(-)	(-)	(-)	
25-169	L	L	-	-	1	✓	×	×	0	×	×	×		(-)			
25-170	L	L	-	-	0	×	×	×	0	×	×	×	(-)	(-)			
25-171	L	L	**H**	H	2	✓	×	✓	2	✓	×	✓					
26-166	H	H	-	-	1	✓	×	×	1	✓	×	×					

26-167	H	H	M	M	2	✓	×	✓	2	✓	×	✓				
26-168	H	H	L	L	2	✓	×	✓	1	✓	×	×				(-)
26-169	H	H	-	-	1	✓	×	×	1	✓	×	×				
26-170	H	H	-	-	1	✓	×	×	1	✓	×	×				
27-165	-	-	-	-	0	×	×	×	0	×	×	×				
27-166	-	-	-	-	0	×	×	×	0	×	×	×				
27-167	-	-	M	M	1	×	×	✓	1	×	×	✓				
27-168	-	-	L	L	0	×	×	×	1	×	×	✓			(-)	
27-169	-	-	-	-	0	×	×	×	0	×	×	×				
28-164	-	-	L	L	0	×	×	×	0	×	×	×			(-)	(-)
28-165	-	-	-	-	0	×	×	×	0	×	×	×				
28-166	-	-	-	-	0	×	×	×	0	×	×	×				
28-167	-	-	M	M	0	×	×	×	1	×	×	✓			(-)	
28-168	-	-	L	L	0	×	×	×	1	×	×	✓			(-)	
29-163	-	-	-	-	1	×	✓	×	1	×	✓	×				
29-164	-	-	L	L	1	×	×	✓	1	×	×	✓				
29-165	-	-	-	-	0	×	×	×	0	×	×	×				
29-166	-	-	-	-	1	×	✓	×	1	×	✓	×				
29-167	-	-	M	M	0	×	×	×	0	×	×	×			(-)	(-)
30-162	M	H	-	-	1	✓	×	×	1	✓	×	×				
30-163	M	H	-	-	0	×	×	×	1	✓	×	×	(-)			
30-164	M	H	L	L	1	×	×	✓	1	×	×	✓	(-)	(-)		
30-165	M	H	-	-	1	✓	×	×	1	✓	×	×				
30-166	M	H	-	-	0	×	×	×	0	×	×	×	(-)	(-)		

31-161	-	-	L	-	0	×	×	×	0	×	×	×		(-)	
31-162	-	-	-	-	1	×	✓	×	1	×	✓	×			
31-163	-	-	-	-	0	×	×	×	1	×	✓	×			
31-164	-	-	L	L	1	×	×	✓	1	×	×	✓			
31-165	-	-	-	-	0	×	×	×	0	×	×	×			
33-160	-	-	M	L	2	×	✓	✓	1	×	✓	×			(-)
33-161	-	-	L	-	1	×	×	✓	2	×	✓	✓			(+)
33-162	-	-	-	-	1	×	✓	×	1	×	✓	×			
33-163	-	-	-	-	2	×	✓	✓	2	×	✓	✓			(+)
33-164	-	-	L	L	2	×	✓	✓	0	×	×	×			(-)
34-159	L	L	-	-	1	✓	×	×	2	×	✓	✓	(-)		
34-160	L	L	M	L	3	✓	✓	✓	2	✓	✓	×			(-)
34-161	L	L	L	-	1	✓	×	×	2	✓	✓	×		(-)	
34-162	L	L	-	-	2	✓	✓	✓	0	×	×	×	(-)		
34-163	L	L	-	-	1	✓	×	×	0	×	×	×	(-)		
35-158	-	-	L	-	0	×	×	×	0	×	×	×		(-)	
35-159	-	-	-	-	2	×	✓	✓	0	×	×	×			
35-160	-	-	M	L	2	×	✓	✓	2	×	✓	✓			
35-161	-	-	L	-	1	×	✓	✓	0	×	×	×			
35-162	-	-	-	-	0	×	×	×	0	×	×	×			

Table 5-5: Comparison of immunoblotting results collected for 1X-Cys mutants to results collected for 2X-Cys mutants resulting in band identification. Results collected for 1X-Cys mutants (118, 147) are compared and contrasted to results collected for 2X-Cys mutants in order to identify the bands that are created. The delta column describes where bands appear (+) or are lost (-) as well as the final column (0% to 15%) which indicated if a band is gained upon stimulus perception (green) or lost upon stimulus perception (red). The table is divided into the sections detailed in **Figure 5-3**, Cytoplasmic end (Purple, 12' interactions present), Membrane Core (Orange, 12' interactions not present) and Periplasmic end (Turquoise, 12' interactions present).

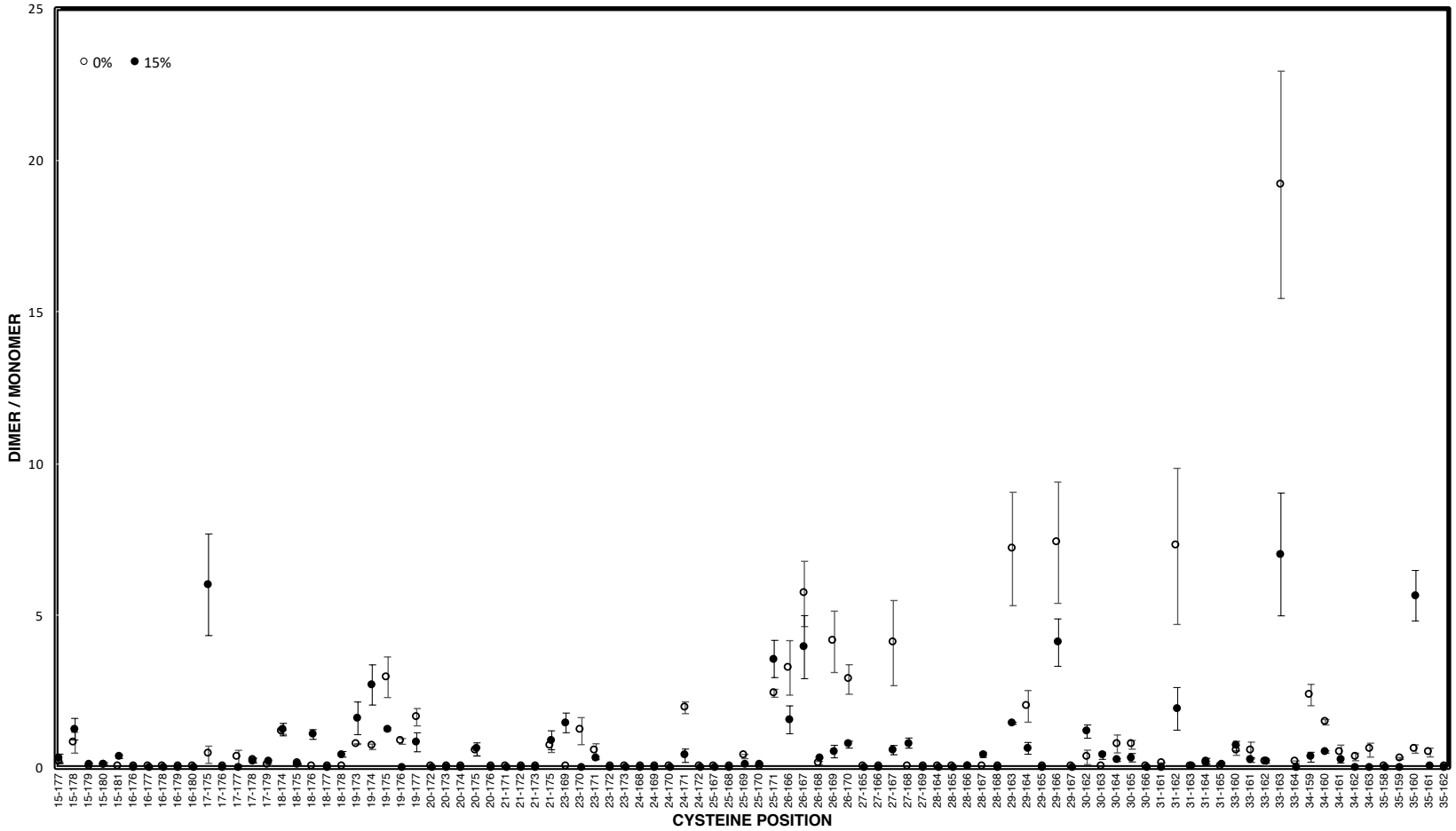

Figure 5-6: Extent of sulphydryl-reactivity for each 2X-Cys containing EnvZ mutant. EPB30/pRD400 cells were grown in low osmolarity media (0% sucrose, empty circles) or high osmolarity media (15% sucrose, filled circles) and subjected to 250 μM molecular iodine for 10 minutes until their OD_{600nm} reached 0.3±0.1. The quantified band intensities for both monomer and dimer(s) are used to calculate a dimer/monomer ratio, the mean values of which are represented in this figure. Error bars represent the standard error of the mean dimer/monomer ratio with a sample size of n=2 for monomer only mutants (ratio recorded as zero) and n≥3 if a dimer or dimers were present.

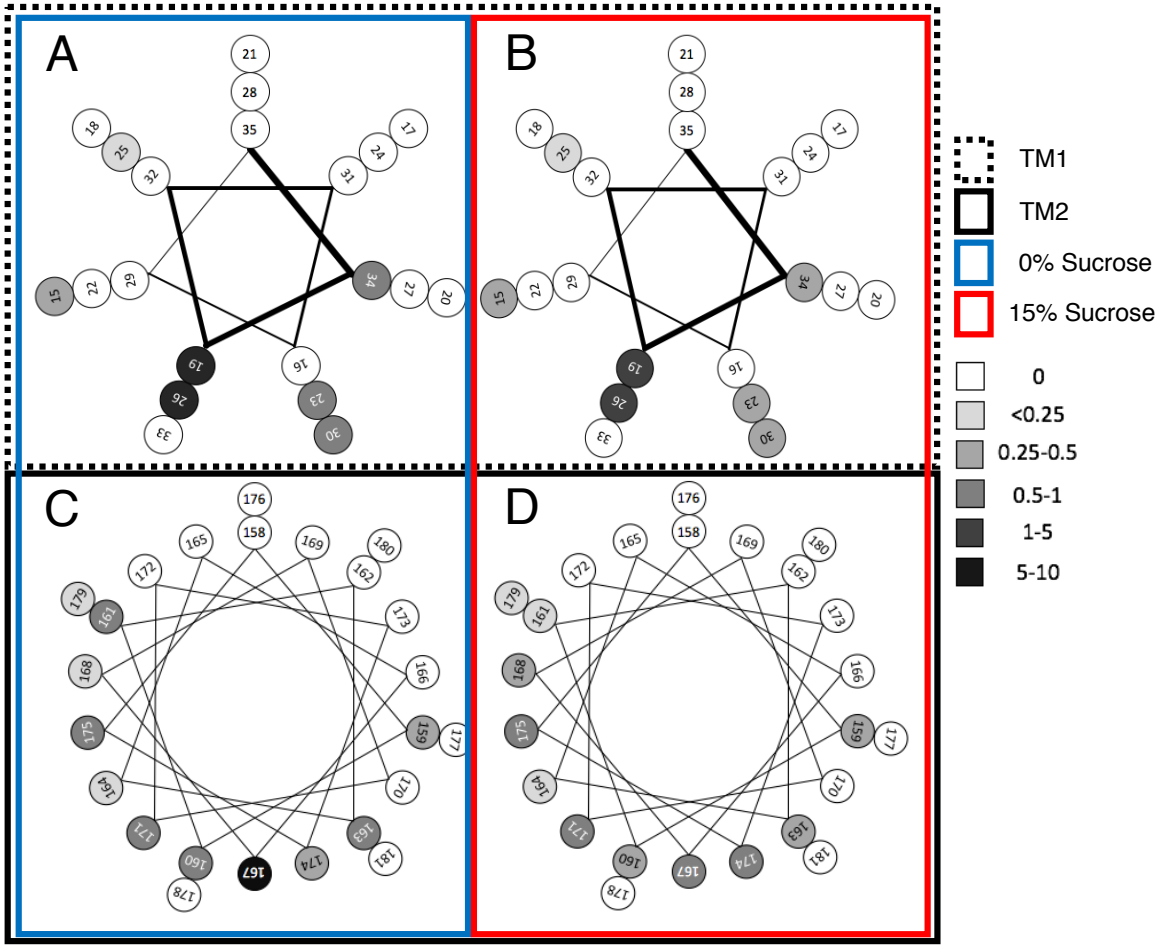

Figure 5-7: Helical wheel diagrams depicting TM1-TM1' and TM2-TM2' interactions within 2X-Cys containing EnvZ mutants. (A) TM1 in a coiled-coil helical formation showing the intensity of D/M ratios calculated for each residue interaction under low osmolarity conditions. (B) TM1 in a coiled-coil helical formation showing the intensity of D/M ratios calculated for each residue interaction under high osmolarity conditions. (C) TM2 in an alpha helical formation showing the intensity of D/M ratios calculated for each residue interaction under low osmolarity conditions. (D) TM2 in an alpha helical formation showing the intensity of D/M ratios calculated for each residue interaction under high osmolarity conditions. Interaction intensities are classified by shade, the classes are detailed in the key to the right of the figure.

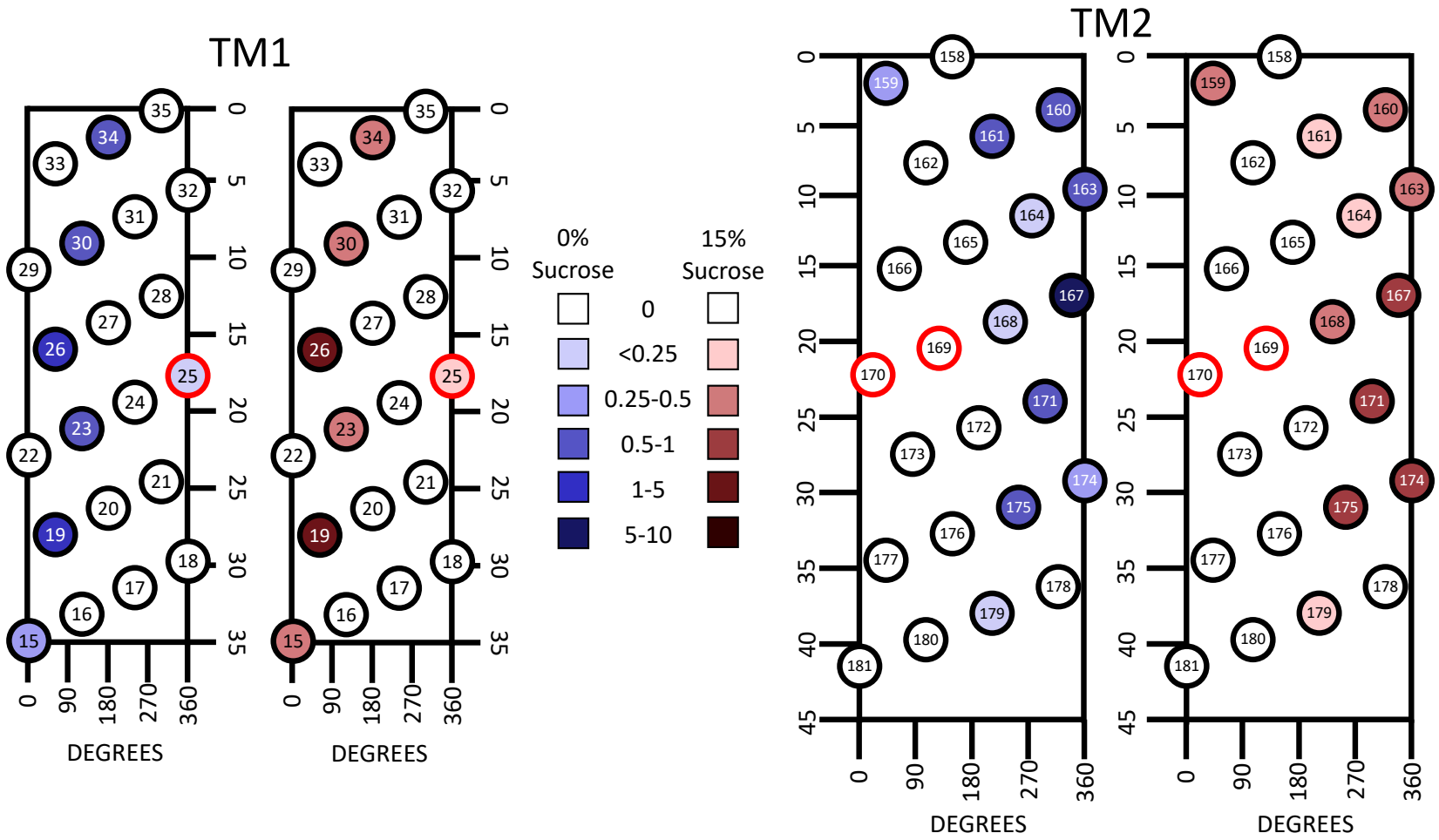

Figure 5-8: Helical net diagrams depicting 1-1' and 2-2' interactions within 2X-Cys containing EnvZ mutants. TM1 (left) and TM2 (right) interactions under low osmolarity (graded blue circles) and high osmolarity (graded red circles). The TM1 helical net is arranged in a coiled coil format and the TM2 helical net is arranged in an alpha helical format. The colour intensities indicate the dimer/monomer ratio for the interactions that are observed. These values are described in the key central to the figure. The central residue within the TM helices is shown via a red circle – TM1=residue 25, TM2= residues 169 & 170).

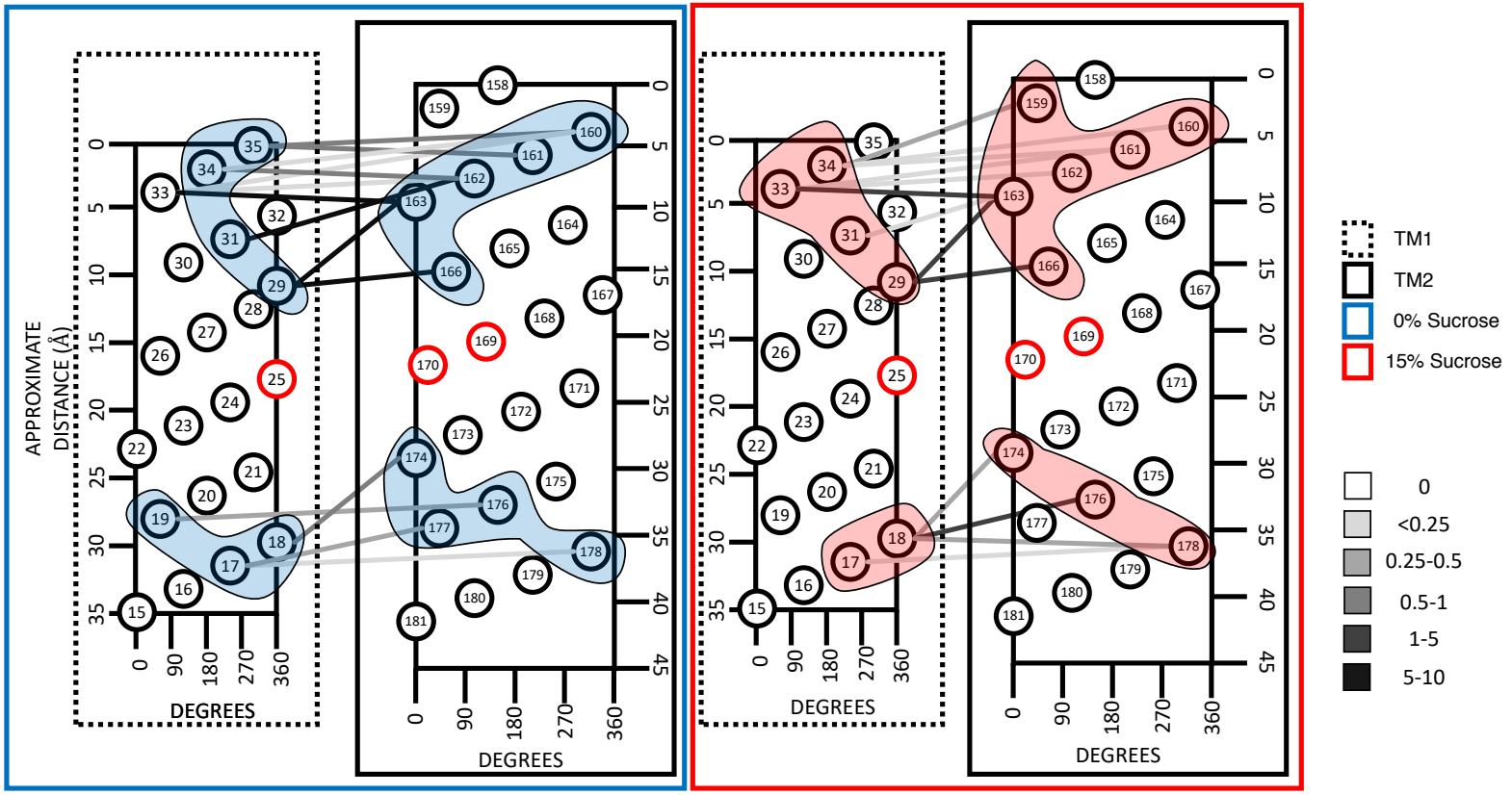

Figure 5-9: Helical net diagrams depicting 1-2' interactions within 2X-Cys containing EnvZ mutants. (Blue area) 1-2' interactions, their intensities and the interaction surfaces, shaded in blue, assumed by these interactions. These samples were grown under low osmolarity conditions. (Red area) 1-2' interactions, their intensities and the interaction surfaces, shaded in red, assumed by these interactions. These samples were grown under high osmolarity conditions. (Interaction intensities are classified by shade; the classes are detailed in the key to the right of the figure. The central residue within the TM helices is shown via a red circle – TM1=residue 25, TM2= residues 169 & 170).

5.2: Baseline helix orientation

Firstly, it has been necessary to ascertain the specific helical formation for both TM1 and TM2 to ensure that the data can be interpreted correctly. Deepcoil (153) showed significant probability of a coiled-coil (CC) formation across 68% of TM1 residues but no significant CC formation was detected within TM2 (**Figure 5-10**). As 5 residues within the periplasmic end of TM1 are not likely to form a CC helix, this section of the protein could be more dynamic during dimer interaction. This supports the suggestion of movement within the periplasmic end of the four-transmembrane helix bundle as this region displays the most movement via immunoblotting data also. Based on this, both helical wheel and helical net diagrams were utilised to judge areas of interaction that have been evidenced from our data.

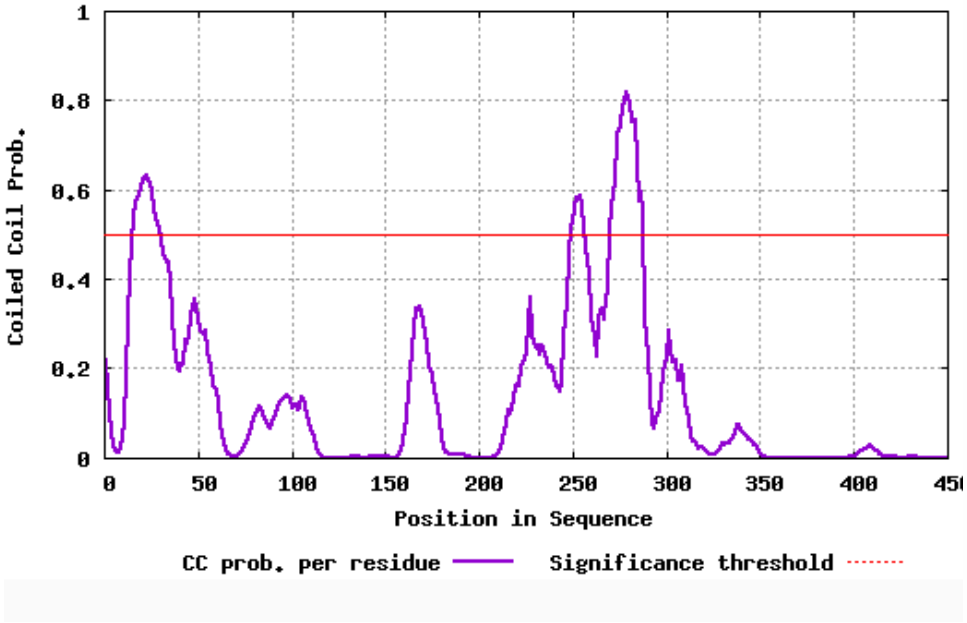

TM1

Res No.	AA	CC Prob
15	T	0.484
16	L	0.535
17	L	0.568
18	L	0.582
19	I	0.588
20	V	0.601
21	T	0.625
22	L	0.623
23	L	0.630
24	F	0.618
25	A	0.611
26	S	0.596
27	L	0.555
28	V	0.535
29	T	0.525
30	T	0.511
31	Y	0.489
32	L	0.459
33	V	0.437
34	V	0.439
35	L	0.394

TM2

Res No.	AA	CC Prob
158	S	0.006
159	P	0.015
160	L	0.037
161	F	0.088
162	R	0.149
163	Y	0.194
164	T	0.239
165	L	0.290
166	A	0.334
167	I	0.328
168	M	0.339
169	L	0.325
170	L	0.304
171	A	0.272
172	I	0.259
173	G	0.203
174	G	0.199
175	A	0.181
176	W	0.148
177	L	0.132
178	F	0.111
179	I	0.081
180	R	0.040
181	I	0.024

Figure 5-10: Identification of helix formation for TM1 and TM2 using Deepcoil. Residues within the TM1 helix overcome the threshold for coiled coil probability indicating a coiled coil (CC) helical structure is adopted within the majority of TM1 (highlighted in grey). 6 TM1 residues (15, 31-35) lie underneath the threshold for CC formation. No residues within the TM2 helix overcome the CC formation threshold, thus it can be concluded that TM2 does not adopt a CC formation.

5.3: Changes upon stimulus perception

Several notable differences between results attained with and without stimulus have been detected. For TM1-TM1' and TM2-TM2' interactions there appears to be a consistent region of interaction that carries through the entire length of the helix, which alters slightly by strength of interaction in the case of the TM2-TM2' interface (**Figures 5-7 and 5-8**). However, the interactions observed for TM1-TM2' have shown to occur at the lower and upper quarters only, with no TM1-TM2' interactions detectable between mutants 19-177 through 28-168 (40 mutants) both with and without stimulus (**Figure 5-9**). This suggests a space is created within that area during the dimer formation, which could have a functional role in the signal perception process. Additionally, there were detected changes in the interactions observed at the periplasmic region during signal perception, specifically the interactions become weaker in the presence of stimulus. This suggests the positions move apart, potentially allowing access to the aforementioned space created between the two transmembrane helices. This theory aligns to data previously collected within a TM2-based 1X-Cys library (137) as differences in immunoblotting data were observed in the periplasmic and cytoplasmic sections of TM2 with and without stimulus. Also, a tilting motion was observed via *in silico* molecular dynamics screening which indicates TM2 and TM2' shift position relative to one another in the presence of stimulus. This movement may also account for changes observed within the 12' interactions recorded within the 2X-Cys data set. As no changes are observed within the interaction surfaces of TM1 and TM1' (104), it can be concluded that these helices are stable in their position throughout signal transduction and could therefore anchor the protein thus allowing the TM2 helices to shift conformation more steadily. At this point, it can only be theorised how these interactions combine into an overall model and further analyses will be required to confirm the theoretical model displayed here (**Figure 5-11**).

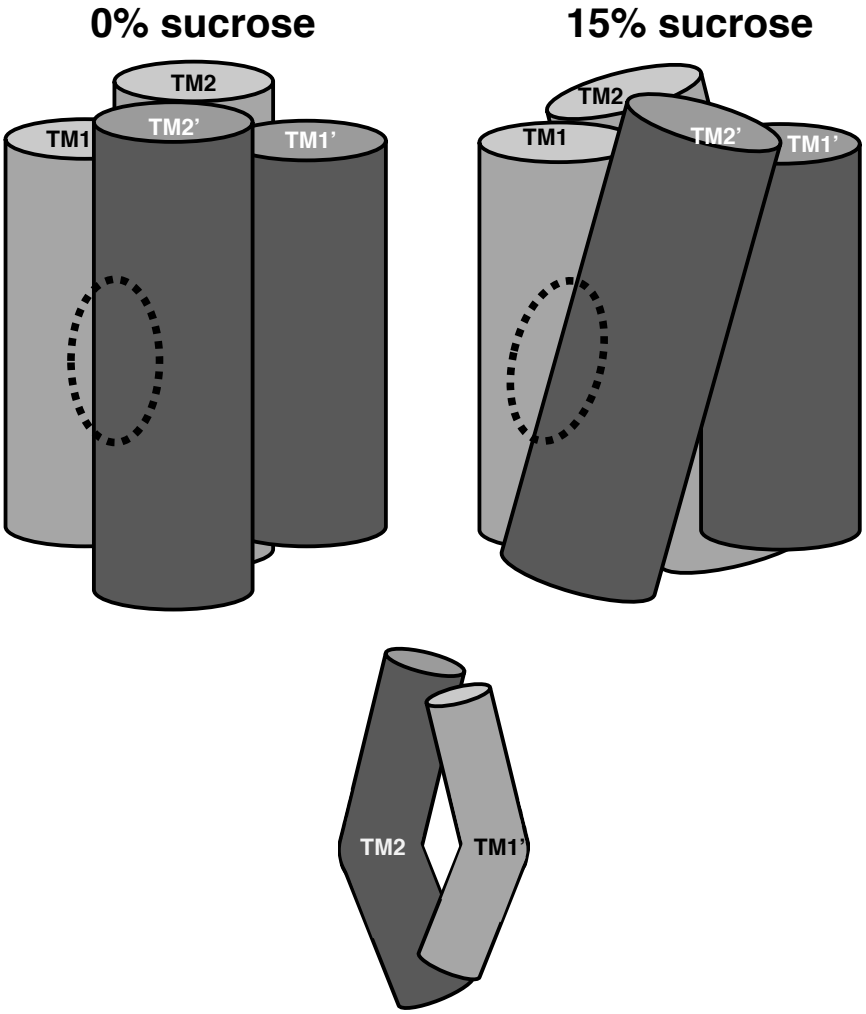

Figure 5-11: Proposal of a non-piston model for EnvZ transmembrane helix movement. This model combines the outcomes of the three cysteine studies detailed within this work and depicts the transmembrane four helix bundle. The dark grey helices represent one EnvZ monomer (TM1 and TM2) and the light grey helices represent the EnvZ monomer that dimerises onto the first (TM1' and TM2'). The larger images show the four-helix bundle in the absence (0% sucrose, left) and presence (15% sucrose, right) of stimulus. The dotted area shows an absence of interaction between TM1 and TM2' (and vice versa) which is also demonstrated with two helices below. Notably, interactions are present within the periplasmic and cytoplasmic regions of the TM1-TM2' interface. At the periplasmic end, evidence of changes in crosslinking was detected upon presence of stimulus. The TM2 helices are shown as moving apart, towards their own TM partner hence the change in TM1-TM2' interactions in this region. Also the TM1 helices remain stationary as no changes were seen in their interaction profile. These changes are detailed two-dimensionally in **Figure 5-8 and 5-9**.

5.4: Signal output of the double cysteine library

Throughout the entire working 2X-Cys library, CFP and YFP levels were recorded under both low (**Figure 5-12A**) and high (**Figure 5-12B**) osmolarity growth. After correction via both optical density of the cells grown and subtraction of MG1655 baseline values, a CFP/YFP ratio was calculated (**Figure 5-13**). The corrected CFP and YFP (cCFP and cYFP) values were averaged for each mutant then compared to control data collected from a Cys-less mutant, C277A. This mutant represents a WT (WT) response without any cysteine involvement, including the naturally occurring Cys residue at position 277. The data collected from C277A was confirmed as normally distributed via the Shapiro-Wilk test across all four populations (*p-value* > 0.05, n=23). A z-score was calculated for mean cCFP and cYFP value in each mutant under both low and high osmolarity using the corresponding C277A data as the normalised population to test within. These comparisons were arranged into 5 categories: shifted on, shifted off, low overall signal, high overall signal and no marked differences (**Table 5-13**).

Under low osmolarity conditions, z-scores of <-2 were reported for both cCFP and cYFP in three mutants (17-176, 20-176, 33-164) which represents significant reduction of signal. Six mutants reported z-scores >+2 for both CFP and YFP, signifying a marked signal output increase overall compared to WT response. Twenty-six mutants reported z-scores that suggest a shifting on compared to WT response (cCFP >+2, cYFP <-2). The remaining fifty-four mutants did not show outlier z-scores (+2<z-score>-2) for both CFP and YFP. Under high osmolarity signal output of a single mutant (17-176) shifted off (cCFP z-score <-2, cYFP z-score >+2). The remaining eighty-eight mutants did not show outlier z-scores (+2<z-score>-2) for both cCFP and cYFP.

The signal output data was juxtaposed to the crosslinking data to identify any patterns (**Table 5-14**). Of the 3 mutants that showed a significant overall reduction in signal output under low osmolarity conditions, only one showed crosslinking interactions (33-164, 1-2' and

2-2'). Although lower than WT average, the signal output under high osmolarity conditions for 33-164 were not significantly reduced, suggesting it may have retained some functionality. Of the 25 mutants that shifted on under low osmolarity conditions, over half (15, 60%) were located in the periplasm proximal third of the transmembrane helix. This area has been previously shown via the crosslinking experiments to be particularly important for TM1-TM2' interactions. Further to this, 7 of these 15 mutants display 12' interactions at low osmolarity and 13 of 15 show interactions of any kind (1-1', 2-2', 1-2'). A mutant of particular interest, 34-160, shows all 3 types of interaction and shifts on under low osmolarity conditions. It is suggested that by mutating these interaction locations, the propensity of a protein to shift into an 'on' state increases.

The substituted amino acids were listed alongside both crosslinking and signal output data in order to identify any patterns. Proline (found at position 159) and glycine (found at positions 173 and 174) have the lowest propensities of all the amino acids to allow helices to form. It would be expected that the helical formation of any mutants with these amino acids removed would become tighter or more stable as the overall helical propensity (HP) would be increased. Similarly, by replacing high helical propensity amino acids (Arginine, Leucine, Alanine) with a cysteine that has a moderate helical propensity, the helical formation could be weakened. This is of particular interest when considering TM1 as a coiled coil format as the heightened stability may be important to the regulation of signal output, thus replacing high HP amino acids with a moderate HP amino acid could have a disruptive effect on this regulation.

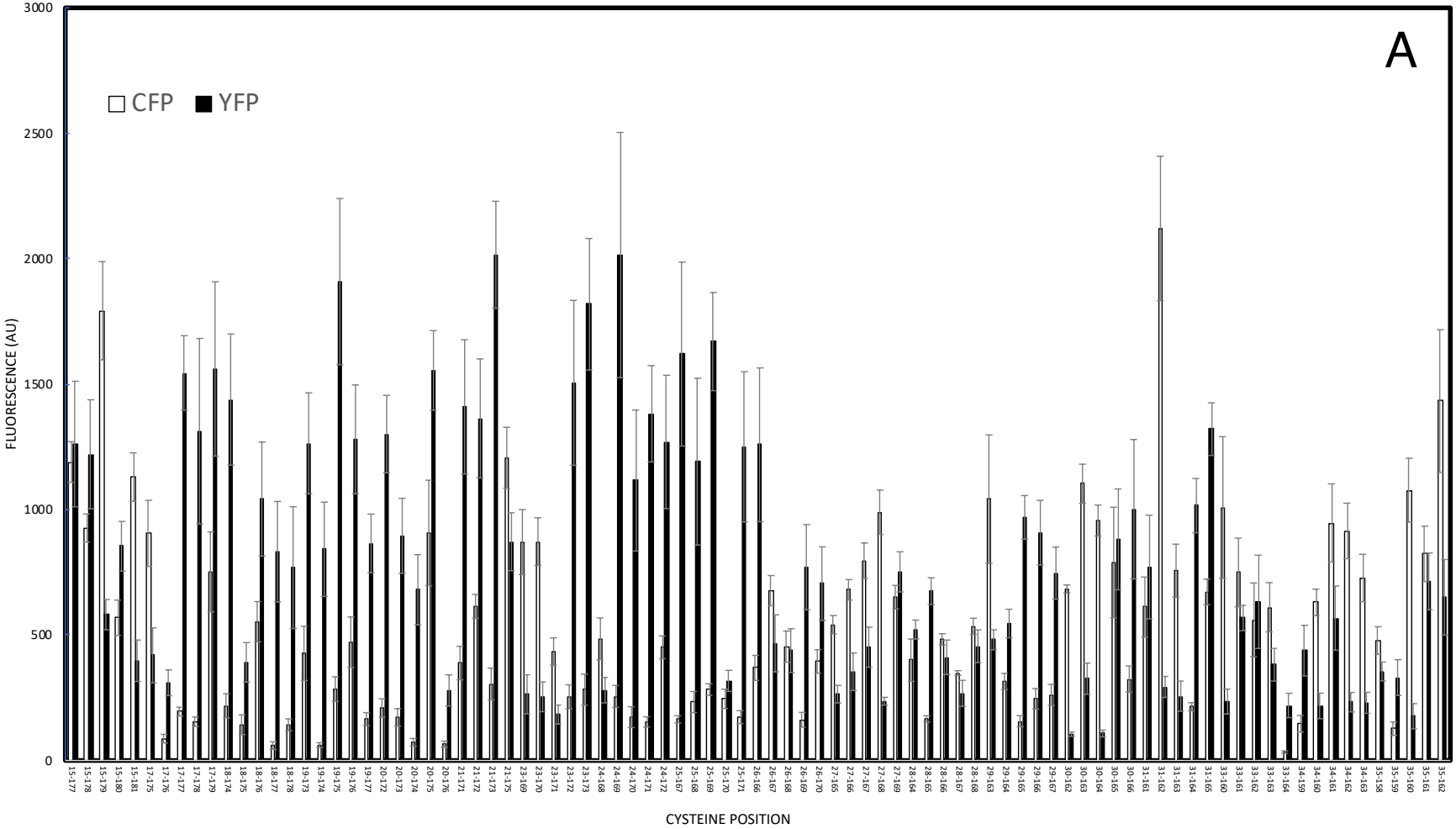
A
CFP
YFP
FLUORESCENCE (AU)
3000
2500
2000
1500
1000
500
0
CYSTEINE POSITION
15-177
15-178
15-179
15-180
15-181
17-175
17-176
17-177
17-178
17-179
18-174
18-175
18-176
18-177
18-178
19-173
19-174
19-175
19-176
19-177
20-172
20-173
20-174
20-175
20-176
21-171
21-172
21-173
21-175
23-169
23-170
23-171
23-172
23-173
24-168
24-169
24-170
24-171
24-172
25-167
25-168
25-169
25-170
25-171
26-166
26-167
26-168
26-169
26-170
27-165
27-166
27-167
27-168
27-169
28-164
28-165
28-166
28-167
28-168
29-163
29-164
29-165
29-166
29-167
30-162
30-163
30-164
30-165
30-166
31-161
31-162
31-163
31-164
31-165
33-160
33-161
33-162
33-163
33-164
34-159
34-160
34-161
34-162
34-163
35-158
35-159
35-160
35-161
35-162

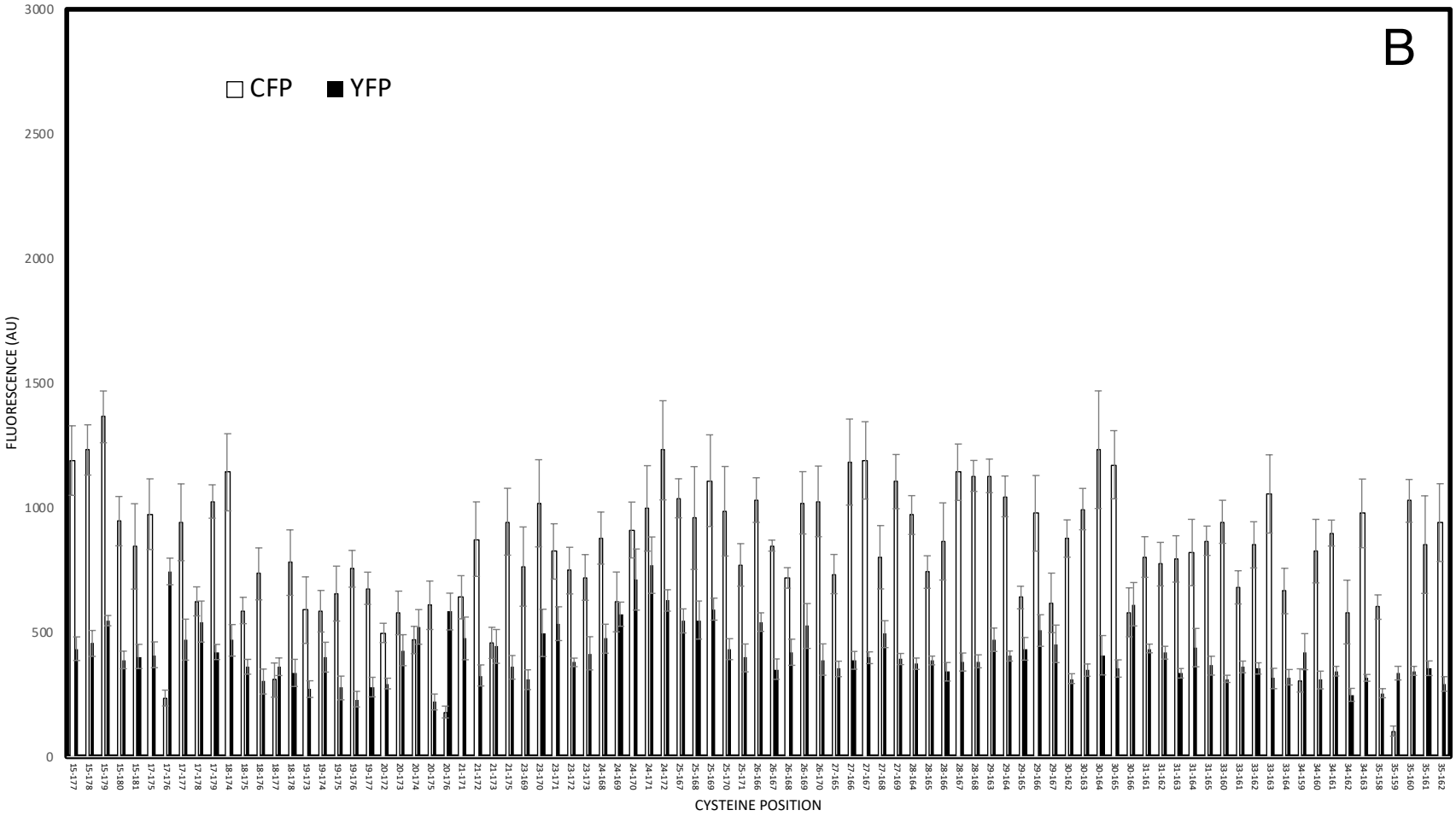

Figure 5-12: Signal output from the 2X-Cys containing EnvZ mutants. (A) CFP (empty bars) and YFP (filled bars) mean fluorescence values collected from EPB30/pRD400 cells expressing a 2X-Cys mutation grown under low osmolarity conditions to an OD_{600nm} of 0.3±0.1, corrected for OD and the estimated background signal (MG1655 CFP and YFP fluorescence output) is subtracted. (B) CFP (empty bars) and YFP (filled bars) mean fluorescence values collected from EPB30/pRD400 cells expressing a 2X-Cys mutation grown under high osmolarity conditions to an OD_{600nm} of 0.3±0.1, corrected for OD and the estimated background signal (MG1655 CFP and YFP fluorescence output) is subtracted. Error bars represent the standard error of the mean in a sample with an $n \geq 3$.

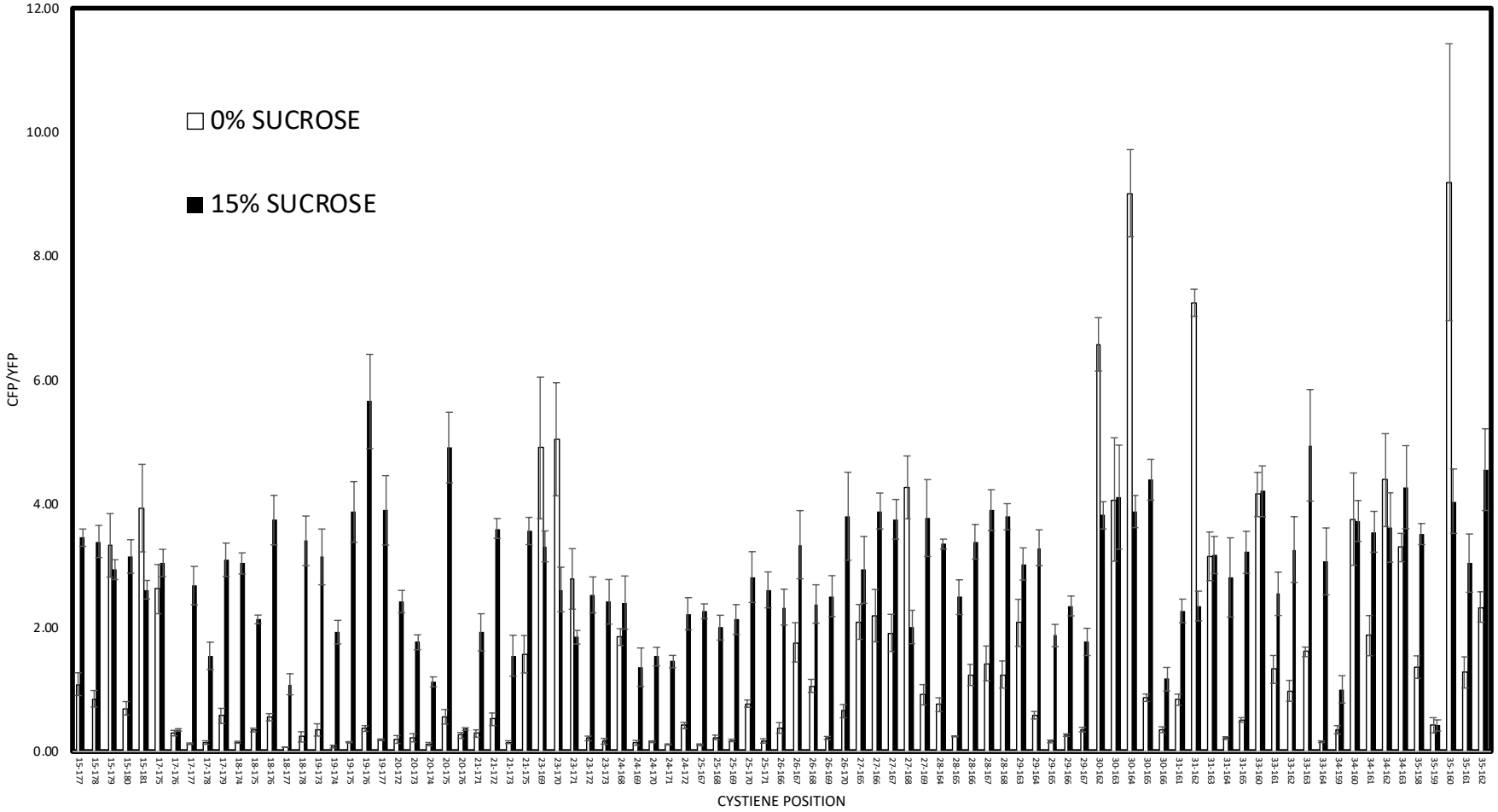

Figure 5-13: Signal output ratio from 2X-Cys containing mutants. EPB30/pRD400 cells expressing 2X-Cys containing EnvZ mutations are grown in low osmolarity (empty bars) and high osmolarity (filled bars) media to an OD_{600nm} of 0.3±0.1. CFP and YFP values are recorded, corrected for OD and the estimated background signal (MG1655 CFP and YFP fluorescence output) is subtracted. A CFP/YFP ratio is calculated indicating the effect of mutation upon signal output with and without stimulus.

A

Cysteine Position	cCFP z-score	cYFP z-score	Shifted on (C+, Y-)	Shifted off (C-, Y+)	Low signal (C-, Y-)	High signal (C+, Y+)	No marked changes
15-177	9.03	2.26				✓	
15-178	6.38	2.00				✓	
15-179	15.09	-2.28	✓				
15-180	2.79	-0.46					✓
15-181	8.43	-3.51	✓				
17-175	6.17	-3.36	✓				
17-176	-2.05	-4.09			✓		
17-177	-0.97	4.16					✓
17-178	-1.37	2.61					✓
17-179	4.63	4.26				✓	
18-174	-0.73	3.45					✓
18-175	-1.49	-3.55					✓
18-176	2.64	0.80					✓
18-177	-2.33	-0.60					✓
18-178	-1.49	-1.02					✓
19-173	1.37	2.28					✓
19-174	-2.31	-0.54					✓
19-175	-0.06	6.58					✓
19-176	1.82	2.39					✓
19-177	-1.27	-0.38					✓
20-172	-0.82	2.53					✓
20-173	-1.20	-0.18					✓
20-174	-2.19	-1.62					✓
20-175	6.19	4.22				✓	
20-176	-2.27	-4.30			✓		
21-171	0.98	3.25					✓
21-172	3.25	2.94				✓	
21-173	0.14	7.30					✓
21-175	9.20	-0.34					✓
23-169	5.82	-4.40	✓				
23-170	5.84	-4.47	✓				
23-171	1.44	-4.94					✓

Cysteine Position	cCFP z-score	cYFP z-score	Shifted on (C+, Y-)	Shifted off (C-, Y+)	Low signal (C-, Y-)	High signal (C+, Y+)	No marked changes
23-172	-0.37	3.89					✓
23-173	-0.09	5.98					✓
24-168	1.95	-4.29					✓
24-169	-0.36	7.29					✓
24-170	-1.19	1.29					✓
24-171	-1.38	3.07					✓
24-172	1.61	2.32					✓
25-167	-1.28	4.66					✓
25-168	-0.58	1.79					✓
25-169	-0.09	4.99					✓
25-170	-0.45	-4.04					✓
25-171	-1.19	2.19					✓
26-166	0.79	2.24					✓
26-167	3.88	-3.04	✓				
26-168	1.63	-3.24					✓
26-169	-1.29	-1.02					✓
26-170	1.04	-1.45					✓
27-165	2.52	-4.39	✓				
27-166	3.91	-3.80	✓				
27-167	5.08	-3.14	✓				
27-168	7.02	-4.58	✓				
27-169	3.62	-1.14					✓
28-164	1.09	-2.67					✓
28-165	-1.26	-1.65					✓
28-166	1.93	-3.41					✓
28-167	0.58	-4.37					✓
28-168	2.45	-3.12	✓				
29-163	7.54	-2.95	✓				
29-164	0.24	-2.51					✓
29-165	-1.35	0.31					✓
29-166	-0.45	-0.10					✓
29-167	-0.29	-1.17					✓

Cysteine Position	cCFP z-score	cYFP z-score	Shifted on (C+, Y-)	Shifted off (C-, Y+)	Low signal (C-, Y-)	High signal (C+, Y+)	No marked changes
30-162	3.95	-5.46	✓				
30-163	8.16	-3.98	✓				
30-164	6.69	-5.44	✓				
30-165	5.01	-0.27					✓
30-166	0.34	0.53					✓
31-161	3.22	-1.01					✓
31-162	18.38	-4.20	✓				
31-163	4.68	-4.45	✓				
31-164	-0.77	0.62					✓
31-165	3.83	2.66				✓	
33-160	7.21	-4.59	✓				
33-161	4.60	-2.37	✓				
33-162	2.71	-1.94					✓
33-163	3.21	-3.61	✓				
33-164	-2.59	-4.70			✓		
34-159	-1.45	-3.24					✓
34-160	3.41	-4.71	✓				
34-161	6.59	-2.37	✓				
34-162	6.27	-4.61	✓				
34-163	4.39	-4.63	✓				
35-158	1.88	-3.79					✓
35-159	-1.65	-3.95					✓
35-160	7.90	-4.98	✓				
35-161	5.35	-1.39					✓
35-162	11.47	-1.82					✓

B

Cysteine Position	cCFP z-score	cYFP z-score	Shifted on (C+, Y-)	Shifted off (C-, Y+)	Low signal (C-, Y-)	High signal (C+, Y+)	No marked changes
15-177	1.78	0.26					✓
15-178	2.06	0.44					✓
15-179	2.95	1.18					✓
15-180	0.15	-0.11					✓
15-181	-0.52	0.01					✓
17-175	0.34	0.06					✓
17-176	-4.59	2.80		✓			
17-177	0.12	0.56					✓
17-178	-2.00	1.23					✓
17-179	0.68	0.15					✓
18-174	1.46	0.54					✓
18-175	-2.24	-0.33					✓
18-176	-1.26	-0.68					✓
18-177	-4.11	-0.33					✓
18-178	-0.96	-0.53					✓
19-173	-2.23	-1.07					✓
19-174	-2.26	-0.02					✓
19-175	-1.79	-1.03					✓
19-176	-1.12	-1.26					✓
19-177	-1.64	-0.86					✓
20-172	-2.84	-0.88					✓
20-173	-2.31	0.21					✓
20-174	-3.03	0.98					✓
20-175	-2.10	-1.49					✓
20-176	-4.96	1.48					✓
21-171	-1.89	0.60					✓
21-172	-0.33	-0.62					✓
21-173	-3.11	0.47					✓
21-175	0.14	-0.35					✓
23-169	-1.06	-0.76					✓
23-170	0.63	0.78					✓

Cysteine Position	cCFP z-score	cYFP z-score	Shifted on (C+, Y-)	Shifted off (C-, Y+)	Low signal (C-, Y-)	High signal (C+, Y+)	No marked changes
23-171	-0.66	1.08					✓
23-172	-1.17	-0.19					✓
23-173	-1.35	0.11					✓
24-168	-0.30	0.74					✓
24-169	-2.01	1.40					✓
24-170	-0.08	2.53					✓
24-171	0.50	3.01					✓
24-172	2.05	1.85					✓
25-167	0.77	1.17					✓
25-168	0.24	1.20					✓
25-169	1.24	1.56					✓
25-170	0.42	0.25					✓
25-171	-1.02	0.09					✓
26-166	0.72	1.14					✓
26-167	-0.50	-0.41					✓
26-168	-1.37	0.15					✓
26-169	0.65	1.08					✓
26-170	0.68	-0.10					✓
27-165	-1.26	-0.40					✓
27-166	1.74	-0.12					✓
27-167	1.78	-0.03					✓
27-168	-0.81	0.74					✓
27-169	1.21	-0.08					✓
28-164	0.32	-0.23					✓
28-165	-1.21	-0.12					✓
28-166	-0.39	-0.50					✓
28-167	1.47	-0.18					✓
28-168	1.37	-0.15					✓
29-163	1.37	0.56					✓
29-164	0.82	0.02					✓
29-165	-1.89	0.26					✓
29-166	0.36	0.86					✓
29-167	-2.04	0.42					✓

Cysteine Position	cCFP z-score	cYFP z-score	Shifted on (C+, Y-)	Shifted off (C-, Y+)	Low signal (C-, Y-)	High signal (C+, Y+)	No marked changes
30-162	-0.31	-0.72					✓
30-163	0.48	-0.44					✓
30-164	2.07	0.05					✓
30-165	1.67	-0.39					✓
30-166	-2.29	1.72					✓
31-161	-0.81	0.27					✓
31-162	-1.00	0.13					✓
31-163	-0.86	-0.55					✓
31-164	-0.69	0.30					✓
31-165	-0.37	-0.30					✓
33-160	0.14	-0.73					✓
33-161	-1.62	-0.34					✓
33-162	-0.48	-0.39					✓
33-163	0.88	-0.72					✓
33-164	-1.72	-0.68					✓
34-159	-4.12	0.16					✓
34-160	-0.65	-0.77					✓
34-161	-0.16	-0.48					✓
34-162	-2.28	-1.25					✓
34-163	0.36	-0.70					✓
35-158	-2.15	-1.20					✓
35-159	-5.47	-0.54					✓
35-160	0.70	-0.47					✓
35-161	-0.47	-0.38					✓
35-162	0.11	-0.90					✓

Table 5-14: Analysis of 2X-Cys mutant CFP/YFP ratio compared to a Cys-less mutant. Fluorescence output (CFP and YFP) was measured for a C277A EnvZ mutant in EPB30/pRD400 cells, representing a WT signal output. These values were used as the mid-point of a z-score scale in order to determine the differences caused by the 2X-Cys mutations that have been employed. (A) Comparison of C277A to 2X-Cys mutants grown in low osmolarity (0%) media. (B) Comparison of C277A to 2X-Cys mutants grown in high osmolarity (15%) media. The colour scale indicates the degree of difference to C277A signal output, ranging from red (lower than WT signal output) to green (higher than WT signal output).

	LOW (0% SUCROSE)					HIGH (15% SUCROSE				
Cysteine position	SHIFT ON/OFF	SIGNAL HIGH/LOW	BAND IDENTITY	AMINO ACIDS		SHIFT ON/OFF	SIGNAL HIGH/LOW	BAND IDENTITY	AMINO ACIDS	
15-177			11	T	L			11	T	L
15-178			11	T	F			11	T	F
15-179	ON		N/A	T	I			N/A	T	I
15-180			N/A	T	R			N/A	T	R
15-181	ON		N/A	T	I			11	T	I
17-175	ON		22	L	A			22	L	A
17-176 *		LOW	N/A	L	W	OFF		N/A	L	W
17-177			12	L	L			N/A	L	L
17-178			12	L	F			12	L	F
17-179			22	L	I			22	L	I
18-174			12I22	L	G			12I22	L	G
18-175			22	L	A			22	L	A
18-176			N/A	L	W			12	L	W
18-177			N/A	L	L			N/A	L	L
18-178			N/A	L	F			12	L	F
19-173			11	I	G			11	I	G
19-174			11	I	G			11	I	G
19-175			11	I	A			11	I	A
19-176			11I12	I	W			N/A	I	W
19-177			11	I	L			11	I	L
20-172			N/A	V	I			N/A	V	I
20-173			N/A	V	G			N/A	V	G
20-174			N/A	V	G			N/A	V	G
20-175			22	V	A			22	V	A

Cysteine position	SHIFT ON/OFF	SIGNAL HIGH/LOW	BAND IDENTITY	AMINO ACIDS		SHIFT ON/OFF	SIGNAL HIGH/LOW	BAND IDENTITY	AMINO ACIDS	
20-176		LOW	N/A	V	W			N/A	V	W
21-171			N/A	T	A			N/A	T	A
21-172			N/A	T	I			N/A	T	I
21-173			N/A	T	G			N/A	T	G
21-175			22	T	A			22	T	A
23-169	ON		N/A	L	L			11	L	L
23-170	ON		11	L	L			N/A	L	L
23-171			11|22	L	A			11	L	A
23-172			N/A	L	I			N/A	L	I
23-173			N/A	L	G			N/A	L	G
24-168			N/A	F	M			N/A	F	M
24-169			N/A	F	L			N/A	F	L
24-170			N/A	F	L			N/A	F	L
24-171			22	F	A			22	F	A
24-172			N/A	F	I			N/A	F	I
25-167			N/A	A	I			N/A	A	I
25-168			N/A	A	M			N/A	A	M
25-169			11	A	L			N/A	A	L
25-170			N/A	A	L			11	A	L
25-171			11|22	A	A			11|22	A	A
26-166			11	S	A			11	S	A
26-167	ON		11|22	S	I			11|22	S	I
26-168			11	S	M			11	S	M
26-169			11	S	L			11	S	L
26-170			11	S	L			11	S	L

Cysteine position	SHIFT ON/OFF	SIGNAL HIGH/LOW	BAND IDENTITY	AMINO ACIDS		SHIFT ON/OFF	SIGNAL HIGH/LOW	BAND IDENTITY	AMINO ACIDS	
27-165	ON		N/A	L	L			N/A	L	L
27-166	ON		N/A	L	A			N/A	L	A
27-167	ON		22	L	I			22	L	I
27-168	ON		N/A	L	M			22	L	M
27-169			N/A	L	L			N/A	L	L
28-164			N/A	V	T			N/A	V	T
28-165			N/A	V	L			N/A	V	L
28-166			N/A	V	A			N/A	V	A
28-167			N/A	V	I			22	V	I
28-168	ON		N/A	V	M			N/A	V	M
29-163	ON		12	T	Y			12	T	Y
29-164			22	T	T			22	T	T
29-165			N/A	T	L			N/A	T	L
29-166			12	T	A			12	T	A
29-167			N/A	T	I			N/A	T	I
30-162	ON		11	T	R			11	T	R
30-163	ON		N/A	T	Y			11	T	Y
30-164	ON		22	T	T			22	T	T
30-165			11	T	L			11	T	L
30-166			N/A	T	A			N/A	T	A
31-161			22	Y	F			N/A	Y	F
31-162	ON		12	Y	R			12	Y	R
31-163	ON		N/A	Y	Y			12	Y	Y
31-164			22	Y	T			22	Y	T
31-165			N/A	Y	L			N/A	Y	L

Cysteine position	SHIFT ON/OFF	SIGNAL HIGH/LOW	BAND IDENTITY	AMINO ACIDS		SHIFT ON/OFF	SIGNAL HIGH/LOW	BAND IDENTITY	AMINO ACIDS	
33-160	ON		12|22	V	L			22	V	L
33-161	ON		22	V	F			12|22	V	F
33-162			12	V	R			12	V	R
33-163	ON		12|22	V	Y			12|22	V	Y
33-164		LOW	12|22	V	T			N/A	V	T
34-159			11	V	P			12|22	V	P
34-160	ON		11|12|22	V	L			11|12|22	V	L
34-161	ON		11	V	F			11|12	V	F
34-162	ON		11|12	V	R			N/A	V	R
34-163	ON		11	V	Y			N/A	V	Y
35-158			N/A	L	S			N/A	L	S
35-159			12|22	L	P			N/A	L	P
35-160	ON		12|22	L	L			12|22	L	L
35-161			12	L	F			N/A	L	F
35-162			N/A	L	R			N/A	L	R

Table 5-15: Comparison of Immunoblotting data to Fluorescence data for 2X-Cys mutants. Results are divided into sections for EPB30/pRD400 cells containing 2XCys EnvZ mutations grown in low osmolarity (0% sucrose) and high osmolarity (15% sucrose) media. SHIFT indicates if the signal output is reversed. SIGNAL indicates the level of overall signal recorded in relation to a C277A variant. BAND IDENTITY summarises the outcomes of **Table 5-5**. AMINO ACIDS indicates the residues that have been replaced with cysteine in each mutation. The colour is either darkened (11' or 22' interaction) or a bolder border is drawn (12') if respective interactions are observed via the position in which that residue has been substituted.

5.5: Correlation of signal output to dynamic range of the osmosensing circuit

The dynamic range of each mutant was plotted against the signal output without stimulus (low osmolarity conditions). An exponential decay curve was formed from 84 of 89 mutants tested, with 5 mutants not following that trend (**Figure 5-16**). Of these 5 mutants, 2 (17-176, 20-176) showed significantly lowered signal output under low osmolarity conditions and 2 others (34-159, 35-159) replaced a proline residue, potentially altering the helical stability of TM2. The remaining outlier mutant (30-166) showed no significant changes overall under low or high osmolarity conditions and of the 5 outliers it lies closest to the normal data trend.

When ordered by decreasing dynamic range, including the values for C277A (WT), the majority of mutants (60 of 89) fell below the WT dynamic range value (**Figure 5-17**). A z-score was calculated for each mutant using the C277A mean and standard deviation. Of the 60 mutants that fell below C277A dynamic range, 40 had a z-score of less than -2 showing that they were in the 2^{nd} percentile or lower compared to the spread of data for C277A. The mutant list was divided into thirds based on where they are positioned in the membrane (15-177 to 21-173 = Cytoplasm, 21-174 to 28-165 = Membrane, 28-166 to 35-162 = Periplasm) and the graph was colour coded according to these groupings. This shows 88% of periplasm mutants to record a dynamic range less than WT and 70% showed a z-score of -2 or less. From this it can be concluded that the osmosensing circuit is less likely to be tolerant of periplasm proximal mutations compared to membrane and cytoplasm proximal mutations.

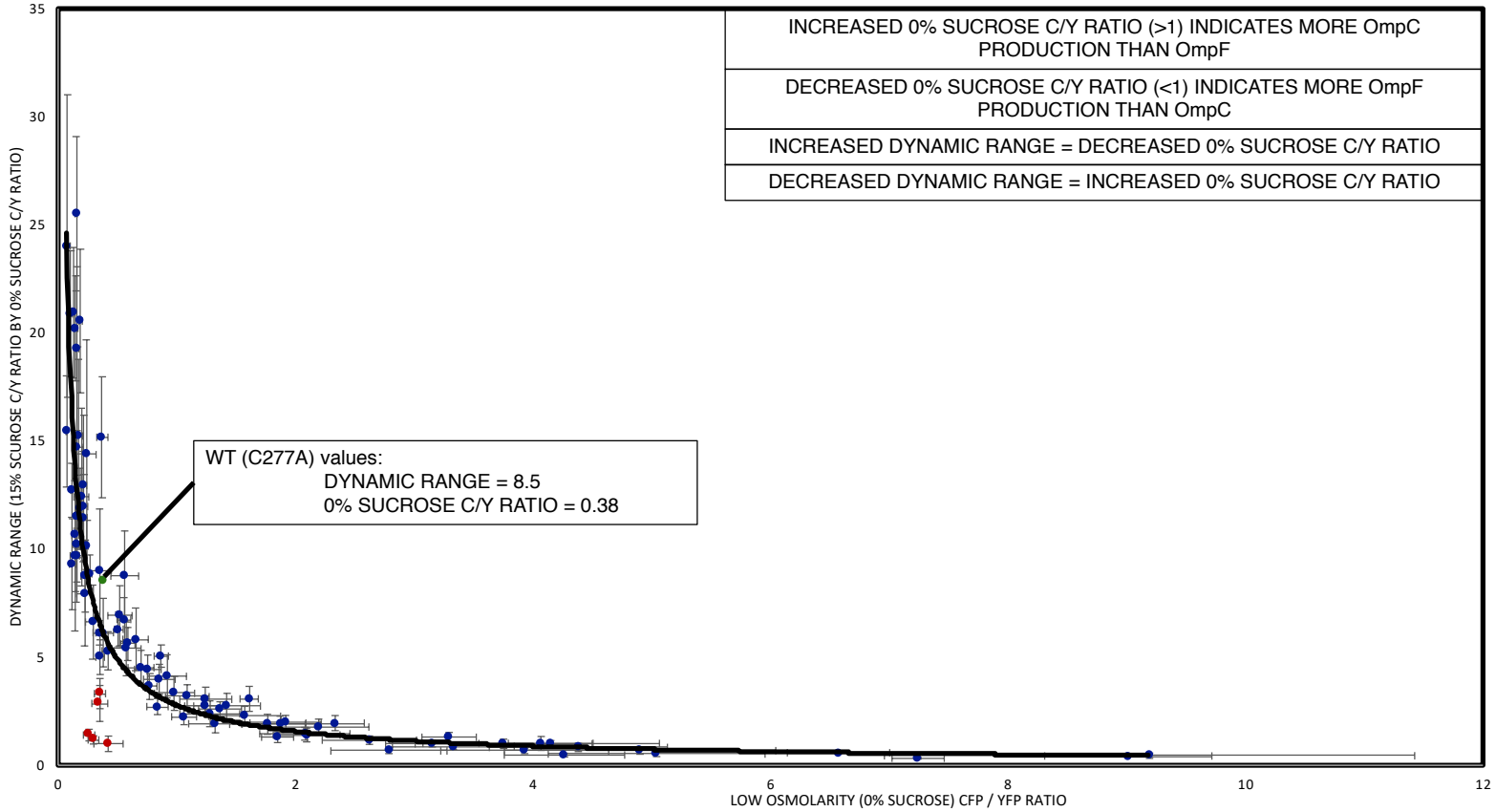

Figure 5-16: Observation of an exponential decay relationship between dynamic range and signal output without stimulus. The dynamic range is the ratio of signal output in the presence of stimulus (high osmolarity media, 15% sucrose) against the signal output in the absence of stimulus (low osmolarity media, 0% sucrose). For EPB30/pRD400 cells containing 2X-Cys EnvZ mutants, the dynamic range is calculated via the fluorescence data recorded in **Figure 5-13** and compared to the low osmolarity calculated in the same figure. Error bars are transferred from **Figure 5-13** for low osmolarity data (horizontal bars) and error forwarding has been employed for the dynamic range error bars (vertical) to combine the separate high and low osmolarity signal output ratios. The trendline (black) represents the exponential decay relationship displayed by the majority of the collected results (blue circles). C277A data represents the WT relationship of dynamic range against signal output in low osmolarity media (green circle). Five mutants did not conform to the exponential decay relationship (red circles).

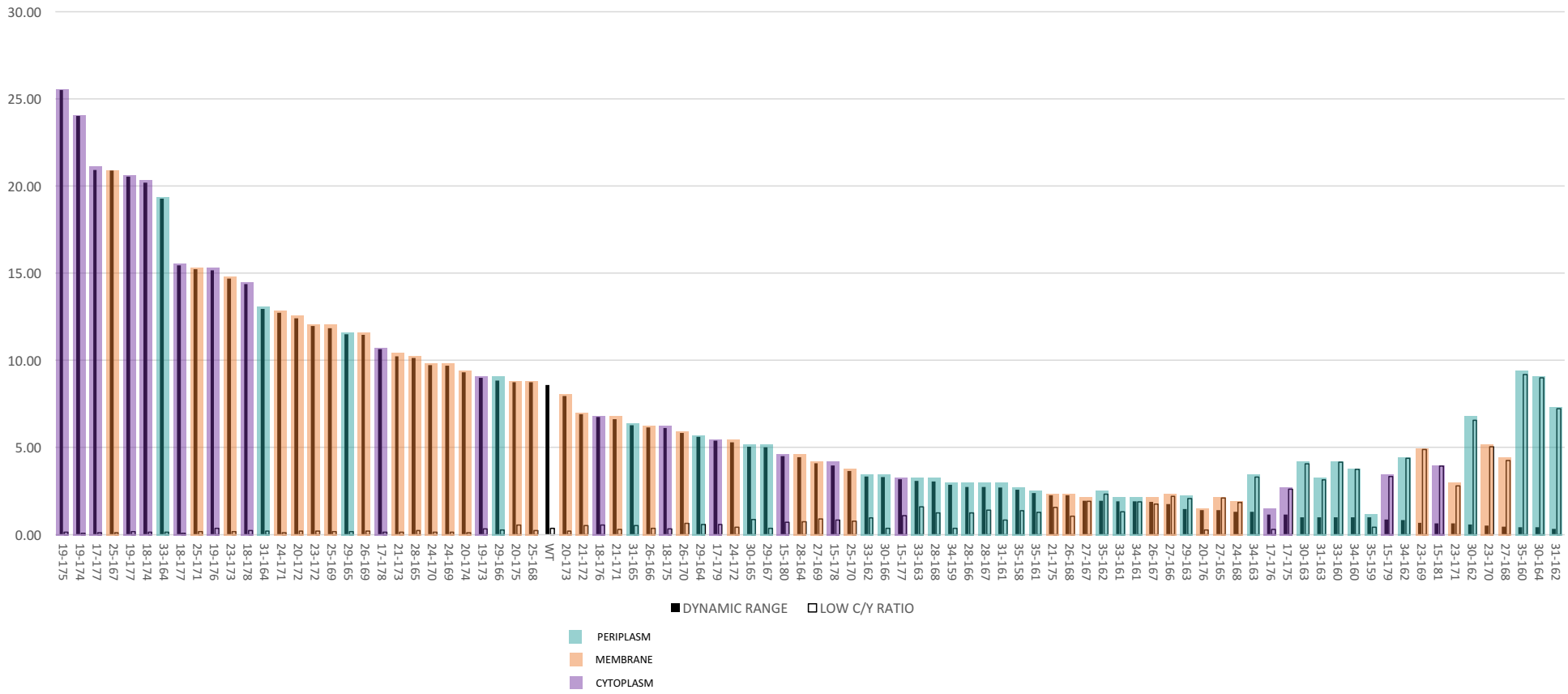

Figure 5-17: 2X-Cys mutants ordered by descending dynamic range and categorised by position within the TM helices. Dynamic range (filled bars) and Low Osmolarity signal output (CFP/YFP ratio) are juxtaposed for each 2X-Cys mutant then ordered by descending dynamic range. Mutants are categorised by the helix sections described in **Figure 5-3** – Cytoplasmic end (purple), Membrane core (orange) and Periplasmic end (turquoise).

Chapter 6: Discussion

6.1: TM1 discussion

6.1.1: Establishing the surface of TM1 that promotes dimerisation

The results of sulphydryl-reactivity experiments were plotted on a helical net (154) to visualise the TM1-TM1' interaction surface. Using the well-defined distance and angular constraints of a disulphide bond (155,156), the relative distance between Cys residues along the TM1-TM1' interface were assessed. These constraints can be estimated from the distance between β-carbons in disulphide bonds, which range from 3.4 to 4.6 Å in protein crystal structures (157). Therefore, when a fixed concentration of molecular iodine (250 μM) and reaction time (10 minutes) is employed, the extent of crosslinking correlates with the distance between the Cys residues (**Figure 3-5**). Based on this correlation, residue positions 23/23' and 26/26' would be in closest proximity. By extension, the significant reduction in crosslinking as the Cys residues become more distal from these positions within the membrane core suggests that the TM1 and TM1' helices cross at an angle that results in increased distance between residues near the membrane boundaries. Therefore, it is proposed that the major TM1-TM1' interaction surface consists of residues Ile-19, Leu-23, Ser-26, Thr-30 and Val-34 (**Figure 6-1A**). In addition, minor reactivity was observed with residues Ser-11 and Thr-15, suggesting that they are quite distant, but most likely reside on the same surface as the TM1-TM1' interface. Adjacent residues at the periplasmic end of TM1, ranging from position 38 to 40 also exhibited extensive cross-linking, however the helical pattern was interrupted suggesting that a less uniform structure exists within these residues (**Figures 3-9** and **6-1A**). Also important to note is that no significant differences in the TM1-TM1' interface were observed when cells were grown under the low- (0% sucrose) or high-osmolarity (15% sucrose) regime (**Figure 3-9**).

From this, it is believed that the residues examined can be formally divided into three distinct regions (**Figure 6-1A**) based on results obtained when changing the concentration of

iodine (**Figure 3-10**) or the reaction time (**Figure 3-11**). The EnvZ variants within Region I (S11C and T15C) follow a distinct pattern of forming disulphide bonds only in the presence of the highest concentration of iodine (250 μM) and the longest duration (10 minutes). These data suggest the Cys residues are either very distant, such that they irregularly form a disulphide bond, or are internal to the inner leaflet of the cytoplasmic membrane. The variants in Region II (I19C, L23C, S26C, T30C, V34C and A25C to a minor extent) all follow a similar pattern that is different than the variants in the first region. Here, a minor extent of crosslinking at the distal ends of the region, namely I19C and V34C, is observed, while a maximal amount is seen near the core that is comprised of L23C and S26C. This is further demonstrated by comparing the extent of crosslinking at the higher concentrations of iodine (100 μM and 250 μM). In addition, unlike residues in Region I, the reaction is complete after 1 minute regardless of the overall extent of crosslinking (**Figure 3-11**). The variants found in Region III (A38C, I39C and L40C) follow a third distinct pattern. EnvZ A38C exhibited a much greater extent of crosslinking than V34C, and thus does not conform to the crossing helix pattern. In addition, EnvZ I39C and L40C show crosslinking at all concentrations of iodine (**Figure 3-10**) and thus suggest that either the helix becomes broken/unwound, or that these residues reside in the periplasm, or both. It is also worth noting that when cells were grown under the low osmolarity regime and in the absence of iodine (**Figure 3-5**), crosslinking occurred at positions 38 through 40, suggesting that they may reside within the oxidising environment of the periplasm.

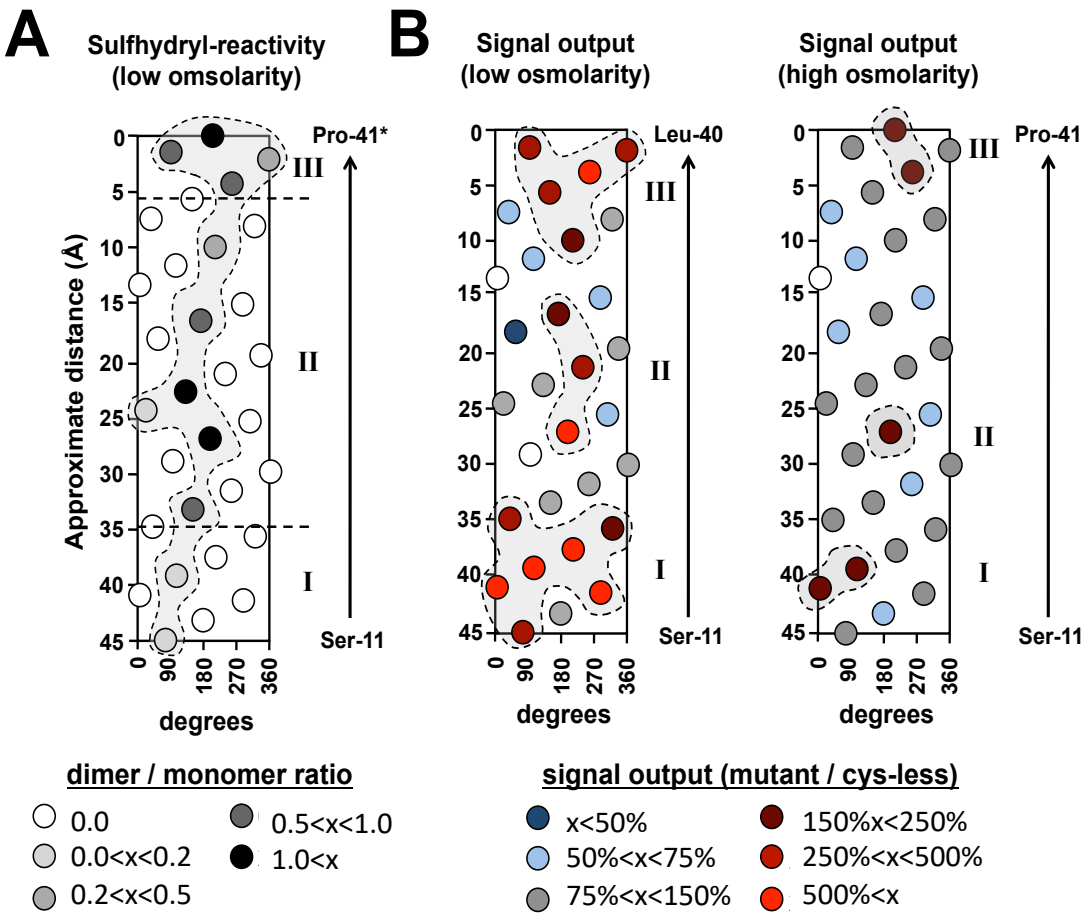

Figure 6-1: Helical net diagrams illustrating the TM1–TM1′ interface and surfaces important for maintenance of baseline EnvZ signal output. (A) The TM1–TM1′ interface remains similar when EPB30/pRD400 cells are grown under the low- (0% sucrose) or high-osmolarity (15% sucrose) regime. The extent of TM1-TM1' crosslinking, measured as the ratio of dimeric:monomeric EnvZ moieties at each position is represented by the intensity of darkness. Residue positions 23 and 26, which reside in close proximity, result in the greatest extent of cross-linking. As the position of the Cys residue is moved toward the cytoplasmic end of the helix, a decrease in reactivity is observed. The divergence from a helical pattern at the periplasmic end of TM1 may indicate that the periplasmic boundary of the membrane has been breached and/or that the helicity is not observed within this region. It should be noted that the P41C, indicated with an asterisk, variant could only be analysed when grown under the high-osmolarity regime. (B) Cys substitutions that result in decreased signal output compared to the cys-less variant are presented in blue colours, while those resulting in increased signal output are indicated in red. Regions responsible for maintenance of baseline signal output fall into three contiguous surfaces (red dots residing under a transparent grey area): one at the cytoplasmic end (surface I), a small one within the membrane core (surface II) and one at the periplasmic end of the helix (surface III). These surfaces are less pronounced when cells are grown under the high-osmolarity regime, possibly because the EnvZ/OmpR circuit is already stimulated by external osmolarity. The white circles represent the Cys-32 mutant that could not be created and the Cys-22 variant that failed to grow under the low-osmolarity regime.

6.1.2: Mapping surfaces of TM1 responsible for maintenance of baseline EnvZ signal output

In order to visualise which surfaces of TM1 are responsible for maintenance of steady-state EnvZ signal output, the signal output of the family of single-Cys-containing receptors was mapped onto a helical net (**Figure 6-1B**). This analysis resulted in the identification of three subdomains intolerant of Cys substitutions (signal output greater than 150% of the cys-less variant): the cytoplasmic end of TM1 (Surface I), three residues in the core of the membrane (Surface II) and the periplasmic end of TM1 (Surface III). Surfaces II and III were not considered as contiguous because surface III may be due to breaching the periplasmic boundary, while surface II remained buried but truly intolerant of Cys substitution. This becomes clearer when cells are grown under the high-osmolarity (15% sucrose) regime (**Figure 6-1B**). It is also important to emphasise that the two residues in the membrane core (positions 17 and 24) are subject to both sulphydryl-reactivity and intolerance of Cys substitution with regard to steady-state signal output. Overall, similar patterns were observed when EPB30/pRD400 cells were grown under the high-osmolarity regime (15% sucrose), although the degree of increased signal output was smaller, perhaps because the EnvZ/OmpR circuit was already activated by osmolarity so the mutation could not increase the signal output further(**Figure 6-1B**).

Two EnvZ mutants that reside within the analysed region (V33E and P41L) were previously shown to result in significantly greater increased steady-state signal output (158,159). Our data with EnvZ P41C is in agreement with the previously published results with P41L, which demonstrates that loss of the Pro residue results in greatly increased steady-state EnvZ signal output. In fact, the P41C variant of EnvZ results in the greatest change in signal output when grown under the high-osmolarity regime (**Figure 3-7**). However, with EnvZ V33C, different results were observed than those previously published with the V33E variant. This difference suggests that the loss of Val-33 is not the major driving force for changing

steady-state signal output and that the increased activation is most likely due to the insertion of a Glu residue. This is not unexpected as it was previously demonstrated (160) that residues with longer side chains within their R-group possess the ability to snorkel and interact with, or be repulsed from in this case, the negatively charged phospholipid head groups in the cytoplasmic membrane. This may explain why our V33C variant did not exhibit similar properties to the previously published EnvZ V33E.

6.1.3: Evaluation within the context of current models for transmembrane communication

The crosslinking and signal output data presented here demonstrate that the TM1-TM1' interface does not significantly change when EPB30/pRD400 cells are grown under regimes possessing different osmolarities (**Figure 3-9**). This suggests that TM1-TM1' might be relatively static in a manner consistent with results previously observed with the aspartate and ribose/galactose chemoreceptors (161) and also recently with DcuS, the C_4-dicarboxylate sensor of *E. coli* (162). However, other types of signaling mechanisms that involve more dynamic roles for TM1 and/or TM1' have been observed. For example, a rotation between TM1 and TM1' within McpB of *Bacillus subtilis* was seen upon addition of arginine (108), its cognate stimulus, whereas our results suggest that no rotation occurs along the TM1-TM1' interface in response to osmolarity. In addition, small piston-type displacements of TM1 have been observed in the periplasmic domain of NarX and the TorT-TorS complex (97,100) and these might not be detectable within the current iteration of the assay.

From another perspective, these results are in agreement with recent analyses involving PhoQ that proposed the existence of water-filled hemichannel spanning through the cytoplasmic end of the TM domain (163). This data suggesting that TM1 and TM1' cross at an angle resulting in an increasing distance between the residues as they become further distal from the membrane core is consistent with the presence of water hemichannel possessing a

cytoplasmic-facing opening. The proposed necessity of a polar residue is also consistent with previous results involving “aromatic tuning” and the repositioning of non-polar hydrophobic residues around the cytoplasmic end of TM2 resulting in modified signal output (6,160,164). Recently, further experimentation proposed a scissor-type model, which would also be consistent with previous helical crossing angles. In light of the plethora of proposed signaling mechanisms, recent publications (165,166) suggest that different subclasses of bacterial receptors may employ alternate mechanisms of signal transmission and that every proposed mechanism should not be imposed upon all bacterial membrane-spanning receptors.

6.2: TM2 Discussion

6.2.1: Non piston transmembrane communication by EnvZ

EnvZ has been shown to allosterically process cytoplasmic changes in osmolarity and upon interaction with MzrA within the periplasmic space. Here, our *in vivo* analysis demonstrated that only the periplasmic end of EnvZ TM2 undergoes a conformational transition upon cytoplasmic stimulus perception and suggests that the asymmetric piston-type displacement employed by Tar is not used by EnvZ. To our knowledge, this is the first example of a periplasmic end of TM2 being affected by a cytoplasmic stimulus observed within EnvZ. Various experimentations have also been performed with the aromatically tuned variants of TM2 from both Tar and EnvZ. Previously, a linear correlation was observed between the position of the aromatic residue in Tar TM2, the position of the helices *in vitro* and *in silico* and the signal output from each Tar receptor (6,98,160,164). Here, *in silico* analysis of EnvZ TM2 demonstrates that such a linear correlation is absent and that EnvZ functions by a non-piston mechanism in which both tilting and azimuthal rotation play a substantial role in modulation of signal output (**Figure A-2**).

6.2.2: Correlation between membrane composition and mechanism of signal transduction

Comparisons of recently published *apo* and *holo* high-resolution (~1.9 Å) crystal structures of the *E. coli* nitrate sensor NarQ that contain the periplasmic, TM and HAMP domains reveal extensive structural rearrangements involving a piston-like motion of TM1 relative to TM2 of approximately 2.5 Å. These displacements result in a lever-like rotation of individual HAMP domains upon binding of cognate ligand (88). Based on these results, the authors posit that receptors containing a membrane-adjacent HAMP domain function by a piston-type displacement of TM helices while those that lack such domains transduce signal by rotation of TM helices. It was previously postulated a related yet different categorization of signaling mechanisms also based on the domain structure of bacterial receptors (166). It is proposed

that receptors containing a periplasmic four-helix bundle transduce signal across the membrane by piston-type displacements and that the attached membrane-adjacent HAMP domains might possess one of a multitude of signaling mechanisms including a gearbox-type rotation (69), a dynamic bundle (87) or potentially other mechanisms (166). Differentiating between these classification systems will provide a theoretical framework for understanding domain-based intra-protein allosteric communication by bacterial receptors. A recent authoritative structural-based review of transmembrane communication by bacterial receptors addresses these different suggestions (167).

The results presented here also examine whether SHKs that possess membrane-adjacent HAMP domains function solely by piston-type displacements or whether other signaling mechanisms might be employed. The results here with EnvZ should be compared with previous findings from the aspartate chemoreceptor (Tar) and the recent NarQ structures (85,88,161,168) as these three are ideal candidates for comparison because they all possess a membrane-adjacent HAMP domain, however, while Tar and NarQ possess a periplasmic four-helix bundle, EnvZ possesses a periplasmic PDC/CACHE domain (169,170). The authors of the recent NarQ structures posit that the presence or absence of the membrane-adjacent HAMP domain may be the difference between receptors employing piston-type mechanisms of transmembrane communication as compared to other mechanisms (88). However, differences employed during transmembrane communication by the Tar and EnvZ TMDs observed here and previously strongly suggest that Tar and EnvZ possess different mechanism of TM communication even though both possess a membrane-adjacent HAMP domain. Our previous work analysed AS1 helices from *E. coli* NarX, *E. coli* Tar, *E. coli* EnvZ and Af1503, the HAMP domain resulting in the initial high-resolution structure (69), and found that the Tar and NarX AS1 helices possess similar properties, which the AS1 helices from both EnvZ and Af1503 fail to possess. Recent comparisons of the *apo* and ligand-bound structures of the combined periplasmic-TM-HAMP domain from *E. coli* NarQ demonstrate that

binding of ligand results in symmetrical displacements of TM1 relative to TM2 of approximately 2.5 Å (88). These results are similar to Tar, which functions by asymmetrical TM2 displacement also possesses a periplasmic four-helix-bundle (85,102,161,168).

6.2.3: Conclusion

Based on these results, it is concluded that *E. coli* EnvZ functions by a non-piston mechanism of transmembrane communication that is different than Tar, NarX and NarQ, which communicate across the membrane by piston-type displacements. Furthermore, it is proposed that TM signaling mechanisms can be predicted and assigned based upon the domain(s) present in the periplasmic region of a bacterial membrane-spanning receptor.

6.3: 2X-Cys Discussion

6.3.1: Piston model comparisons

The evidence presented supports the non-piston theory previously presented as part of the TM2 investigations (137). To demonstrate this support, the results must again be compared to the piston movements observed within the transmembrane helices of both the NarQ and HtrII proteins in order to highlight the differences/similarities that are present.

The dimeric TM domains of both NarQ and HtrII consist of 4 helices yet their structures are notably different (88) (**Figure 6-2**). The NarQ TM region conforms to a 4-helix coiled coil in its *holo* form and has a dimeric coiled-coil core made up of the TM1 from each subunit. HtrII has a coiled coil dimeric core consisting instead of the TM2 helices (171,172). Despite these differences, both display piston-type displacement following presence of signal. These systems both include well defined mechanisms of ligand/protein interaction which allows for a connection between this interaction and its conformation effects upon the protein to be more easily defined. While EnvZ has conclusively been shown to react to changes in osmolarity, the specific mechanisms have not been conclusively stated. Therefore, it is more difficult to connect the conformational adjustments that can be demonstrated within its various regions, including the transmembrane helices, to a ligand binding event or a protein interaction. However, the discovery of these conformational changes may provide a route to the discovery of a sensing mechanism in retrospect.

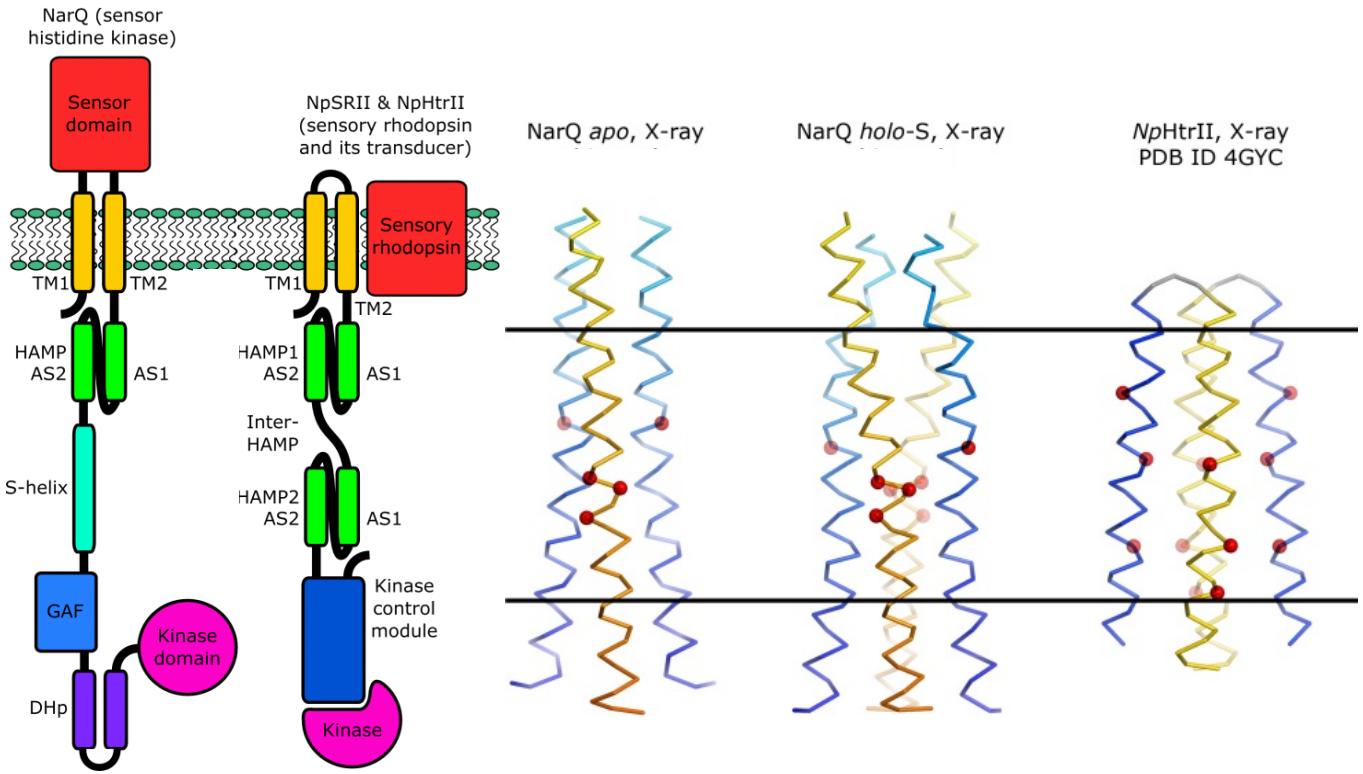

Figure 6-2: NarQ and HtrII domain organisation and TM conformation. The apo and holo structures of NarQ show a displacement of the TM helices out of the membrane, suggesting piston type movement. Evidence demonstrating this motion would be required to suggest a piston type model in the TM helix of a similar protein.

Regarding the comparison of data collected within this body of work with the work completed to conclude piston-type movements of NarQ and HtrII, some assumptions must be made as the methodologies do not match. However, it can be postulated from the data that has been collected for these proteins how a disulphide crosslinking map could look for a piston type displacement. If a helix has shifted out of the membrane an approximate distance (~2.5Å as concluded by Gushchin et al (88)) then the crosslinking profile would be expected to shift accordingly. This would result in aligned residues (off-state) crosslinking followed by either a reduction in or complete lack of crosslinking upon piston shift and subsequent unalignment of the residues. Along a helix interaction surface that is demonstrated to run the entire length of the helix, all crosslinking interactions would be expected to either reduce or disappear to demonstrate a piston type movement.

Heininger et al demonstrated TM1 within EnvZ does not alter its crosslinking interaction profile to any significant degree between off (low osmolarity conditions) and on (high osmolarity conditions) states (104). While these helices do not move in relation to one another, this does not rule out the possibility of the dimerised TM1 helices moving as a whole without breaking their interaction profile with one another. A different approach would be required in order to determine whether they are entirely immobile throughout signal transduction or if they move in sync. Results collected from the 2XCys library could suggest movement of the TM1-TM1' dimer structure, but it is currently impossible to draw any conclusions regarding this with the data currently collected.

Additionally, Yusuf et al demonstrated TM2 within EnvZ displays changes in it crosslinking interaction profile that do not fit to the previously described expectation for a piston type movement to be postulated (137). Again, the data collected here does not indicate overall movement of the TM2-TM2' dimer structure which could alter within the membrane. As piston-type movement was not detected, it is assumed that movement remains within the membrane however further testing would be required in order to corroborate this assumption.

Finally, the data generated from a 2X-Cys mutant library of EnvZ corroborates the evidence collected for TM1/TM1' and TM2/TM2' interactions. Additionally, it adds further dimension to these observations via a TM1/TM2' interaction profile that also does not display interaction profiles that appear to change between "on" and "off" states in a way that would suggest piston-type displacement. Instead, an unexpected result is presented in which the TM1/TM2' interaction profile appears to lack any crosslinking interaction within the membrane core of the TM helices (**Figure 5-8**). This is particularly interesting when compared to the interaction profiles demonstrated by both TM1/TM1' and TM2/TM2' as these interaction surfaces are uninterrupted along the entire length of the helices (**Figure 5-7**). Additionally, the areas of interaction are located at both ends of the helices and the periplasmic end in particular displays changes between on and off states.

Within the 2X-Cys mutant library results, multiple mutants contained a residue that crosslinked as a 1X-Cys mutant but did not crosslink in the presence of its paired mutation. There are multiple examples of this occurrence, both within TM1-TM1' and TM2-TM2' interactions. A TM1 residue expected to crosslink from 1X-Cys data collected would not necessarily lose its crosslinking capability throughout its five TM2 pairings. This suggests that specific pairings would prevent the successful interactions of one, if not both residues with their identical dimer partner. Taking 19-175 as an example, from 1X-Cys data both 19-19' and 175-175' crosslinking was expected to be strong yet only a 19-19' band was recorded from the 19-175 mutant. Additionally, this band was far more intense than its 1X-Cys iteration suggesting that the addition of a 175 position cysteine increased the positional proximity of the 19-19' interaction.

6.3.2: Limitations of the Methodology

6.3.2.1: Disulphide crosslinking

The mutants created are sequenced to confirm the cysteines are substituted into the correct positions both when they are ligated and transformed into DH10B cells and when they are transformed into EPB30 cells. However, there remains a possibility that these sequences could be disrupted during the transcription/translation process. It is not currently possible to circumvent this eventuality; therefore, the results should be trusted if the sequenced plasmid transformed into EPB30 cells contains cysteine residues in the expected positions for each mutant.

When designing the 2X-Cys library, it was theorised that a monomer could crosslink with itself, leading to an alternate monomer band forming, indicating a TM1-TM2 interaction surface. In theory, a crosslinked monomer could form differently enough to the non-crosslinked monomer and allow it to migrate a distinctly different distance through an SDS PAGE gel. However, no bands were observed leading to two separate suggestions. Firstly, the crosslinked monomer could have migrated the same distance as the non-crosslinked monomer, therefore the two bands would have been indistinguishable. Alternatively, the crosslinking event is not possible within a monomer, therefore no band would have been present. The former of these suggestions is more logical, as it would be expected that within a 4-helix bundle where all other combinations of interaction are evident, there should be a TM1-TM2 interaction also. A possible solution to distinguish whether any monomer band was disguising a crosslinked monomer band would be to compare mutant results with and without iodine making note of any differences in the monomer band intensity.

6.3.2.1: Signal output measurements

The signal output measurements throughout this work have been taken using a fluorescence photospectrometer, which detects the overall fluorescence of the sample input. However,

within a population of mutant cells there may exist subpopulations that behave differently to the representation of the overall fluorescence values produced. For example, a population of cells for one mutant may display normal fluorescent values comparable to WT of CFP/YFP<1 without stimulus. If the overall CFP level is low without stimulus and the YFP level is high without stimulus, such a ratio would be expected. However, these values could hide opposing subpopulations within. If the overall value for CFP is 100, there may be an extremely low subpopulation of 10 and a much higher subpopulation of 300, neither of which would be represented by the overall recorded value of 100. In order to avoid this misclassification of a population, the cells must be individually measured for their fluorescence output via flow cytometry. This method, while costly, would reveal any subpopulation of fluorescence behaviour by any mutant, therefore eliminating the risk of misclassification via fluorescence photospectrometry.

6.3.2.3: Deepcoil predictions

The Deepcoil predictions completed to suggest the helical formations of TM1 and TM2 may not be entirely accurate. In particular, the suggested coiled coil formation of TM1 may not be correct as the helix could be too short for this formation. Further computational modelling involving energy minimisation will be required to specifically characterise the formation of this helix.

6.4: Conclusion

While these data show promise in elucidating the mechanism of EnvZ/OmpR signal transduction, the transmembrane domain helices are merely one section of the overall function within EnvZ. For example, the cytoplasmic domains of EnvZ (EnvZc) have been shown to support transcription of ompC/ompF via OmpR, albeit without retaining the robustness of full EnvZ when EnvZc is overexpressed. This indicates there is a sensory function within the cytoplasmic domains, yet it could either be secondary to a sensory domain within the transmembrane/periplasmic domains or these domains are required for proper regulation of the cytoplasmic sensory functions. Further to this, the MzrA protein function must be taken into account as it could either directly or indirectly modulate transmembrane helix conformation regardless of media osmolarity. Further experimentation, using similar methods to those employed here, would be required to fully understand the physical interactions that occur between MzrA and EnvZ. As MzrA dimerises itself, with a single transmembrane crossing, it would also be useful to understand interactions that occur within its own dimeric conformation.

As the data shows evidence for an entirely new type of model within transmembrane helices of SHKs, the next stages directly related to this line of research will involve further proving that model. Firstly, the evidence must be corroborated by a different method, for example *in silico* modelling of the transmembrane four-helix bundle. If a pocket is shown to form, there will be specific residues that line this pocket and it is likely that one or more of those residues plays a significant role in sensing within the pocket. Exhaustive mutations of the pocket-lining residues (substituting each residue for every other amino acid) could help to isolate which of these positions is most critical to normal signal transduction via the dual fluorescence reporter system. Next, the identity of the molecule(s) entering the pocket would need to be ascertained. As EnvZ has osmosensory capability, it would be logical to predict that water may enter the pocket when the bundle formation allows, leading to a mechanistic

alteration in the overall dimeric formation which allows signal transduction. Both *in vivo* and *in silico* methods could be used to test this theory, the former providing the most conclusive evidence and the latter serving as a time/cost saving route to expedite decisions made for *in vivo* experimentation.

Overall, this data will inspire research in multiple directions that will hopefully lead to a fuller understanding of the mechanisms associated with EnvZ/OmpR signal transduction. With this knowledge, the role of this system within the overall TCS network can also be discovered leading to more effective research into disrupting that network for antibacterial purposes.

Chapter 7: Connections to Antibiotic Resistance

7.1: Connecting the TCS to Antibiotic Resistance

Research is only as good as its eventual application to a real-life issue. The TCS has been connected with antibiotic resistance mechanisms and this section first details the crisis including its effect upon the world and the antibiotic drug discovery conundrum. Further to this, the connections of the TCS family to antibiotic drug discovery are outlined.

7.2: The Antibiotic Crisis

Global misuse of antibiotics has brought about the era of resistance with respect to antibacterial drug discovery and development (173). Consequently, an increasing number of pharmaceutical companies have abandoned their endeavours into antibacterials (174). With the situation deteriorating, it has become an obligatory task to explore alternative potential mechanisms of antibacterial action. The mechanisms of antibacterial resistance are myriad and diverse but are usually categorised into three groups. Firstly, bacteria acquire resistance via the capture of resistance genes, generally through mobilisation and horizontal gene transfer from the environment. Secondly, the protection of polymorphisms in genes targeted by antibiotics via secondary mutations that neutralise fitness reductions caused by resistance mutations (175). Fitness reductions refers to the usual decrease in survival capability that is conferred by genetic mutations within bacteria. Thirdly, upregulation of intrinsic resistance mechanisms such as antibiotic efflux, bacterial impermeability to antibacterial agents or antibiotic inactivating enzymes (173,176,177). It has been suggested that targeting the intrinsic resistome offers potential for both novel therapeutic targets and employing combinatorial therapies with antibacterials that had been rendered ineffective as a direct result of the resistance mechanism targeted (176). For example, if changes in outer membrane permeability are rectified, the ability of an organism to limit antibiotic entry could be corrected and resistance could be overcome (178). In certain instances of antibacterial resistance,

membrane permeability has been shown to be reduced, which resulted in decreased antimicrobial uptake. This usually manifests as decreased expression of the outer membrane porin C (OmpC) and F (OmpF) following prolonged exposure to antibacterials (179). Based on this, specific protein systems, such as two-component regulatory systems (TCS), that contribute to the management of these resistance mechanisms could serve as novel antibacterial targets if their activity could be inhibited or modulated (180,181). Due to this possibility, EnvZ signal transduction and how signal transduction might be harnessed for signal output modulation and subsequent changes in porin balance within the outer membrane of Gram-negative organisms is reviewed.

7.3: Statistically summarising a slippery slope

There exists a multitude of research that conclusively describes our current situation of antibiotic resistance as a crisis (182–186). Seventeen million people die globally each year as a result of bacterial infections, making it the second most common cause of mortality after heart disease (187). In the United States of America, 2.8 million people are infected with antibiotic-resistant (ABR) strains of bacteria each year and 35,000 of those people will die as a result of these infections (187). These statistics have steadily risen across the globe and will continue to rise at an ever-increasing rate without prompt intervention. It is therefore possible to state that antibiotic resistance represents the single greatest threat to public health today (188). It also has severe economic consequences, as the O'Neill report estimated that ABR infections would cost the healthcare industry trillions of US dollars with annual deaths worldwide rising to 10 million by 2050 (189). The best example of the presence of resistant bacteria is the increasing difficulty with which gonorrhoea is treated, this disease is now resistant even to third-generation cephalosporins when it had originally been treated with penicillin during the 1970s (190). This dramatic reduction in treatment options will inevitably occur in many other infectious diseases without prompt intervention. Therefore, the

underpinning concepts of bacterial resistance mechanisms must be fully understood in order to overcome this downward trajectory of bacterial treatment options.

7.4: Pushing past the futility

Presently, the crucial issues impacting the endurance of antimicrobial efficacy are firstly any novel antibiotic that may be conceived will inevitably be resisted in some form by the bacteria it is designed to combat, secondly, the rate at which it is possible to design, create and approve novel antimicrobial agents is consistently slower than the rate of genetic diversification within bacteria. Thirdly, with concerted efforts from the scientific community to overcome these issues, economic barriers exist to further prevent the spread of ABR bacteria. Antibiotics are of diminishing financial value to the pharmaceutical industry, as they are often curative and used for short periods. Compared to medications designed for chronic illnesses, they are not economically wise investments which is supported by trends in the financial decisions made by pharmaceutical companies (184,191). This suggests research into new antibiotics and antibacterial resistance could ultimately be a Sisyphean endeavour. However, the human spirit for survival is nothing if not indomitable, therefore we shall continue to roll the boulder up the mountainside, figuratively speaking, and our search for new ways to control bacterial survival and, infection shall continue regardless.

7.5: Drug Discovery to prevent a Post-Antibiotic Era

During the golden and medicinal chemistry eras of antibiotic discovery, technologies were progressing rapidly allowing for the adaptation of existing antibiotic structures to improve their pharmacological profiles as well as identifying new targets via newly invented genetic techniques. As we progressed into the resistance era, discovery became target-based and the success rate diminished rapidly. If these trends continue as predicted, small injuries and minor infections will become increasingly serious if not fatal as they were before the discovery of antibiotics (192). Going forward, it is crucial that new and unconventional methods of drug

discovery be conceived and implemented, else the current period of drug discovery decline will persist and worsen (173). The first step in designing new models of discovery is to identify the key failures of the previous models. Firstly, conventional drug discovery methods such as target-based and phenotypic high throughput screening, have not worked for discovering novel antibacterial therapies. Also, the compound portfolios for clinical trials consist largely of derivatives of chemicals that have underlying resistance mechanisms against them Finally, the lack of knowledge concerning novel targets, in terms of their identity, function and integration with other bacterial processes poses a difficult starting point for discovery of novel antibacterials. (193–195). Combinatorial therapies have been proven to allow certain antibiotics to avoid the intrinsic resistance mechanisms imposed upon them by ABR bacteria. For example, beta lactam antibacterials, such as ampicillin, are prevented from working by beta-lactamases. Thus, beta-lactamase inhibitors, such as sulbactam (which can be combined with ampicillin due to similar half-lives) were developed to prevent the beta lactamase from inactivating the beta lactam drug. Further strategies may then be devised based on nullifying other resistance mechanisms that either directly or indirectly impact on the efficacy of current antimicrobial therapies. Identifying both essential and non-essential genes within the genomes of specific bacteria may lead to direct and specific targeting of these genes in order to attenuate virulence or decrease chance of survival. Finally, by assessing genetic networks within bacteria, genes reliant on one or more other genes to function effectively can be identified. This creates an opportunity to disrupt multiple genes and therefore multiple proteins by targeting a single gene, efficiently reducing bacterial survival or virulence. By focussing on these specific areas through which antibiotic resistance can be countered, discovery of novel antibiotics may be expedited.

7.5.1: Combinatorial therapies

The lack of knowledge surrounding bacterial membrane permeation and efflux systems holds back the creation of efficacious compounds, especially in the case of Gram-negative bacteria (173). If these systems can be understood and subsequently targeted, they could be used in combination with older antibiotics otherwise rendered powerless due either to inability to enter the cell or inability to remain within the cell long enough to be efficacious. Such combinatorial therapies, such as a beta-lactam and a beta-lactamase inhibitor, have already proven synergistic effects and it is an increasingly favourable therapeutic strategy. This is an especially important example as the additional therapy (the inhibitor) tackles the resistance mechanism employed by the bacteria therefore allowing the original antibiotic to retain its efficacy. This method could be replicated for other therapies that are made ineffective by a specific resistance mechanism by targeting that mechanism in combination with the original therapy. In order to capitalise on this, further discoveries must be made into systems that may be targeted by an adjuvant, thereby reducing the minimum inhibitory concentration of the main bacteriostatic/cidal agent and minimise toxicity.

7.5.2: Essential genes

Further on the subject of understanding the inner workings of bacteria, it is important to identify the essential genes within the bacterial genome. If a gene encodes a protein that could be described as dispensable to the ongoing survival of that bacterium, then that protein may be considered to be of less worth as a potential antibiotic target. The *E. coli* genome consists of 4290 genes, seven percent of which are considered to be essential genes (EG) for growth in nutrient rich media and a further ten percent are considered conditionally essential genes (CEG)(23, 24). Adding to this, a distinction between an EG and a CEG must be addressed, as several genes could be considered essential in one environmental context but not another. Because of this, CEGs have often been overlooked for drug discovery purposes despite

occupying large portions of bacterial genomes. As the conditions effect the essentiality of these genes, it is important to assess their importance within an *in vivo* model (e.g. mouse model) rather than performing *in vitro* experiments using model microorganisms. Therefore, the function of these genes within the context of infection is poorly understood and further *in vivo* experimentation will be required. It has also been shown that removal of a subset of non-essential genes completely attenuated the virulence of a highly virulent mycoplasma bacterium (198). This suggests that while survival may not be directly affected, the pathogenicity of the bacteria could be altered via non-essential targets. If the conditions of indispensability for this wide array of genes could be understood, a multitude of target options would become available. Also, experiments into defining EGs have been dominated by *in vitro* experimentation and in model microorganisms, reducing opportunities to assess the effect of different environmental contexts. Therefore *in vivo* experimentation of EGs within a host (e.g. mouse model) could allow assessment of a group of potential EG targets within an appropriate environment therefore producing the *in vivo* phenotype. This phenotype represents the specific genetic outcome that would occur *in vivo* and therefore would be the most clinically relevant target. However, the pool of targets within this *in vivo* infection gene set is vast and the majority of genes identified through *in vitro* experimentation with both nutrient-rich and nutrient-limited media can be found within this set yet represent a smaller pool of targets (**Figure 7-1**). It is therefore a greater innovation risk to pharmaceutical companies to develop novel antibacterials based on these targets as the pool of potential targets is so large that it will significantly reduce the success rate of discovery.

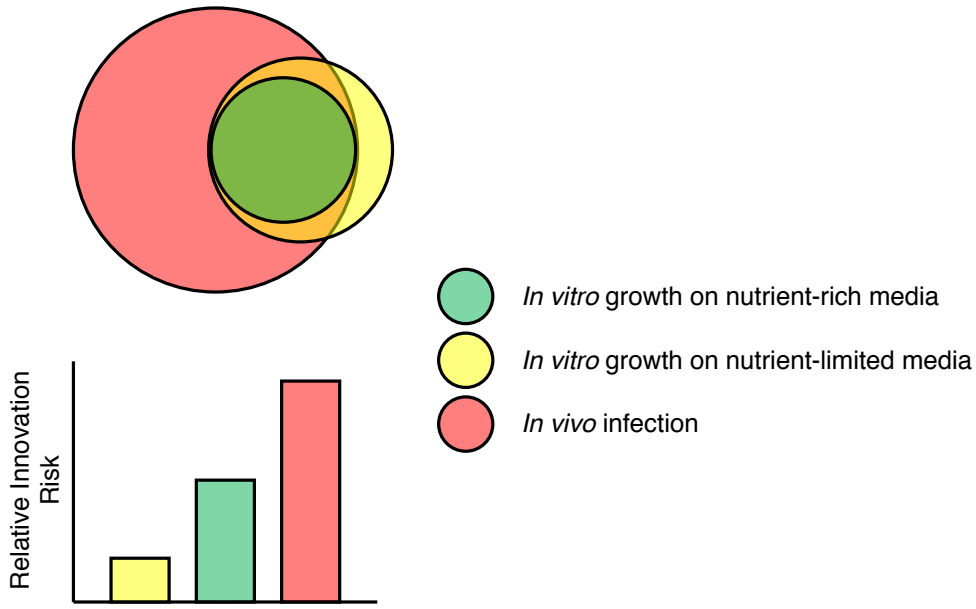

Figure 7-1: A Venn diagram showing the relative pool of target genes within a hypothetical bacterial pathogen. Three pools are set with an assigned innovation risk (indicated by the bar chart) to modern drug discovery. The largest pool (red) contains genes required for infection within a relevant animal model. These genes require extensive validation thus the risk is greatest. The pool containing genes required for growth on nutrient-limited media (yellow) is well documented, yet a portion of these genes will not be required for in vivo infection. The risk for these genes is lowest as the pool is large and mainly consists of genes of potential clinical relevance. The pool containing genes required for growth on nutrient-rich media (green) have been the conventional targets for many years. This pool is the smallest yet many of these genes will have been checked for validation as a potential target previously (173).

7.5.3: Gene interaction networks

The network of genetic interactions across a bacterial genome can be considered functional, complex and abundant (26, 27). As previously discussed, certain genes may be considered essential, yet this may be context-dependant. The context may include the availability of connected genes, for example, a gene may be essential if a connected gene is not present but dispensable when that gene is present. Experiments have been conducted in which both single and paired gene deletions are implemented within a bacterium, in which thousands of the latter were synthetically lethal (201). Further on from this, the double deletions showed significant fitness reduction compared to their corresponding single deletion mutants. Unsurprisingly, this contributes to the evidence base that supports combinatorial therapies as disruption of two linked targets has potential to increase bactericidal capabilities. However, as certain genes are deleted, other genes may become dispensable thereby reducing its viability as a drug target. Overall, as our understanding of genetic-interaction networks becomes deeper it will become easier to identify targets that will have the required effect within that network.

7.6 Summary

Understanding the mechanisms behind antimicrobial resistance (AMR) in a general sense must lead into more specific investigation into protein families that confer resistance to bacteria. The TCSs can be logically connected as they are found across almost all bacteria which sense changes in the bacterial environment and alter systems accordingly to promote cell survival. As antibiotic compounds are regularly present in the environment, and because several antibiotics are developed from compounds produced by bacteria, there will be TCSs that either directly or indirectly impede antibiotic mechanisms.

7.7: TCS and Drug Discovery

The TCS holds a number of attributes that suggest that it would be a successful target for antimicrobial therapy (202). Perhaps the most attractive of these is its complete absence throughout mammalian eukaryotic cells and ubiquity within bacterial cells. When considering the intrinsic resistance mechanisms employed by bacteria, it is unsurprising that the TCS protein family, designed to protect a bacterium from its environment, is frequently involved. As previously discussed, combinatorial therapies are recommended to become employed and designed with increasing frequency. A TCS involved in an antibiotic prevention mechanism, such as the EnvZ/OmpR system that controls porin expression and therefore membrane permeability, could be targeted in order to allow the formerly resisted compound to regain efficacy. As these protein systems are not found in mammalian cells, the chance of side effects is significantly reduced, thereby eliminating the concern of increased side effects, which usually accompanies combinatorial therapies. TCSs also contribute to bacterial virulence, cell growth and biofilm formation (40,41,203,204), yet understanding behind their mechanisms of virulence is poor. However, the mechanisms have been proven to exist as TCS knockout strains have resulted in attenuation of virulence, suggesting that such a strain would serve as viable option for live vaccines against bacterial infections (202,205–208). For example, deletion of PhoP genes in *Mycobacterium* and *Salmonella* attenuates their virulence and remains immunogenic in animal models. Further to this, deletion of the *phoP/phoQ* TCS in *Salmonella typhi* provides a useful strain for a live vaccine against typhoid fever (208).

As most antibiotics derive from natural products, often from fungi, it would be wise to investigate natural TCS inhibitors and modulators. Further to this, there exist conserved homologies across multiple TCSs (209,210) and it is therefore suggested that a single drug could be capable of targeting a conserved domain then inhibiting several TCSs that share it. This approach should also protect against any molecular mutations that would usually affect ligand target affinity (211,212). Compared to targeting individual sensor domains for specific

SHKs, this may be the most effective course of action (203,213). However, this approach holds a severe disadvantage in that the ATP-binding pocket within the SHK that may be targeted in this way exhibits considerable homology to multiple human protein families (213). As previously mentioned, the TCS family is not found in human cells yet certain domains will be similar or the same, as this example demonstrates. Therefore, such an approach must be investigated cautiously to eliminate any chance of any side effect-generating human interactions.

Consequently, several groups have looked at specific TCSs in order to find potentially efficacious inhibitors specific to those systems. Examples include WalKR, essential for cell survival, QseCB, involved in virulence and VanSR, a TCS specifically evolved for antibiotic resistance. In addition to these, several TCSs control envelope transporter proteins with efflux capability that provide multidrug resistance in well-known human pathogens such as *Acinetobacter baumannii* and *Klebsiella pneumoniae* (214,215). Of particular interest, VanSR specifically confers resistance to vancomycin and this mechanism has been reported in several bacteria including *Staphylococcus aureus, Enterococcus faecalis* and *Enterococcus faecium*. Several inhibitors have been identified for this TCS, but as they have a negative effect on mitochondrial respiration within human cells they could not be used safely as a therapeutic (213,216–218). This discovery could, however, serve as a viable template upon which to develop a VanSR adjunct therapy. In the case of the PhoPR TCS, molecules from natural sources have been shown to bind to the PhoP protein (219), eliciting an antimicrobial effect in *Corynebacterium pseudotuberculosis*.

Returning to the EnvZ/OmpR TCS, as it is the best characterised and has a role in virulence in multiple organisms (220–222), any further investigation into its functionality would be extremely advantageous towards targeting this system. With the recent discovery of **M**odulator of Env**Z**/Omp**R A** (MzrA), a protein designed to modulate EnvZ activity (79,80), and inconclusive evidence on the specific mechanism by which EnvZ senses changes in

osmolarity it is important to define specific elements of the overall signaling mechanism in greater detail. Without such information, it would be far more difficult to specify viable targets within the protein system. It has therefore been necessary to investigate the research currently available regarding transmembrane communication both generally and in direct relation to the EnvZ/OmpR TCS.

Chapter 8: Future work

8.1: Future works

While I have suggested a model for the mechanism within the TM helices of EnvZ during signal transduction, the data is ultimately insufficient to conclusively state it as concrete fact. Further experiments will be required to solidify the findings from these projects.

8.1.1: Increase in Number of 2X-Cys mutants

The simplest way to gain more information utilising the information already acquired would be to extend the library by increasing the pairings to involve a wider range of potential interactions. Results gathered in the 2X-Cys project would inform these new pairings as there may be a pattern that would continue with further adjacent mutations. For example, the 2X-Cys library contains pairing 19-173 through 177. There may be interactions for 19-172 or 19-178 and so on which may illuminate us to more specific information about the dynamics of the transmembrane domains.

8.1.2: Investigation into MzrA

The structure of MzrA has been discovered as well as its general function, yet the specific mechanisms behind that function remain mysterious (79,80). The *mzrA* gene, formerly known as *yqjB* was discovered via mutational analyses within a *ΔbamBΔdegP E. coli* mutant. This mutant displays a lethal phenotype at 37°C, therefore the study aimed to find mutations within the *ΔbamBΔdegP* that allowed survival at 37°C. Subsequent experiments narrowed the removal of the lethal phenotype to the *mzrA* gene. MzrA was then overexpressed in the *ΔbamBΔdegP* mutant, improving cell growth, and the reasons for this were elucidated by examining the outer membrane protein (OMP) profile. In response to MzrA overexpression, OmpF levels are dramatically reduced while OmpC levels are unaffected even within a *bamB+degP+* strain. This led to the MzrA protein being connected to the EnvZ/OmpR and

subsequently a more specific characterisation of this relationship (79). As EnvZ-MzrA interactions are enhanced, EnvZ kinase activity is increased and therefore phosphorylated OmpR levels rise. This could also be caused by MzrA reducing phosphatase capabilities of EnvZ, either in combination with increased kinase activity or instead of it. Despite these discoveries, the specific biophysical interactions between the MzrA and EnvZ proteins have not been concretely established. Therefore, to understand the full function of EnvZ within the context of a WT *E. coli* all interactions must be characterised fully.

Disulphide crosslinking experiments similar to those carried out within the EnvZ TMs should be carried out to first establish inter-protein interactions within its homodimer formation. Following this step, Cys-mutants of both EnvZ and MzrA will be combined in order to determine EnvZ-MzrA interactions (**Figure 8-1**). Results collected from the first set of MzrA mutants and from the EnvZ TM mutants will be used to determine the best areas of the protein to target when creating EnvZ/MzrA mutant combinations. With the information gathered from such experiments, interacting domains can be identified within the MzrA-MzrA' homodimer and within the EnvZ/MzrA interface

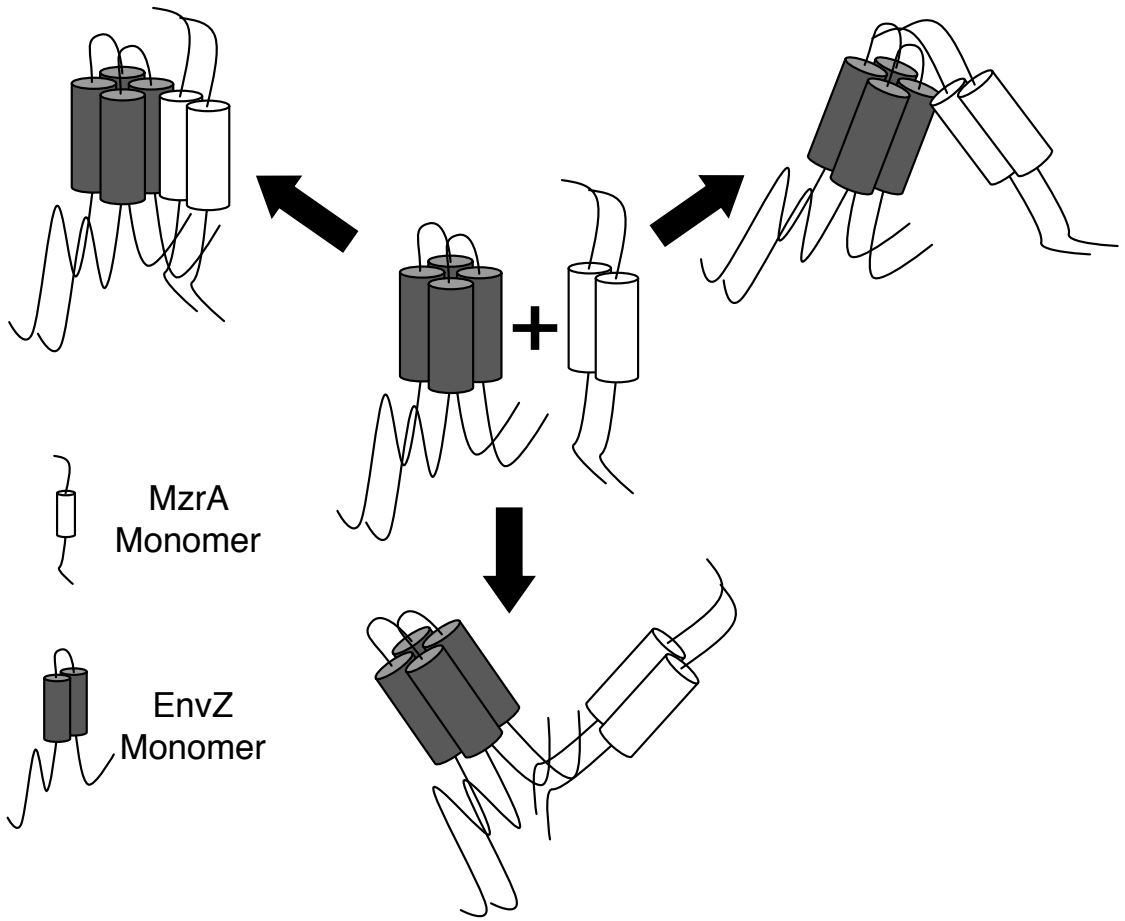

Figure 8-1: EnvZ-MzrA interactions are yet to be established. The interaction surfaces between EnvZ and MzrA have not been mapped. Experiments involving the combination of a library containing 1X-Cys substitutions at every available position within MzrA and the existing 1X-Cys mutant libraries would show where MzrA/EnvZ TM helix interactions occur. This figure shows three possibilities, only one of which, interaction directly with EnvZ transmembrane helices (top left), would be possible through these combination experiments. To test the possibilities of MzrA interacting with other parts of EnvZ (periplasmic and cytoplasmic domains) a library of EnvZ 1X-Cys mutations would need to be created for every available position within the protein. This library would then be combined with all mutations within the MzrA library. However, these methods, whilst exhaustive of every possible interaction, would be time consuming and costly to run due to the high number of mutant combinations possible.

8.2: Crosstalk Research

EnvZ/OmpR has been shown to engage in some crosstalk with the ArcB-ArcA TCS, which could highlight an excellent starting point for investigation into the overall *E. coli* TCS network. Evidence shows OmpR is phosphorylated by the SHK ArcB as OmpC levels are increased when cells are grown under anaerobic conditions, the activating factor for the ArcB phosphorylation mechanism (223). To show this activation of OmpR is achieved through ArcB function and not EnvZ function, the same experiments were carried out in the absence of EnvZ and the same results were seen. Lastly, purified ArcB phosphorylates both ArcA and OmpR *in vitro*, yet other RRs such as UvrY and KdpE are not affected. While these results are highly suggestive of cross phosphorylation between these TCSs, activation of OmpR via ArcA has not been ruled out. Regardless, the systems evidently interact with one another and further investigation into the survival advantages for this crosstalk mechanism will be the logical next step.

Generally considering the potential reasons for crosstalk overcoming specificity in TCS function, it is worth considering the relationship between signal input and signal output. If a TCS detects a particular environmental change, the outputs that are produced by this detection and subsequent activation will be specifically designed to allow the cell to adapt to its specific environment in that moment. As environments are diverse and complex, there will undoubtedly be occurrences in which multiple TCSs are activated simultaneously from the various environmental stimuli. If a RR is deliberately affected by another TCSs SHK, especially in the absence of the RRs stimulus, then it could be theorised that the non-cognate outputs address that stimulus as well as the usual stimulus. To take the previously discussed EnvZ/OmpR – ArcB/ArcA crosstalk as an example, if anaerobic conditions cause OmpR activation then the presence of the outer membrane porin OmpC could contribute to cell survival in an anaerobic environment. Further to this with regards to the importance of porin regulation, it may be important to alter porin expression in response to a variety of

environmental stimuli especially if they are in combination. For example, a bacterium will have a survival advantage if it reduces membrane permeability in response to the presence of antibiotic compounds within its environment despite the osmolarity of its environment being low, which would usually lead to increased membrane permeability. This would likely be achieved via allosteric modulation of the EnvZ protein, activating the SHK via a different signal pathway than its osmosensing mechanism. This could be delivered by MzrA or it could be a separate sensing capability – there is ample room for further investigation into these areas. Particularly regarding MzrA, there would logically be another signal receiving element further upstream of this signaling cascade that needs to be identified and understood. This could be another TCS, a different protein system altogether or even MzrA receiving direct stimulus itself. These inquiries should initially concern the role of EnvZ in deliberate crosstalk and membrane protein networking but ultimately branch out into other TCSs and understanding the network of communication as a whole. The clearer we can depict this network, the easier it will be to develop ways in which we can disrupt and sabotage it leading to decreased bacterial survival within regular environments.

8.3: Developing a Biotechnology Application for Two-Component Systems

As previously discussed, TCSs are promising targets for future antibacterials, thus methods must be developed in order to screen potential compounds for their antibacterial properties specifically regarding their capability to interact with TCS function. As multiple TCSs are found in pathogenic bacteria and influence pathogenic mechanisms, the practicalities of experimentation are ultimately affected. A pathogenic bacterium will need increased health and safety measures to perform any experiment, which increases the cost and complexities of protective equipment and practices. If experiments can include only the least pathogenic bacteria, these costs can be drastically reduced, then the overall speed and efficiency of

experiments will be significantly increased. As non-pathogenic *E. coli* is a hazard group 1 bacterium (224) (least pathogenic concern), experiments will require far less protective personal equipment and safety procedures will be less restrictive. Therefore, we can move forward using *E. coli* and the EnvZ/OmpR TCS as a basis for investigating how best to target TCSs in general, especially considering the infrastructure and knowledge we have in place for developing new experiments around these systems. However, a method must be developed to discover new information about pathogenic bacteria and their TCSs while still using *E. coli* and the EnvZ/OmpR system.

Chimeric proteins fuse domains of two similarly functioning proteins in order to gain information about the domain(s) of one protein via the output of the other protein. In the case of TCSs, the SHK of two separate systems can be fused to create a chimera that senses like one but generates a signal output like the other. As the signal output system of EnvZ/OmpR is easily quantifiable by the dual fluorescence reporter system described earlier in this thesis, the cytoplasmic domains of EnvZ will be used in these chimeras. This leaves the sensory domains, areas potential antibacterials may interact with, to be filled by a variety of different SHKs that are involved in pathogenic processes or found in pathogenic bacteria. This will allow quantification of the effect a novel compound has on an SHK within a pathogenic bacterium, via the signal output of EnvZ/OmpR within a non-pathogenic strain of *E. coli*.

To reach this stage, the chimeric protein must be tested for its robustness compared to the normal functioning forms of its WT constituents. Robustness is defined as the ability for a signaling circuit to maintain a steady response across a wide concentration/intensity range of stimulus input. For example, if 0.01M of a substance is added then it should illicit the same response as 1M of the same substance with very little fluctuation in between. If the robustness of a chimeric system is much lower than this range, the results that are gained from it will be unrepresentative of either of its constituents. In most cases, a chimeric protein will not be robust and therefore it must be tuned in order to restore that robustness. The key area of

interest when tuning a chimera is the point of fusion as one protein becomes the next, which is an unnatural connection and therefore highly susceptible to improper positioning or reduced dynamism. A way in which dynamism can be restored to this fusion point is a method known as aromatic tuning. This method involves the repositioning of aromatic residues at the point of fusion to improve dynamism and restore robustness to the signaling circuit. Multiple positions are used for aromatic tuning in order to locate the ideal positioning for the aromatic residues. This is gauged by the usual method for signal output measurement, the dual fluorescence reporter system, and the aromatically tuned chimeric protein will be tested across a range of stimulus input concentrations/intensities to determine an appropriately robust response. Once this has been determined, novel compounds can be delivered to the chimeric protein in order to ascertain any reduction or abolishment of signal. As several thousand compounds would be screened via this method, once entirely optimised and functional, it is likely that a wide variety of results will be seen. Results that may be categorised with “potential antibacterial properties” should be tested further in addition to finding compounds with similar chemical structures that have not been tested. As an *in vivo* experiment, this process will expedite progression into the next stages of drug discovery and ultimately reduce the overall cost of development into a viable therapeutic.

Closing Remarks

This body of work investigated one small part of a much bigger mechanism in terms of EnvZ, the TCS network it operates within and the overall bacterial survival mechanisms that protect *E. coli* and other organisms from antibacterial interventions. The result of that investigation proved fruitful in beginning to define something that could be truly novel within the current understanding of TCS signaling mechanisms. As previously mentioned, the various paths of research that have been illuminated from these discoveries could each contain their own discoveries and a multitude of paths after that. If there is one thing that inspires me to conduct research, it is being happy that there will always be so much left to discover and those discoveries will always pose more questions than they answer. It is unlikely that I will discover the full working mechanisms of EnvZ/OmpR during my career, yet I can rest easy knowing that I pushed that section of knowledge a step further towards that end goal. The reference list of this thesis alone holds over 200 contributions informing my work and now my findings will inform other research for many years to come. Some may interpret the data differently and others may dispute it entirely but it will make people think and discuss the subject and ultimately that is all you can ask from research – to further the conversation.

Appendix

Ethics

FORM UPR16

Research Ethics Review Checklist

Please include this completed form as an appendix to your thesis (see the Research Degrees Operational Handbook for more information

UNIVERSITY OF PORTSMOUTH

Postgraduate Research Student (PGRS) Information				**Student ID:**	652740		
PGRS Name:	Robert John Lawrence						
Department:	PHBM		**First Supervisor:**	Dr Roger R. Draheim			
Start Date: (or progression date for Prof Doc students)	**01/10/2016**						
Study Mode and Route:	Part-time ☐	Full-time ☒	MPhil ☐	PhD ☒	MD ☐	Professional Doctorate ☐	

Title of Thesis:	Unravelling the Choreography of the EnvZ/OmpR Transmembrane Pas de Deux
Thesis Word Count: (excluding ancillary data)	47913

If you are unsure about any of the following, please contact the local representative on your Faculty Ethics Committee for advice. Please note that it is your responsibility to follow the University's Ethics Policy and any relevant University, academic or professional guidelines in the conduct of your study

Although the Ethics Committee may have given your study a favourable opinion, the final responsibility for the ethical conduct of this work lies with the researcher(s).

UKRIO Finished Research Checklist: (If you would like to know more about the checklist, please see your Faculty or Departmental Ethics Committee rep or see the online version of the full checklist at: http://www.ukrio.org/what-we-do/code-of-practice-for-research/)	
a) Have all of your research and findings been reported accurately, honestly and within a reasonable time frame?	YES ☒ NO ☐
b) Have all contributions to knowledge been acknowledged?	YES ☒ NO ☐
c) Have you complied with all agreements relating to intellectual property, publication and authorship?	YES ☒ NO ☐
d) Has your research data been retained in a secure and accessible form and will it remain so for the required duration?	YES ☒ NO ☐
e) Does your research comply with all legal, ethical, and contractual requirements?	YES ☒ NO ☐

Candidate Statement:		
I have considered the ethical dimensions of the above named research project, and have successfully obtained the necessary ethical approval(s)		
Ethical review number(s) from Faculty Ethics Committee (or from NRES/SCREC):		ETHIC-2019-1520
If you have *not* submitted your work for ethical review, and/or you have answered 'No' to one or more of questions a) to e), please explain below why this is so:		
Signed *(PGRS)*:		**Date:** 25/11/2019

UPR16 – April 2018

Bibliography

1. Batchelor E, Goulian M. Robustness and the cycle of phosphorylation and dephosphorylation in a two-component regulatory system. Proc Natl Acad Sci. 2003;100(2):691–6.
2. Siryaporn A, Goulian M. Cross-talk suppression between the CpxA-CpxR and EnvZ-OmpR two-component systems in E. coli. Mol Microbiol. 2008;70(2):494–506.
3. Casadaban MJ, Cohen SN. Analysis of gene control signals by DNA fusion and cloning in Escherichia coli. J Mol Biol. 1980;138(2):179–207.
4. Batchelor E, Silhavy TJ, Goulian M. Continuous control in bacterial regulatory circuits. J Bacteriol. 2004;186(22):7618–25.
5. Hsing W, Silhavy TJ. Function of conserved histidine-243 in phosphatase activity of EnvZ, the sensor for porin osmoregulation in Escherichia coli. J Bacteriol. 1997;179(11):3729–35.
6. Nørholm MHH, Von Heijne G, Draheim RR. Forcing the issue: Aromatic tuning facilitates stimulus-independent modulation of a two-component signaling circuit. ACS Synth Biol. 2015;4(4):474–81.
7. Dubrac S, Bisicchia P, Devine KM, Msadek T. A matter of life and death: Cell wall homeostasis and the WalKR (YycGF) essential signal transduction pathway. Mol Microbiol. 2008;70(6):1307–22.
8. Freeman ZN, Dorus S, Waterfield NR. The KdpD/KdpE Two-Component System: Integrating K+ Homeostasis and Virulence. PLoS Pathog. 2013;9(3).
9. Hsieh YJ, Wanner BL. Global regulation by the seven-component Pi signaling system. Curr Opin Microbiol. 2010;13(2):198–203.
10. Raivio TL. Everything old is new again: An update on current research on the Cpx envelope stress response. Biochim Biophys Acta - Mol Cell Res. 2014;1843(8):1529–41.

11. Kato A, Latifi T, Groisman EA. Closing the loop: The PmrA/PmrB two-component system negatively controls expression of its posttranscriptional activator PmrD. Proc Natl Acad Sci. 2003;100(8):4706–11.

12. Groisman EA. The pleiotropic two-component regulatory system PhoP-PhoQ. J Bacteriol. 2001;183(6):1835–42.

13. Ryndak M, Wang S, Smith I. PhoP, a key player in Mycobacterium tuberculosis virulence. Trends Microbiol. 2008;16(11):528–34.

14. Lynn DG, Lin YH, Gao R, Binns AN. Capturing the VirA/VirG TCS of Agrobacterium tumefaciens. Adv Exp Med Biol. 2008;631:161–77.

15. Raghavan V, Groisman EA. Orphan and hybrid two-component system proteins in health and disease. Curr Opin Microbiol. 2010;13(2):226–31.

16. Norsworthy AN, Visick KL. Signaling between two interacting sensor kinases promotes biofilms and colonization by a bacterial symbiont. Mol Microbiol. 2015;96(2):233–48.

17. Quon KC, Marczynski GT, Shapiro L. Cell cycle control by an essential bacterial two-component signal transduction protein. Cell. 1996;84(1):83–93.

18. Alkhuder K, Meibom KL, Dubail I, Dupuis M, Charbit A. Identification of trkH, Encoding a Potassium Uptake Protein Required for Francisella tularensis Systemic Dissemination in Mice. Aziz RK, editor. PLoS One [Internet]. 2010 Jan 29 [cited 2020 May 28];5(1):e8966. Available from: https://dx.plos.org/10.1371/journal.pone.0008966

19. Stingl K, Brandt S, Uhlemann EM, Schmid R, Altendorf K, Zeilinger C, et al. Channel-mediated potassium uptake in Helicobacter pylori is essential for gastric colonization. EMBO J. 2007 Jan 10;26(1):232–41.

20. Chen YC, Chuang YC, Chang CC, Jeang CL, Chang MC. A K+ Uptake Protein, TrkA, is Required for Serum, Protamine, and Polymyxin B Resistance in Vibrio vulnificus. Infect Immun. 2004 Feb;72(2):629–36.

21. Su J, Gong H, Lai J, Main A, Lu S. The potassium transporter trk and external potassium

modulate Salmonella enterica protein secretion and virulence. Infect Immun. 2009 Feb;77(2):667–75.

22. Nikaido H. Molecular Basis of Bacterial Outer Membrane Permeability Revisited. Microbiol Mol Biol Rev. 2003;67(4):593–656.

23. Groisman EA. Feedback Control of Two-Component Regulatory Systems. Annu Rev Microbiol. 2016;70(1):103–24.

24. Laub MT, Goulian M. Specificity in Two-Component Signal Transduction Pathways. Annu Rev Genet. 2007;41(1):121–45.

25. Verhamme DT, Arents JC, Postma PW, Crielaard W, Hellingwerf KJ. Investigation of in vivo cross-talk between key two-component systems of Escherichia coli. Microbiology. 2002;148(1):69–78.

26. Skerker JM, Prasol MS, Perchuk BS, Biondi EG, Laub MT. Two-component signal transduction pathways regulating growth and cell cycle progression in a bacterium: A system-level analysis. PLoS Biol. 2005;3(10):1043–54.

27. Casino P, Rubio V, Marina A. Structural Insight into Partner Specificity and Phosphoryl Transfer in Two-Component Signal Transduction. Cell. 2009;139(2):325–36.

28. Huynh TN, Noriega CE, Stewart V. Conserved mechanism for sensor phosphatase control of two-component signaling revealed in the nitrate sensor NarX. Proc Natl Acad Sci. 2010;107(49):21140–5.

29. Willett JW, Kirby JR. Genetic and Biochemical Dissection of a HisKA Domain Identifies Residues Required Exclusively for Kinase and Phosphatase Activities. PLoS Genet. 2012;8(11).

30. Igo MM, Ninfa AJ, Stock JB, Silhavy TJ. Phosphorylation and dephosphorylation of a bacterial transcriptional activator by a transmembrane receptor. Genes Dev. 1989;3(11):1725–34.

31. Huynh TN, Stewart V. Negative control in two-component signal transduction by

transmitter phosphatase activity. Mol Microbiol. 2011;82(2):275–86.

32. Klein AH, Shulla A, Reimann SA, Keating DH, Wolfe AJ. The intracellular concentration of acetyl phosphate in Escherichia coli is sufficient for direct phosphorylation of two-component response regulators. J Bacteriol [Internet]. 2007 Aug 1 [cited 2019 Aug 8];189(15):5574–81. Available from: http://www.ncbi.nlm.nih.gov/pubmed/17545286

33. Lukat GS, McCleary WR, Stock AM, Stock JB. Phosphorylation of bacterial response regulator proteins by low molecular weight phospho-donors. Proc Natl Acad Sci U S A [Internet]. 1992 Jan 15 [cited 2019 Aug 8];89(2):718–22. Available from: http://www.ncbi.nlm.nih.gov/pubmed/1731345

34. McCleary WR, Stock JB, Ninfa AJ. Is acetyl phosphate a global signal in Escherichia coli? J Bacteriol [Internet]. 1993 May 1 [cited 2019 Aug 8];175(10):2793–8. Available from: http://www.ncbi.nlm.nih.gov/pubmed/8491699

35. Miyashiro T, Goulian M. High stimulus unmasks positive feedback in an autoregulated bacterial signaling circuit. Proc Natl Acad Sci. 2008;105(45):17457–62.

36. Cai SJ, Inouye M. EnvZ-OmpR interaction and osmoregulation in Escherichia coli. J Biol Chem. 2002;277(27):24155–61.

37. Carpenter BM, West AL, Gancz H, Servetas SL, Pich OQ, Gilbreath JJ, et al. Crosstalk between the HpArsRS two-component system and HpNikR is necessary for maximal activation of urease transcription. Front Microbiol [Internet]. 2015 [cited 2019 Aug 8];6(JUN):558. Available from: http://www.ncbi.nlm.nih.gov/pubmed/26124751

38. Pei G, Niu X, Zhou Y, Chen L, Zhang W. Crosstalk of two-component signal transduction systems in regulating central carbohydrate and energy metabolism during autotrophic and photomixotrophic growth of Synechocystis sp. PCC 6803. Integr Biol [Internet]. 2017 May 1 [cited 2019 Aug 8];9(5):485–96. Available from: https://academic.oup.com/ib/article/9/5/485-496/5115391

39. Novotna GB, Kwun MJ, Hong HJ. In vivo characterization of the activation and

interaction of the VanR-VanS two-component regulatory system controlling glycopeptide antibiotic resistance in two related streptomyces species. Antimicrob Agents Chemother. 2016;60(3):1627–37.

40. Eguchi Y, Utsumi R. Introduction to bacterial signal transduction networks. Adv Exp Med Biol [Internet]. 2008;631:1–6. Available from: http://eutils.ncbi.nlm.nih.gov/entrez/eutils/elink.fcgi?dbfrom=pubmed&id=18792678&retmode=ref&cmd=prlinks%5Cnpapers2://publication/doi/10.1007/978-0-387-78885-2_1

41. Mitrophanov AY, Groisman EA. Signal integration in bacterial two-component regulatory systems. Genes Dev. 2008;22(19):2601–11.

42. Cai SJ, Inouye M. Spontaneous subunit exchange and biochemical evidence for trans-autophosphorylation in a dimer of Escherichia coli histidine kinase (EnvZ). J Mol Biol. 2003;329(3):495–503.

43. Kellogg SL, Little JL, Hoff JS, Kristich CJ. Requirement of the CroRS two-component system for resistance to cell wall-targeting antimicrobials in Enterococcus faecium. Antimicrob Agents Chemother. 2017;61(5).

44. Zhang S, Hu Y, Fan Q, Wang X, He J. Two-component system yvqEC-dependent bacterial resistance against vancomycin in bacillus thuringiensis. Antonie van Leeuwenhoek, Int J Gen Mol Microbiol. 2015;108(2):365–76.

45. Kristich CJ, Snyder H, Little JL, Kellogg SL, Skarda LM. Nutritional Control of Antibiotic Resistance via an Interface between the Phosphotransferase System and a Two-Component Signaling System. Antimicrob Agents Chemother. 2013;58(2):957–65.

46. Weatherspoon-Griffin N, Yang D, Kong W, Hua Z, Shi Y. The CpxR/CpxA Two-component Regulatory System Up-regulates the Multidrug Resistance Cascade to Facilitate *Escherichia coli* Resistance to a Model Antimicrobial Peptide. J Biol Chem [Internet]. 2014 Nov 21 [cited 2019 Aug 1];289(47):32571–82. Available from: http://www.ncbi.nlm.nih.gov/pubmed/25294881

47. Adler M, Anjum M, Andersson DI, Sandegren L. Combinations of mutations in envZ, ftsI, mrdA, acrB and acrR can cause high-level carbapenem resistance in Escherichia coli. J Antimicrob Chemother. 2016;71(5):1188–98.

48. Ferris HU, Coles M, Lupas AN, Hartmann MD. Crystallographic snapshot of the Escherichia coli EnvZ histidine kinase in an active conformation. J Struct Biol [Internet]. 2014 [cited 2020 Jun 25];186(3):376–9. Available from: https://pubmed.ncbi.nlm.nih.gov/24681325/

49. Slauch JM, Garrett S, Jackson DE, Silhavy TJ. EnvZ functions through OmpR to control porin gene expression in Escherichia coli K-12. J Bacteriol. 1988;170(1):439–41.

50. Yoshida T, Phadtare S, Inouye M. Functional and Structural Characterization of EnvZ, an Osmosensing Histidine Kinase of E. coli. In: Methods in Enzymology [Internet]. Academic Press Inc.; 2007 [cited 2020 Jun 24]. p. 184–202. Available from: https://pubmed.ncbi.nlm.nih.gov/17609132/

51. Egger LA, Inouye M. Purification and characterization of the periplasmic domain of EnvZ osmosensor in Escherichia Coli. Biochem Biophys Res Commun. 1997;231(1):68–72.

52. Khorchid A, Inouye M, Ikura M. Structural characterization of Escherichia coli sensor histidine kinase EnvZ: The periplasmic C-terminal core domain is critical for homodimerization. Biochem J. 2005;385(1):255–64.

53. Forst S, Comeau D, Norioka S, Inouye M. Localization and membrane topology of EnvZ, a protein involved in osmoregulation of OmpF and OmpC in Escherichia coli. J Biol Chem. 1987;262(34):16433–8.

54. Roberts DL, Bennett DW, Forst SA. Identification of the site of phosphorylation on the osmosensor, EnvZ, of Escherichia coli. J Biol Chem. 1994;269(12):8728–33.

55. Delgado J, Forst S, Harlocker S, Inouye M. Identification of a phosphorylation site and functional analysis of conserved aspartic acid residues of OmpR, a transcriptional

activator for ompF and ompC in Escherichia coli. Mol Microbiol. 1993;10(5):1037–47.

56. Aiba H, Nakasai F, Mizushima S, Mizuno T. Evidence for the physiological importance of the phosphotransfer between the two regulatory components, EnvZ and OmpR, in osmoregulation in Escherichia coli. J Biol Chem. 1989;264(24):14090–4.

57. Yang Y, Inouye M. Intermolecular complementation between two defective mutant signal-transducing receptors of Escherichia coli (signal transduction/protein kinase/phosphatase/outer membrane porins/OmpR) [Internet]. Vol. 88, Proc. NatI. Acad. Sci. USA. 1991 [cited 2020 Apr 22]. Available from: https://www.pnas.org/content/88/24/11057.short

58. Qin L, Dutta R, Kurokawa H, Ikura M, Inouye M. A monomeric histidine kinase derived from EnvZ, an Echerichia coli osmosensor. Mol Microbiol. 2000;36(1):24–32.

59. Pukklay P, Nakanishi Y, Nitta M, Yamamoto K, Ishihama A, Shiratsuchi A. Involvement of EnvZ-OmpR two-component system in virulence control of Escherichia coli in Drosophila melanogaster. Biochem Biophys Res Commun. 2013;438(2):306–11.

60. Dutta R, Inouye M. GHKL, an emergent ATPase/kinase superfamily. Trends Biochem Sci. 2000;25(1):24–8.

61. Parkinson JS, Kofoid EC. Communication Modules in Bacterial Signaling Proteins. Annu Rev Genet. 1992 Dec;26(1):71–112.

62. Hidaka Y, Park H, Inouye M. Demonstration of dimer formation of the cytoplasmic domain of a transmembrane osmosensor protein, EnvZ, of Escherichia coli using Ni-histidine tag affinity chromatography. FEBS Lett. 1997 Jan 3;400(2):238–42.

63. Park H, Inouye M. Mutational analysis of the linker region of EnvZ, an osmosensor in Escherichia coli [Internet]. Vol. 179, Journal of Bacteriology. 1997 [cited 2020 Apr 21]. Available from: http://jb.asm.org/

64. Park H, Saha SK. Two-domain reconstitution of a functional protein histidine kinase [Internet]. Vol. 95, National Acad Sciences. 1998 [cited 2020 Apr 22]. Available from:

www.pnas.org.

65. Zhu Y, Qin L, … TY-P of the, 2000 undefined. Phosphatase activity of histidine kinase EnvZ without kinase catalytic domain. Natl Acad Sci [Internet]. [cited 2020 Apr 22]; Available from: https://www.pnas.org/content/97/14/7808.short

66. Tomomori C, Tanaka T, Dutta R, Park H, Saha SK, Zhu Y, et al. Solution structure of the homodimeric core domain of Escherichia coli histidine kinase EnvZ [Internet]. nature.com. 1999 [cited 2020 Apr 22]. Available from: http://www.biochem.ucl.ac.uk/bsm/PP/server

67. Tanaka T, Saha S, Tomomori C, Ishima R, Nature DL-, 1998 undefined. NMR structure of the histidine kinase domain of the E. coli osmosensor EnvZ [Internet]. nature.com. 1998 [cited 2020 Apr 22]. Available from: www.nature.com

68. Inouye M. Signaling by Transmembrane Proteins Shifts Gears. Cell. 2006;126(5):829–31.

69. Hulko M, Berndt F, Gruber M, Linder JU, Truffault V, Schultz A, et al. The HAMP Domain Structure Implies Helix Rotation in Transmembrane Signaling. Cell. 2006;126(5):929–40.

70. Eftink MR. The Use of Fluorescence Methods to Monitor Unfolding Transitions in Proteins [Internet]. Vol. 66, Biophysical Journal. 1994 [cited 2020 Apr 22]. Available from: https://www.cell.com/biophysj/pdf/S0006-3495(94)80799-4.pdf

71. Sevvana M, Vijayan V, Zweckstetter M, Reinelt S, Madden DR, Herbst-Irmer R, et al. A Ligand-Induced Switch in the Periplasmic Domain of Sensor Histidine Kinase CitA. Elsevier [Internet]. 2008 [cited 2020 Apr 22]; Available from: www.sciencedirect.com

72. Cheung J, Structure WH-, 2009 undefined. Structural analysis of ligand stimulation of the histidine kinase NarX. Elsevier [Internet]. [cited 2020 Apr 22]; Available from: https://www.sciencedirect.com/science/article/pii/S0969212609000306

73. Blain KY, Kwiatkowski W, Choe S. The functionally active mistic-fused histidine kinase

receptor, EnvZ. Biochemistry. 2010 Oct 26;49(42):9089–95.

74. Reinelt S, Hofmann E, Gerharz T, Bott M, Madden DR. The Structure of the Periplasmic Ligand-binding Domain of the Sensor Kinase CitA Reveals the First Extracellular PAS Domain*. ASBMB [Internet]. 2003 [cited 2020 Apr 22]; Available from: http://www.jbc.org/

75. Teale F, Journal GW-B, 1957 undefined. Ultraviolet fluorescence of the aromatic amino acids. ncbi.nlm.nih.gov [Internet]. [cited 2020 Apr 22]; Available from: https://www.ncbi.nlm.nih.gov/pmc/articles/PMC1199900/

76. Royer CA. Probing protein folding and conformational transitions with fluorescence. Vol. 106, Chemical Reviews. 2006. p. 1769–84.

77. Cheung J, Hendrickson WA. Crystal Structures of C 4-Dicarboxylate Ligand Complexes with Sensor Domains of Histidine Kinases DcuS and DctB * □ S. ASBMB [Internet]. 2008 [cited 2020 Apr 22]; Available from: http://www.jbc.org/

78. Cheung J, Hendrickson WA. Sensor domains of two-component regulatory systems. Vol. 13, Current Opinion in Microbiology. Elsevier Current Trends; 2010. p. 116–23.

79. Gerken H, Charlson ES, Cicirelli EM, Kenney LJ, Misra R. MzrA: A novel modulator of the EnvZ/OmpR two-component regulon. Mol Microbiol. 2009;72(6):1408–22.

80. Gerken H, Misra R. MzrA-EnvZ interactions in the periplasm influence the EnvZ/OmpR two-component regulon. J Bacteriol. 2010;192(23):6271–8.

81. Liu Y, Rose J, Huang S, Hu Y, Wu Q, Wang D, et al. A pH-gated conformational switch regulates the phosphatase activity of bifunctional HisKA-family histidine kinases. Nat Commun. 2017;8(1).

82. Chakraborty S, Winardhi RS, Morgan LK, Yan J, Kenney LJ. Non-canonical activation of OmpR drives acid and osmotic stress responses in single bacterial cells. Nat Commun [Internet]. 2017 Dec 14 [cited 2019 Aug 2];8(1):1587. Available from: http://www.ncbi.nlm.nih.gov/pubmed/29138484

83. Foo YH, Gao Y, Zhang H, Kenney LJ. Cytoplasmic sensing by the inner membrane histidine kinase EnvZ. Prog Biophys Mol Biol. 2015;118(3):119–29.

84. Dunin-Horkawicz S, Lupas AN. Comprehensive Analysis of HAMP Domains: Implications for Transmembrane Signal Transduction. J Mol Biol [Internet]. 2010 Apr 16 [cited 2019 Aug 2];397(5):1156–74. Available from: http://www.ncbi.nlm.nih.gov/pubmed/20184894

85. Parkinson JS, Hazelbauer GL, Falke JJ. Signaling and sensory adaptation in Escherichia coli chemoreceptors: 2015 update. Trends Microbiol. 2015;23(5):257–66.

86. Elliott KT, Zhulin IB, Stuckey JA, DiRita VJ. Conserved Residues in the HAMP Domain Define a New Family of Proposed Bipartite Energy Taxis Receptors. J Bacteriol [Internet]. 2009 Jan 1 [cited 2019 Aug 2];191(1):375–87. Available from: http://jb.asm.org/cgi/doi/10.1128/JB.00578-08

87. Zhou Q, Ames P, Parkinson JS. Mutational analyses of HAMP helices suggest a dynamic bundle model of input-output signalling m chemoreceptors. Mol Microbiol. 2009;73(5):801–14.

88. Gushchin I, Melnikov I, Polovinkin V, Ishchenko A, Yuzhakova A, Buslaev P, et al. Mechanism of transmembrane signaling by sensor histidine kinases. Science (80-). 2017;356(6342).

89. Ames P, Hunter S, Parkinson JS. Evidence for a Helix-Clutch Mechanism of Transmembrane Signaling in a Bacterial Chemoreceptor. J Mol Biol. 2016;428(19):3776–88.

90. Wright GA, Crowder RL, Draheim RR, Manson MD. Mutational analysis of the transmembrane helix 2-HAMP domain connection in the Escherichia coli aspartate chemoreceptor Tar. J Bacteriol. 2011;193(1):82–90.

91. Kitanovic S, Ames P, Parkinson JS. A trigger residue for transmembrane signaling in the Escherichia coli serine chemoreceptor. J Bacteriol. 2015;197(15):2568–79.

92. Kitanovic S, Ames P, Parkinson JS. Mutational analysis of the control cable that mediates transmembrane signaling in the Escherichia coli serine chemoreceptor. J Bacteriol. 2011;193(19):5062–72.

93. Hall BA, Armitage JP, Sansom MSP. Transmembrane helix dynamics of bacterial chemoreceptors supports a piston model of signalling. PLoS Comput Biol. 2011;7(10):e1002204.

94. Miller AS, Falke JJ. Side Chains at the Membrane-Water Interface Modulate the Signaling State of a Transmembrane Receptor. Biochemistry. 2004;43(7):1763–70.

95. Park H, Im W, Seok C. Transmembrane signaling of chemotaxis receptor tar: Insights from molecular dynamics simulation studies. Biophys J. 2011;100(12):2955–63.

96. Ottemann KM, Xiao W, Shin YK, Koshland DE. A piston model for transmembrane signaling of the aspartate receptor. Science (80-). 1999;

97. Cheung J, Hendrickson WA. Structural Analysis of Ligand Stimulation of the Histidine Kinase NarX. Structure. 2009;17(2):190–201.

98. Draheim RR, Bormans AF, Lai RZ, Manson MD. Tuning a bacterial chemoreceptor with protein-membrane interactions. Biochemistry. 2006;45(49):14655–64.

99. Draheim RR, Bormans AF, Lai RZ, Manson MD. Tryptophan residues flanking the second transmembrane helix (TM2) set the signaling state of the Tar chemoreceptor. Biochemistry. 2005;44(4):1268–77.

100. Moore JO, Hendrickson WA. Structural Analysis of Sensor Domains from the TMAO-Responsive Histidine Kinase Receptor TorS. Structure. 2009;17(9):1195–204.

101. Lai WC, Beel BD, Hazelbauer GL. Adaptational modification and ligand occupancy have opposite effects on positioning of the transmembrane signalling helix of a chemoreceptor. Mol Microbiol. 2006;61(4):1081–90.

102. Mise T. Structural Analysis of the Ligand-Binding Domain of the Aspartate Receptor Tar from Escherichia coli. Biochemistry. 2016;55(26):3708–13.

103. Bi S, Jin F, Sourjik V. Inverted signaling by bacterial chemotaxis receptors. Nat Commun [Internet]. 2018 Dec 26 [cited 2019 Aug 2];9(1):2927. Available from: http://www.ncbi.nlm.nih.gov/pubmed/30050034

104. Heininger A, Yusuf R, Lawrence RJ, Draheim RR. Identification of transmembrane helix 1 (TM1) surfaces important for EnvZ dimerisation and signal output. Biochim Biophys Acta - Biomembr [Internet]. 2016 Aug 1 [cited 2019 Jul 30];1858(8):1868–75. Available from: https://www.sciencedirect.com/science/article/pii/S0005273616301444?via%3Dihub

105. Gao R, Stock AM. Biological Insights from Structures of Two-Component Proteins. Annu Rev Microbiol. 2009 Oct;63(1):133–54.

106. Xu J, Chiang HC, Bjursell MK, Gordon JI. Message from a human gut symbiont: Sensitivity is a prerequisite for sharing. Vol. 12, Trends in Microbiology. Elsevier Ltd; 2004. p. 21–8.

107. Corbett MSP, Poger D, Mark AE. Revisiting the scissor-like mechanism of activation for the erythropoietin receptor. FEBS Lett. 2016;590(18):3083–8.

108. Szurmant H, Bunn MW, Cho SH, Ordal GW. Ligand-induced conformational changes in the Bacillus subtilis chemoreceptor McpB determined by disulfide crosslinking in vivo. J Mol Biol. 2004;344(4):919–28.

109. Saita E, Abriata LA, Tsai YT, Trajtenberg F, Lemmin T, Buschiazzo A, et al. A coiled coil switch mediates cold sensing by the thermosensory protein DesK. Mol Microbiol [Internet]. 2015 Oct [cited 2019 Aug 2];98(2):258–71. Available from: http://doi.wiley.com/10.1111/mmi.13118

110. Abriata LA, Albanesi D, Dal Peraro M, de Mendoza D. Signal Sensing and Transduction by Histidine Kinases as Unveiled through Studies on a Temperature Sensor. Acc Chem Res [Internet]. 2017 Jun 20 [cited 2019 Aug 2];50(6):1359–66. Available from: http://pubs.acs.org/doi/10.1021/acs.accounts.6b00593

111. Molnar KS, Bonomi M, Pellarin R, Clinthorne GD, Gonzalez G, Goldberg SD, et al. Cys-Scanning disulfide crosslinking and bayesian modeling probe the transmembrane signaling mechanism of the histidine kinase, PhoQ. Structure. 2014;22(9):1239–51.

112. Wang B, Zhao A, Novick RP, Muir TW. Activation and Inhibition of the Receptor Histidine Kinase AgrC Occurs through Opposite Helical Transduction Motions. Mol Cell [Internet]. 2014 Mar [cited 2019 Aug 2];53(6):929–40. Available from: https://linkinghub.elsevier.com/retrieve/pii/S1097276514002019

113. Ferris HU, Dunin-Horkawicz S, Mondéjar LG, Hulko M, Hantke K, Martin J, et al. The mechanisms of HAMP-mediated signaling in transmembrane receptors. Structure. 2011;19(3):378–85.

114. Ferris HU, Dunin-Horkawicz S, Hornig N, Hulko M, Martin J, Schultz JE, et al. Mechanism of regulation of receptor histidine kinases. Structure. 2012;20(1):56–66.

115. Mondéjar LG, Lupas A, Schultz A, Schultz JE. HAMP domain-mediated signal transduction probed with a mycobacterial adenylyl cyclase as a reporter. J Biol Chem. 2012;287(2):1022–31.

116. Smock RG, Gierasch LM. Sending signals dynamically. Science [Internet]. 2009 Apr 10 [cited 2019 Aug 15];324(5924):198–203. Available from: http://www.ncbi.nlm.nih.gov/pubmed/19359576

117. Sourjik V, Berg HC. Receptor sensitivity in bacterial chemotaxis. Proc Natl Acad Sci [Internet]. 2002 Jan 8 [cited 2019 Aug 15];99(1):123–7. Available from: http://www.ncbi.nlm.nih.gov/pubmed/11742065

118. Bornhorst JA, Falke JJ. Evidence That Both Ligand Binding and Covalent Adaptation Drive a Two-State Equilibrium in the Aspartate Receptor Signaling Complex. J Gen Physiol [Internet]. 2001 Dec 1 [cited 2019 Aug 15];118(6):693–710. Available from: http://www.ncbi.nlm.nih.gov/pubmed/11723162

119. Li G, Weis RM. Covalent modification regulates ligand binding to receptor complexes

in the chemosensory system of Escherichia coli. Cell [Internet]. 2000 Feb 4 [cited 2019 Aug 15];100(3):357–65. Available from: http://www.ncbi.nlm.nih.gov/pubmed/10676817

120. Starrett DJ, Falke JJ. Adaptation Mechanism of the Aspartate Receptor: Electrostatics of the Adaptation Subdomain Play a Key Role in Modulating Kinase Activity †. Biochemistry [Internet]. 2005 Feb 8 [cited 2019 Aug 15];44(5):1550–60. Available from: http://www.ncbi.nlm.nih.gov/pubmed/15683239

121. Kim S-H, Wang W, Kim KK. Dynamic and clustering model of bacterial chemotaxis receptors: Structural basis for signaling and high sensitivity. Proc Natl Acad Sci [Internet]. 2002 Sep 3 [cited 2019 Aug 15];99(18):11611–5. Available from: http://www.ncbi.nlm.nih.gov/pubmed/12186970

122. Stewart V. The HAMP signal-conversion domain: static two-state or dynamic three-state? Mol Microbiol [Internet]. 2014 Mar 1 [cited 2019 Aug 15];91(5):853–7. Available from: http://doi.wiley.com/10.1111/mmi.12516

123. Kalli AC, Campbell ID, Sansom MSP. Multiscale simulations suggest a mechanism for integrin inside-out activation. Proc Natl Acad Sci. 2011;108(29):11890–5.

124. Sukomon N, Widom J, Borbat PP, Freed JH, Crane BR. Stability and Conformation of a Chemoreceptor HAMP Domain Chimera Correlates with Signaling Properties. Biophys J. 2017;112(7):1383–95.

125. Wang LC, Morgan LK, Godakumbura P, Kenney LJ, Anand GS. The inner membrane histidine kinase EnvZ senses osmolality via helix-coil transitions in the cytoplasm. EMBO J. 2012;31(11):2648–59.

126. Dardalhon M, Kumar C, Iraqui I, Vernis L, Kienda G, Banach-Latapy A, et al. Redox-sensitive YFP sensors monitor dynamic nuclear and cytosolic glutathione redox changes. Free Radic Biol Med. 2012 Jun 1;52(11–12):2254–65.

127. Østergaard H, Tachibana C, Winther JR. Monitoring disulfide bond formation in the

eukaryotic cytosol. J Cell Biol. 2004 Aug 2;166(3):337–45.

128. Lai W, Hazelbauer GL. Analyzing Transmembrane Chemoreceptors Using In Vivo Disulfide Formation Between Introduced Cysteines. In: Methods in enzymology [Internet]. 2007 [cited 2019 Aug 19]. p. 299–316. Available from: http://www.ncbi.nlm.nih.gov/pubmed/17609137

129. Careaga CL, Falke JJ. Thermal motions of surface alpha-helices in the D-galactose chemosensory receptor. Detection by disulfide trapping. J Mol Biol [Internet]. 1992 Aug 20 [cited 2019 Aug 19];226(4):1219–35. Available from: http://www.ncbi.nlm.nih.gov/pubmed/1518053

130. Hughson AG, Hazelbauer GL. Detecting the conformational change of transmembrane signaling in a bacterial chemoreceptor by measuring effects on disulfide cross-linking in vivo. Proc Natl Acad Sci [Internet]. 1996 Oct 15 [cited 2019 Aug 19];93(21):11546–51. Available from: http://www.ncbi.nlm.nih.gov/pubmed/8876172

131. Metcalf DG, Kulp DW, Bennett JS, DeGrado WF. Multiple Approaches Converge on the Structure of the Integrin αIIb/β3 Transmembrane Heterodimer. J Mol Biol [Internet]. 2009 Oct 2 [cited 2019 Aug 19];392(4):1087–101. Available from: http://www.ncbi.nlm.nih.gov/pubmed/19527732

132. Rivera-Cancel G, Ko WH, Tomchick DR, Correa F, Gardner KH. Full-length structure of a monomeric histidine kinase reveals basis for sensory regulation. Proc Natl Acad Sci U S A [Internet]. 2014 Dec 16 [cited 2020 Jun 25];111(50):17839–44. Available from: https://www.pnas.org/content/111/50/17839

133. Guyer MS, Reed RR, Steitz JA, Low KB. Identification of a sex-factor-affinity site in E. coli as gamma delta. Cold Spring Harb Symp Quant Biol. 1981;45 Pt 1(1):135–40.

134. Lai RZ, Bormans AF, Draheim RR, Wright GA, Manson MD. The region preceding the C-terminal NWETF pentapeptide modulates baseline activity and aspartate inhibition of Escherichia coli Tar. Biochemistry. 2008;47(50):13287–95.

135. Cantwell BJ, Draheim RR, Weart RB, Nguyen C, Stewart RC, Manson MD. CheZ phosphatase localizes to chemoreceptor patches via CheA-short. J Bacteriol. 2003;185(7):2354–61.

136. Southern JA, Young DF, Heaney F, Baumgartner WK, Randall RE. Identification of an epitope on the P and V proteins of simian virus 5 that distinguishes between two isolates with different biological characteristics. J Gen Virol. 1991;72(7):1551–7.

137. Yusuf R, Nguyen TL, Heininger A, Lawrence RJ, Hall BA, Draheim RR. In vivo cross-linking and transmembrane helix dynamics support a bidirectional non-piston model of signaling within E. coli EnvZ. bioRxiv. 2018;

138. Oropeza R, Calva E. The cysteine 354 and 277 residues of Salmonella enterica serovar Typhi EnvZ are determinants of autophosphorylation and OmpR phosphorylation. FEMS Microbiol Lett. 2009;292(2):282–90.

139. Cai SJ, Khorchid A, Ikura M, Inouye M. Probing catalytically essential domain orientation in histidine kinase EnvZ by targeted disulfide crosslinking. J Mol Biol. 2003;328(2):409–18.

140. Adase CA, Draheim RR, Manson MD. The residue composition of the aromatic anchor of the second transmembrane helix determines the signaling properties of the aspartate/maltose chemoreceptor tar of escherichia coli. Biochemistry. 2012;51(9):1925–32.

141. Adase CA, Draheim RR, Rueda G, Desai R, Manson MD. Residues at the cytoplasmic end of transmembrane helix 2 determine the signal output of the TarEc chemoreceptor. Biochemistry. 2013;52(16):2729–38.

142. The W, Partitioning P, Ag B, Mc-icpms NP, Zurich ETH. Supplementary information. Nature. 2010;450:1–7.

143. Krogh A, Larsson B, Von Heijne G, Sonnhammer ELL. Predicting transmembrane protein topology with a hidden Markov model: Application to complete genomes. J Mol

Biol. 2001;305(3):567–80.

144. Nyholm TKM, Özdirekcan S, Antoinette Killian J. How protein transmembrane segments sense the lipid environment. Biochemistry. 2007;46(6):1457–65.

145. Hessa T, Meindl-Beinker NM, Bernsel A, Kim H, Sato Y, Lerch-Bader M, et al. Molecular code for transmembrane-helix recognition by the Sec61 translocon. Nature. 2010;450:1026–30.

146. Ausubel FM, Brent R, Kingston RE, Moore DD, Seidman JG, Smith JA, et al. Current Protocols in Molecular Biology: Preface. Current Protocols in Molecular Biology. 2010;(SUPPL. 90).

147. Schneider CA, Rasband WS, Eliceiri KW. NIH Image to ImageJ: 25 years of image analysis. Nat Methods. 2012;9(7):671–5.

148. Yaku H, Mizuno T. The membrane-located osmosensory kinase, EnvZ, that contains a leucine zipper-like motif functions as a dimer in Escherichia coli. FEBS Lett. 1997;417(3):409–13.

149. Bass RB, Butler SL, Chervitz SA, Gloor SL, Falke JJ. Use of Site-Directed Cysteine and Disulfide Chemistry to Probe Protein Structure and Dynamics: Applications to Soluble and Transmembrane Receptors of Bacterial Chemotaxis. In: Methods in Enzymology. 2007. p. 25–51.

150. Hammack LJ, Kusmierczyk AR. Assembly of proteasome subunits into non-canonical complexes in vivo. Biochem Biophys Res Commun [Internet]. 2017 Jan 1 [cited 2019 Nov 24];482(1):164–9. Available from: http://www.ncbi.nlm.nih.gov/pubmed/27833017

151. Kuhn A. Crosslinking and Reconstitution Approaches to Study Protein Transport. Protein J [Internet]. 2019 Jun 29 [cited 2019 Nov 24];38(3):229–35. Available from: http://www.ncbi.nlm.nih.gov/pubmed/31144202

152. Taylor BL, Watts KJ, Johnson MS. Oxygen and Redox Sensing by Two-Component Systems That Regulate Behavioral Responses: Behavioral Assays and Structural

Studies of Aer Using In Vivo Disulfide Cross-Linking. In: Methods in enzymology [Internet]. 2007 [cited 2019 Nov 24]. p. 190–232. Available from: http://www.ncbi.nlm.nih.gov/pubmed/17628141

153. Ludwiczak J, Winski A, Szczepaniak K, Alva V, Dunin-Horkawicz S. DeepCoil—a fast and accurate prediction of coiled-coil domains in protein sequences. Hancock J, editor. Bioinformatics [Internet]. 2019 Aug 15 [cited 2019 Nov 28];35(16):2790–5. Available from: http://www.ncbi.nlm.nih.gov/pubmed/30601942

154. Dunnill P. The Use of Helical Net-Diagrams to Represent Protein Structures. Biophys J. 1968;8(7):865–75.

155. Careaga CL, Falke JJ. Structure and dynamics of Escherichia coli chemosensory receptors. Engineered sulfhydryl studies. Biophys J. 1992;62(1):209–19.

156. Balaji VN, Mobasser A, Rao SN. Modification of protein stability by introduction of disulfide bridges and prolines: Geometric criteria for mutation sites. Biochem Biophys Res Commun. 1989;160(1):109–14.

157. SRINIVASAN N, SOWDHAMINI R, RAMAKRISHNAN C, BALARAM P. Conformations of disulfide bridges in proteins. Int J Pept Protein Res. 1990;36(2):147–55.

158. Leatham-Jensen MP, Frimodt-Møller J, Adediran J, Mokszycki ME, Banner ME, Caughron JE, et al. The streptomycin-treated mouse intestine selects Escherichia coli envZ missense mutants that interact with dense and diverse intestinal microbiota. Infect Immun. 2012;80(5):1716–27.

159. Adediran J, Leatham-Jensen MP, Mokszycki ME, Frimodt-Møller J, Krogfelt KA, Kazmierczak K, et al. An escherichia coli nissle 1917 missense mutant colonizes the streptomycin-treated mouse intestine better than the wild type but is not a better probiotic. Infect Immun. 2014;82(2):670–82.

160. Botelho SC, Enquist K, Von Heijne G, Draheim RR. Differential repositioning of the second transmembrane helices from E. coli Tar and EnvZ upon moving the flanking

aromatic residues. Biochim Biophys Acta - Biomembr. 2015;1848(2):615–21.

161. Falke JJ, Hazelbauer GL. Transmembrane signaling in bacterial chemoreceptors. Trends Biochem Sci. 2001;26(4):257–65.

162. Monzel C, Unden G. Transmembrane signaling in the sensor kinase DcuS of Escherichia coli : A long-range piston-type displacement of transmembrane helix 2 . Proc Natl Acad Sci. 2015;112(35):11042–7.

163. Goldberg SD, Clinthorne GD, Goulian M, DeGrado WF. Transmembrane polar interactions are required for signaling in the Escherichia coli sensor kinase PhoQ. Proc Natl Acad Sci. 2010;107(18):8141–6.

164. Yusuf R, Draheim RR. Employing aromatic tuning to modulate output from two-component signaling circuits. J Biol Eng. 2015;9(1):7.

165. Falke JJ. Piston versus Scissors: Chemotaxis receptors versus sensor his-kinase receptors in two-component signaling pathways. Structure. 2014;22(9):1219–20.

166. Unnerståle S, Mäler L, Draheim RR. Structural characterization of AS1-membrane interactions from a subset of HAMP domains. Biochim Biophys Acta - Biomembr. 2011;1808(10):2403–12.

167. Gushchin I, Gordeliy V. Transmembrane Signal Transduction in Two-Component Systems: Piston, Scissoring, or Helical Rotation? BioEssays. 2018;40(2).

168. Hazelbauer GL, Falke JJ, Parkinson JS. Bacterial chemoreceptors: high-performance signaling in networked arrays. Trends Biochem Sci. 2008;33(1):9–19.

169. Hwang E, Cheong HK, Kim SY, Kwon O, Blain KY, Choe S, et al. Crystal structure of the EnvZ periplasmic domain with CHAPS. FEBS Lett. 2017;591(10):1419–28.

170. Upadhyay AA, Fleetwood AD, Adebali O, Finn RD, Zhulin IB. Cache Domains That are Homologous to, but Different from PAS Domains Comprise the Largest Superfamily of Extracellular Sensors in Prokaryotes. PLoS Comput Biol. 2016;12(4).

171. Gordeliy VI, Labahn J, Moukhametzianov R, Efremov R, Granzin J, Schlesinger R, et

al. Molecular basis of transmembrane signalling by sensory rhodopsin II-transducer complex. Nature. 2002 Oct 3;419(6906):484–7.

172. Ishchenko A, Round E, Borshchevskiy V, Grudinin S, Gushchin IY, Klare JP, et al. Ground state structure of D75N mutant of sensory rhodopsin II in complex with its cognate transducer. J Photochem Photobiol B Biol [Internet]. 2013 [cited 2020 May 1];(123):55–8. Available from: https://hal.inria.fr/hal-00881553

173. Brown ED, Wright GD. Antibacterial drug discovery in the resistance era. Nature. 2016;529(7586):336–43.

174. Spellberg B. The future of antibiotics. Crit Care. 2014;18(3).

175. Dcosta VM, King CE, Kalan L, Morar M, Sung WWL, Schwarz C, et al. Antibiotic resistance is ancient. Vol. 477, Nature. Nature Publishing Group; 2011. p. 457–61.

176. Cox G, Wright GD. Intrinsic antibiotic resistance: Mechanisms, origins, challenges and solutions. Vol. 303, International Journal of Medical Microbiology. 2013. p. 287–92.

177. Nikaido H. Preventing drug access to targets: Cell surface permeability barriers and active efflux in bacteria. Semin Cell Dev Biol. 2001;12(3):215–23.

178. Delcour AH. Outer membrane permeability and antibiotic resistance. Biochim Biophys Acta - Proteins Proteomics. 2009;1794(5):808–16.

179. Fadli M, Chevalier J, Hassani L, Mezrioui NE, Pagès JM. Natural extracts stimulate membrane-associated mechanisms of resistance in Gram-negative bacteria. Lett Appl Microbiol. 2014;58(5):472–7.

180. Bem AE, Velikova N, Pellicer MT, Baarlen P Van, Marina A, Wells JM. Bacterial histidine kinases as novel antibacterial drug targets. Vol. 10, ACS Chemical Biology. 2015. p. 213–24.

181. Brown ED, Wright GD. New targets and screening approaches in antimicrobial drug discovery. Chem Rev. 2005;105(2):759–74.

182. Martens E, Demain AL. The antibiotic resistance crisis, with a focus on the United

States. J Antibiot (Tokyo). 2017;70(5):520–6.

183. Rossolini GM, Arena F, Pecile P, Pollini S. Update on the antibiotic resistance crisis. Curr Opin Pharmacol. 2014;18:56–60.

184. Ventola CL. The Antibiotic Resistance: Part 1: Causes and Threats. P T a peer Rev J Formul Manag. 2015;40(4):277–83.

185. Ventola CL. The antibiotic resistance crisis: part 2: management strategies and new agents. P T [Internet]. 2015;40(5):344–52. Available from: http://www.ncbi.nlm.nih.gov/pubmed/25987823%0Ahttp://www.pubmedcentral.nih.gov/articlerender.fcgi?artid=PMC4422635

186. Alós J-I. Resistencia bacteriana a los antibióticos: una crisis global. Enferm Infecc Microbiol Clin [Internet]. 2015;33(10):692–9. Available from: https://linkinghub.elsevier.com/retrieve/pii/S0213005X14003413

187. Centers for Disease Control U. Antibiotic Resistance Threats in the United States, 2019. [cited 2020 Jun 2]; Available from: http://dx.doi.org/10.15620/cdc:82532.

188. Laxminarayan R. Antibiotic effectiveness: Balancing conservation against innovation. Science (80-). 2014;345(6202):1299–301.

189. O'Neill J. Antimicrobial Resistance: Tackling a crisis for the health and wealth of nations [Internet]. 2014 [cited 2019 Aug 6]. Available from: https://amr-review.org/sites/default/files/AMR Review Paper - Tackling a crisis for the health and wealth of nations_1.pdf

190. Unemo M, Shafer WM. Antimicrobial Resistance in Neisseria gonorrhoeae in the 21st Century: Past, Evolution, and Future. Clin Microbiol Rev [Internet]. 2014 Jul 1 [cited 2019 Aug 5];27(3):587–613. Available from: http://www.ncbi.nlm.nih.gov/pubmed/24982323

191. Gould IM, Bal AM. New antibiotic agents in the pipeline and how they can help overcome microbial resistance. Virulence [Internet]. 2013 Feb 15 [cited 2019 Aug

6];4(2):185–91. Available from: http://www.ncbi.nlm.nih.gov/pubmed/23302792

192. World Health Organisation. Antimicrobial resistance: global report on surveillance 2014 [Internet]. 2014 [cited 2019 Aug 5]. Available from: www.paprika-annecy.com

193. Tommasi R, Brown DG, Walkup GK, Manchester JI, Miller AA. ESKAPEing the labyrinth of antibacterial discovery. Nat Rev Drug Discov. 2015;14(8):529–42.

194. Gwynn MN, Portnoy A, Rittenhouse SF, Payne DJ. Challenges of antibacterial discovery revisited. Ann N Y Acad Sci. 2010;1213(1):5–19.

195. Payne DJ, Gwynn MN, Holmes DJ, Pompliano DL. Drugs for bad bugs: Confronting the challenges of antibacterial discovery. Nat Rev Drug Discov. 2007;6(1):29–40.

196. Joyce AR, Reed JL, White A, Edwards R, Osterman A, Baba T, et al. Experimental and computational assessment of conditionally essential genes in Escherichia coli. J Bacteriol. 2006;188(23):8259–71.

197. Nichols RJ, Sen S, Choo YJ, Beltrao P, Zietek M, Chaba R, et al. Phenotypic landscape of a bacterial cell. Cell. 2011;144(1):143–56.

198. Jores J, Ma L, Ssajjakambwe P, Schieck E, Liljander A, Chandran S, et al. Removal of a Subset of Non-essential Genes Fully Attenuates a Highly Virulent Mycoplasma Strain. Front Microbiol [Internet]. 2019 Apr 3 [cited 2019 Nov 18];10:664. Available from: http://www.ncbi.nlm.nih.gov/pubmed/31001234

199. Butland G, Peregrin-Alvarez JM, Li J, Yang W, Yang X, Canadien V, et al. Interaction network containing conserved and essential protein complexes in Escherichia coli. Nature. 2005;433(7025):531–7.

200. Babu M, Díaz-Mejía JJ, Vlasblom J, Gagarinova A, Phanse S, Graham C, et al. Genetic interaction maps in Escherichia coli reveal functional crosstalk among cell envelope biogenesis pathways. PLoS Genet. 2011;7(11).

201. Costanzo M, Baryshnikova A, Bellay J, Kim Y, Spear ED, Sevier CS, et al. The genetic landscape of a cell. Science (80-). 2010;327(5964):425–31.

202. Tiwari S, Jamal SB, Hassan SS, Carvalho PVSD, Almeida S, Barh D, et al. Two-component signal transduction systems of pathogenic bacteria as targets for antimicrobial therapy: An overview. Front Microbiol. 2017;8(OCT).

203. Gotoh Y, Eguchi Y, Watanabe T, Okamoto S, Doi A, Utsumi R. Two-component signal transduction as potential drug targets in pathogenic bacteria. Curr Opin Microbiol. 2010;13(2):232–9.

204. Schaefers MM, Liao TL, Boisvert NM, Roux D, Yoder-Himes D, Priebe GP. An Oxygen-Sensing Two-Component System in the Burkholderia cepacia Complex Regulates Biofilm, Intracellular Invasion, and Pathogenicity. PLoS Pathog. 2017;13(1).

205. Martin C, Williams A, Hernandez-Pando R, Cardona PJ, Gormley E, Bordat Y, et al. The live Mycobacterium tuberculosis phoP mutant strain is more attenuated than BCG and confers protective immunity against tuberculosis in mice and guinea pigs. Vaccine. 2006;24(17):3408–19.

206. Vancott JL, Chatfield SN, Roberts M, Hone DM, Hohmann EL, Pascual DW, et al. Regulation of host immune responses by modification of Salmonella virulence genes. Nat Med. 1998;4(11):1247–52.

207. Link C, Ebensen T, Ständner L, Déjosez M, Reinhard E, Rharbaoui F, et al. An SopB-mediated immune escape mechanism of Salmonella enterica can be subverted to optimize the performance of live attenuated vaccine carrier strains. Microbes Infect. 2006;8(8):2262–9.

208. Hohmann EL, Oletta CA, Miller SI. Evaluation of a phoP/phoQ-deleted, aroA-deleted live oral Salmonella typhi vaccine strain in human volunteers. Vaccine. 1996;14(1):19–24.

209. Domagala JM, Alessi D, Cummings M, Gracheck S, Huang L, Huband M, et al. Bacterial Two-Component Signalling as a Therapeutic Target in Drug Design. In: Advances in experimental medicine and biology [Internet]. 2011 [cited 2019 Aug 8]. p. 269–86.

Available from: http://link.springer.com/10.1007/978-1-4615-4897-3_14

210. Barrett JF, Hoch JA. Two-component signal transduction as a target for microbial anti-infective therapy. Antimicrob Agents Chemother. 1998;42(7):1529–36.

211. Worthington RJ, Blackledge MS, Melander C. Small-molecule inhibition of bacterial two-component systems to combat antibiotic resistance and virulence. Future Med Chem. 2013;5(11):1265–84.

212. Okada A, Gotoh Y, Watanabe T, Furuta E, Yamamoto K, Utsumi R. Targeting Two-Component Signal Transduction: A Novel Drug Discovery System. Methods Enzymol. 2007;422:386–95.

213. Bem AE, Velikova N, Pellicer MT, Baarlen P Van, Marina A, Wells JM. Bacterial histidine kinases as novel antibacterial drug targets. ACS Chem Biol. 2015;10(1):213–24.

214. Gallego del Sol F, Marina A. Structural Basis of Rap Phosphatase Inhibition by Phr Peptides. PLoS Biol. 2013;11(3).

215. Howell A, Dubrac S, Andersen KK, Noone D, Fert J, Msadek T, et al. Genes controlled by the essential YycG/YycF two-component system of Bacillus subtilis revealed through a novel hybrid regulator approach. Mol Microbiol. 2003;49(6):1639–55.

216. Healy VL, Lessard IA, Roper DI, Knox JR, Walsh CT. Vancomycin resistance in enterococci: reprogramming of the D-ala-D-Ala ligases in bacterial peptidoglycan biosynthesis. Chem Biol [Internet]. 2000 May [cited 2019 Aug 9];7(5):R109-19. Available from: http://www.ncbi.nlm.nih.gov/pubmed/10801476

217. Pootoolal J, Neu J, Wright GD. GLYCOPEPTIDE ANTIBIOTIC RESISTANCE. Annu Rev Pharmacol Toxicol [Internet]. 2002 Apr [cited 2019 Aug 9];42(1):381–408. Available from: http://www.ncbi.nlm.nih.gov/pubmed/11807177

218. Macielag MJ, Demers JP, Fraga-Spano SA, Hlasta DJ, Johnson SG, Kanojia RM, et al. Substituted Salicylanilides as Inhibitors of Two-Component Regulatory Systems in

Bacteria. J Med Chem [Internet]. 1998 Jul [cited 2019 Nov 23];41(16):2939–45. Available from: https://pubs.acs.org/doi/10.1021/jm9803572

219. Tiwari S, Da Costa MP, Almeida S, Hassan SS, Jamal SB, Oliveira A, et al. C. pseudotuberculosis Phop confers virulence and may be targeted by natural compounds. Integr Biol (United Kingdom). 2014;6(11):1088–99.

220. Reboul A, Lemaitre N, Titecat M, Merchez M, Deloison G, Ricard I, et al. Yersinia pestis Requires the 2-Component Regulatory System OmpR-EnvZ to Resist Innate Immunity During the Early and Late Stages of Plague. J Infect Dis [Internet]. 2014 Nov 1 [cited 2019 Aug 9];210(9):1367–75. Available from: http://www.ncbi.nlm.nih.gov/pubmed/24813471

221. Bernardini ML, Fontaine A, Sansonetti PJ. The two-component regulatory system ompR-envZ controls the virulence of Shigella flexneri. J Bacteriol [Internet]. 1990 [cited 2019 Aug 9];172(11):6274. Available from: https://www.ncbi.nlm.nih.gov/pmc/articles/PMC526810/

222. Dorman CJ, Chatfield S, Higgins CF, Hayward C, Dougan G. Characterization of porin and ompR mutants of a virulent strain of Salmonella typhimurium: ompR mutants are attenuated in vivo. Infect Immun [Internet]. 1989 Jul [cited 2019 Aug 9];57(7):2136–40. Available from: http://www.ncbi.nlm.nih.gov/pubmed/2543631

223. Matsubara M, Kitaoka S, Takeda S, Mizuno T. Tuning of the porin expression under anaerobic growth conditions by His-to-Asp cross-phosphorelay through both the EnvZ-osmosensor and ArcB-anaerosensor in Escherichia coli. Genes to Cells [Internet]. 2000 Jul 1 [cited 2019 Sep 23];5(7):555–69. Available from: http://doi.wiley.com/10.1046/j.1365-2443.2000.00347.x

224. Advisory Committee on Dangerous Pathogens (ACDP). The Approved List of Biological Agents. Heal Saf Exec. 2013;

225. Hazelbauer GL, Lai WC. Bacterial chemoreceptors: providing enhanced features to

two-component signaling. Vol. 13, Current Opinion in Microbiology. Elsevier Current Trends; 2010. p. 124–32.

226. Lowe EC, Baslé A, Czjzek M, Firbank SJ, Bolam DN. A scissor blade-like closing mechanism implicated in transmembrane signaling in a Bacteroides hybrid two-component system. Proc Natl Acad Sci U S A. 2012 May 8;109(19):7298–303.

227. Forst SA, Roberts DL. Signal transduction by the EnvZ-OmpR phosphotransfer system in bacteria. Res Microbiol. 1994;145(5–6):363–73.

228. Rampersaud A, Inouye M. Procaine, a local anesthetic, signals through the EnvZ receptor to change the DNA binding affinity of the transcriptional activator protein OmpR. J Bacteriol. 1991;173(21):6882–8.